Universidad de Valladolid

Escuela de Doctorado Universidad de Valladolid

PROGRAMA DE DOCTORADO EN INVESTIGACION BIOMEDICA

TESIS DOCTORAL

BIOENGINEERED DYNAMIC SYSTEMS BASED ON ELASTIN-LIKE RECOMBINAMERS

Presentada por Tatjana Flora para optar al grado de Doctora por la Universidad de Valladolid

Dirigida por:

Prof. Jose Carlos Rodriguez-Cabello

INDEX

ABSTRACT

Abstract

Tissue engineering and regenerative medicine are interdisciplinary fields that aims to develop biological substitutes that restore, maintain, or improve the function of a tissue or whole organ lost to injury or disease. Biomaterials used in biomedical application provide essential features that promote the new tissue morphogenesis supplying a favourable environment for cell growth as well as adequate physical and chemical properties required for a given tissue. In past decades, several obstacles have been encountered to select functional biomaterials that mimic the natural extracellular matrix (ECM). For example, synthetic polymers are often biocompatible, but they lack cues for cell attachment and tissue growth, which has led to the need for modification of many of these materials with bioactive sequences and factors. Conversely, naturally occurring polymers derived from extracellular matrix proteins, offer the advantage of biological signalling, but can be antigenic and their physical properties are more difficult to modulate than synthetic polymers. Biodegradation is a crucial feature for constructs used in biomedical applications and its modulation has been extensively studied namely to have a degradation process that occurs simultaneously with new tissue formation. Degradation rate is influenced by many characteristics including morphology and chain orientation of the polymers, initial

crystallinity, molecular weight, presence of residual monomers and oligomers and purity. There are several methods to change and control the degradation rate of synthetic and natural polymers such as copolymerization, blending, additives and irradiation but these methods show different drawbacks like changes in mechanical properties, loss of biocompatibility as well as delay in bioabsorption. Due to these drawbacks, it may be useful to produce biomaterials that are sensitive to certain enzymes taking advantage in this case of inflammatory response. Advances in genetic engineering have facilitated production of engineered proteins allowing in such a way tailoring a wide range of their properties and different functionalities such as cell adhesion, cell signalling, elasticity, and biodegradability. Currently, elastin-like recombinamers (ELRs) show outstanding properties for application in tissue regeneration. ELRs are artificial polypeptides with a high content in elastin that made them paramount materials able to mimic the ECM. The most commonly used is the penta-peptide VPGXG, where X stands for any amino acid except L-proline. They are synthetized by recombinant technology allowing an absolute control over their amino acid composition affording exquisite control over final protein functionality. They have interesting mechanical properties ranging between ideal elastomers to plastic that enable hence repetitive mechanical stress and confer mechanical resistance

through separate mechanism supporting several tissue functions. Lastly, they are extremely biocompatible due to their amino acidic composition that involves repeating sequences based on the recurring sequences found in the mammalian elastic protein. They recombinant nature allow the inclusion of specific epitopes such as adhesion sequences, proteolytic sites, antimicrobial peptides and so on. For all these advantages that they present, the biopolymers designed and used in this thesis are ELRs.

In the first study of this thesis two ELRs with a complementary bioactivity (CC-RGD and CCC-REDV), including cysteines at the amino terminal region, were employed to develop a 2D system where selective cell adhesion is spatially controlled for subsequent application in cellular biosensor technology as diagnostic devices or tissue engineering and regenerative medicine application. Specifically, in this study, model gold surfaces were functionalized with different percentages of two ELRs (CC-RGD and CCC-REDV) demonstrating that an optimal composition of 75% CCC-REDV and 25% CC-RGD leads to a selective adhesion of endothelial cells in a co-culture system. Afterwards, once the whole surface was functionalized with 100% CC-RGD, specific areas were cleaned by laser ablation without interfering in topographic, hydrophobic and mechanical properties of the surfaces. These areas were functionalized with 75% CCC-REDV and 25% CC-RGD and after *in vitro* studies it was

observed a well-defined distribution of HUVEC and HFF1 cells namely a selective spatial control over HUVEC adhesion. These findings suggest an innovative approach for biosensors generation e/o scaffolds that require spatial and temporal organization of cells.

Following, the second study of this thesis consists on the enhancement of angiogenic activity of ELR-based hydrogels when tethered chemically a small VEGF mimetic peptide called QK. In addition to cell adhesion sequences (RGD and REDV), an ELR used in this work present a proteolytic site (VGVAPG) that belong to elastase enzyme. The angiogenic acticity of these hydrogels were studied *in vitro* demonstrating that it does not alter the mechanical and morphological properties of the ELRs but the biological activity such as cell adhesion and proliferation. When injected *in vivo* an improved microvasculature formation was observed that facilitate perfusion and connection with the surrounding tissue. These results showed that ELR-QK-based hydrogels are optimal engineered constructs with a potential angiogenic activity that could be employed in tissue engineering and regenerative medicine for treatment of cardiovascular diseases.

The third study of this thesis aims to control in time and space cell infiltration and biodegradation in a three dimensional (3D)-structured system. The ELRs employed in this work, in addition to a universal cell

adhesion sequence (RGD), contain proteolytic target sites that degrade in response to urokinase plasminogen activator (uPA) with different degradation rate (fast and slow). Exploiting these features, in this study a 3D system was developed which consist in a three-layer disk hydrogel with an internal layer that contains the rapid degrading component and the external layers that contain the slow-degrading ELR. Those disks have been implanted subcutaneously in mice and its evolution was followed over time. As a result of the design and the programmed cell infiltration sequence, the internal layer was colonized firstly following an inside-to-outside pattern. These results demonstrated that the 3D-ELR based system could be applied as a tissue substitute for biomedical application that require a controlled regeneration and vascularization over time.

In summary, the studies showed in this thesis provides new insights regarding ELR-based hydrogels to be used in tissue engineering and regenerative medicine. Specifically, it describes the importance of the inclusion of several epitopes into the backbone of the ELR such as for example universal and specific adhesion sequences that influence cell behaviour. Furthermore, the presence of a VEGF mimetic peptide called QK enhance the angiogenic properties of ELR-based hydrogels and on the other hand, ELRs with a controlled degradation rate could be implicated

in the construction of complex biological structures that require specific time to regenerate.

OBJECTIVES

Objectives

- The main objective of this thesis is the development of multifunctional systems based on ELRs for their subsequent application in tissue engineering and regenerative medicine. For that we aim to take advantage of their features such as the possibility to tailor them at the genetic level allowing the inclusion of specific epitopes that lead to an efficient and faster cell responses promoting a better regeneration.
- The aim of the first study is to develop a 2D system for biomedical application such as cell-based biosensors or diagnostic devices. This approach consists on using model gold surfaces functionalized with ELRs codifying into their backbone complementary bioactivities as RGD and REDV sequences. The purpose is to obtain a simple system for cell selectivity and spatially controlled cell adhesion onto the surfaces exploiting the synergy between two bioactivities.
- The objective of the second study is to enhance vascularization in ELR-based hydrogels tethering chemically the so-called QK peptide. The presence of cell adhesiveness motifs into their peptide chain (RGD and REDV) increase cell recruitment into the construct and the inclusion of a VGVAPG sequence, sensitive to

proteases, favors its biodegradation which is an important pre-requisite for the scaffolds implied in tissue engineering.

- Lastly, the aim of the third study is to design and obtain advanced functional structures with a preprogrammed cell-infiltration and biodegradation pattern. These are 3D systems composed of two ELRs with differences in peptide cleavage kinetic and coupling cell adhesiveness bioactivity. Theoretically this 3D system should invert conventional cell infiltration patterns conducting cell invasion.

RESUMEN

Resumen

La ingeniería tisular y la medicina regenerativa son campos interdisciplinares que tienen como objetivo desarrollar sustitutos biológicos que restauren, mantengan o mejoren la función de un tejido o de un órgano perdida por lesión o enfermedad. Los biomateriales utilizados en aplicaciones biomédicas persiguen alcanzar características esenciales que promuevan la nueva morfogénesis tisular creando un entorno favorable para el crecimiento celular, así como las propiedades físicas y químicas adecuadas requeridas para un tejido determinado. En décadas pasadas, se han encontrado varios obstáculos para seleccionar biomateriales funcionales que imiten la matriz extracelular natural (MEC). Por ejemplo, algunos de los polímeros sintéticos a menudo son biocompatibles, pero carecen de interacción con las células y el crecimiento del tejido, lo que ha llevado a la necesidad de modificar muchos de estos materiales con secuencias y factores bioactivos. A la inversa, los polímeros naturales derivados de proteínas de la matriz extracelular ofrecen la ventaja de la señalización biológica, pero pueden ser antigénicas y sus propiedades físicas son más difíciles de modular que en los polímeros sintéticos. La biodegradación es una característica crucial en los implantes biomédicos y su modulación ha sido ampliamente estudiada. Presentar un tiempo de degradación sincronizado con la

formación de los nuevos tejidos es un objetivo altamente perseguido. La tasa de degradación está influenciada por muchas características de los polímeros, incluida la morfología y la orientación de la cadena, la cristalinidad inicial, el peso molecular, la presencia de monómeros y oligómeros residuales y la pureza. Existen varios métodos para cambiar y controlar la velocidad de degradación de los polímeros sintéticos y naturales, como la copolimerización, la mezcla, los aditivos y la irradiación, pero estos métodos presentan diferentes inconvenientes, como el cambio en las propiedades mecánicas, la pobre biocompatibilidad y el retraso en la bioabsorción. Debido a estos inconvenientes, puede ser útil producir biomateriales que sean sensibles a ciertos enzimas que se valgan de la respuesta inflamatoria que se produce por la propia lesión o introducción del implante.

Los avances en ingeniería genética han facilitado la producción de proteínas modificadas que abarcan una amplia gama de propiedades y funcionalidades, como la adhesión celular, la señalización celular, la elasticidad y la biodegradabilidad. Actualmente, los recombinamers de tipo elastina (ELR) muestran propiedades sobresalientes para su aplicación en regeneración de tejidos. Los ELR son polipéptidos artificiales con un alto contenido en elastina que los convirtió en materiales capaces de imitar la ECM. El más comúnmente utilizado es el penta-péptido VPGXG, donde

X representa cualquier aminoácido excepto la L-prolina. Como ya se ha mencionado se sintetizan mediante tecnología recombinante que permite no sólo un control absoluto sobre su composición de aminoácidos y funcionalidades de la proteína final, pudiendo incluir epítopos específicos, tales como secuencias de adhesión, dianas de degradación, péptidos antimicrobianos, etc., sino también de propiedades como su peso molecular. Tienen interesantes propiedades mecánicas que van desde los elastómeros ideales hasta el plástico que permiten, por lo tanto, un esfuerzo mecánico repetitivo y confieren resistencia mecánica a través de un mecanismo separado que soporta varias funciones del tejido. Por último, son extremadamente biocompatibles debido a su composición aminoácidica que implica la repetición de secuencias basadas en las secuencias encontradas en la elastina de los mamíferos.

En el primer estudio de esta tesis se emplearon dos ELRs con una bioactividad complementaria (CC-RGD y CCC-REDV), las cisteínas están incluidas en la región amino terminal, para desarrollar un sistema 2D en el que la adhesión celular selectiva está controlada espacialmente para su posterior aplicación en la tecnología de biosensores como dispositivos de diagnóstico o en la aplicación de ingeniería de tejidos y medicina regenerativa. Específicamente, en este estudio, las superficies modelo de oro se funcionalizaron con diferentes porcentajes de dos ELRs (CC-RGD

y CCC-REDV), lo que demuestra que una composición óptima de 75% CCC-REDV y 25% CC-RGD conduce a una adhesión selectiva de células endoteliales en un sistema de co-cultivo. Luego, una vez que se funcionalizó toda la superficie con 100% de CC-RGD, se limpiaron áreas específicas mediante ablación con láser sin interferir en las propiedades topográficas, hidrófobas y mecánicas de las superficies. Estas áreas se funcionalizaron con un 75% de CCC-REDV y un 25% de CC-RGD y después de los estudios in vitro, se observó una distribución bien definida de células HUVEC y HFF1, es decir, un control espacial selectivo sobre la adhesión de las células HUVEC. Estos hallazgos sugieren un enfoque innovador para la generación de biosensores y / o andamios que requieren la organización espacial y temporal de las células.

A continuación, el segundo estudio de esta tesis consiste en la mejora de la actividad angiogénica de los hidrogeles basados en ELR cuando se pega químicamente un pequeño péptido llamado QK que mima el factor de acrecimiento VEGF. Además de las secuencias de adhesión celular (RGD y REDV), un ELR utilizado en este trabajo presenta un sitio proteolítico (VGVAPG) que pertenece a la enzima elastasa. La actividad angiogénica de estos hidrogeles se estudió *in vitro*, demostrando que no altera las propiedades mecánicas y morfológicas de los ELR, sino la actividad biológica, como la adhesión y proliferación celular. Cuando se inyectó *in*

vivo, se observó una mejor formación de microvasculatura que facilita la perfusión y la conexión con el tejido circundante. Estos resultados mostraron que los hidrogeles basados en ELR-QK son construcciones diseñadas óptimas con una potencial actividad angiogénica que podría emplearse en ingeniería de tejidos y medicina regenerativa para el tratamiento de enfermedades cardiovasculares.

El tercer estudio de esta tesis tiene como objetivo lo de controlar en tiempo y espacio la infiltración célular y la biodegradación en un sistema estructurado tridimensional (3D). Los ELR empleados en este trabajo, además de una secuencia de adhesión celular universal (RGD), contienen sitios proteolíticos que se degradan en respuesta al activador de plasminógeno uroquinasa (uPA) con diferente tasa de degradación (rápida y lenta). Aprovechando estas características, en este estudio se desarrolló un sistema 3D que consiste en discos de hidrogeles de tres capas, con una capa interna que contiene el componente de degradación rápida y las capas externas que contienen el ELR de degradación lenta. Esos discos se han implantado por vía subcutánea en ratones y su evolución se siguió a lo largo del tiempo. Como resultado del diseño y de la secuencia de infiltración celular programada, la capa interna se colonizó primero siguiendo un patrón de adentro hacia afuera. Estos resultados demostraron que el sistema basado en 3D-ELR podría aplicarse como un sustituto

tisular para la aplicación biomédica que requiere una regeneración controlada y vascularización a lo largo del tiempo.

En resumen, los estudios mostrados en esta Tesis brindan nuevos conocimientos sobre los hidrogeles basados en ELR que se utilizarán en ingeniería de tejidos y medicina regenerativa. Específicamente, describe la importancia de la inclusión de varios epítopos en el esqueleto de la ELR, como por ejemplo secuencias de adhesión universales y específicas que influyen en el comportamiento celular. Además, el hidrogel basado en ELRs presenta mejores propiedades angiogénicas cuando un péptido mimético de VEGF llamado QK está pegado químicamente. Por otro lado, los ELRs con una tasa de degradación controlada podrían estar implicados en la construcción de estructuras biológicas complejas para su empleo en la regeneración de tejidos.

INTRODUCTION

1. Introduction

1.1 Biomaterials for tissue engineering

Nowadays, there is a significant demand for advanced biomaterials able to replace or regenerate the biological functions of the tissues or organs that have been damaged through diseases or trauma. [1] The definition of the ideal biomaterial has changed considerably during the past 50 years and, in fact, it changes depending on the area of application. [2] The basic role of a biomaterial in tissue regeneration is to provide support and scaffolding for cell growth namely there must be a combination of cells, biological matrices, signals and biophysical cues mimicking in this way the extracellular matrix (ECM). [3][4][5] Biomaterials used in tissue engineering are divided into three groups such as bioceramics materials, polymer-based materials and protein-based materials.

In most cases, bioceramic materials (alumina, zirconia, bioactive glasses, calcium phosphates, and glass-ceramics) have been used for hard tissue regeneration due to their low elasticity but they are characterized by optimal mechanical stiffness and biocompatibility. However, their clinical applications for tissue engineering has been limited because of their brittleness, difficulty of shaping for implantation and difficulties to control their degradation rate. [6]

Polymer-based materials have been developed both from natural and synthetic resources. Regarding synthetic polymers such as polystyrene, poly-l-lactic acid (PLLA), polyglycolic acid (PGA) and poly-dl-lactic-co-glycolic acid (PLGA) are attractive biomaterials for tissue engineering scaffold applications as they can be fabricated with a tailored architecture. However, these polymers are hydrophobic which can be disadvantageous in tissue engineering application due to poor wetting and lack of cellular attachment and interaction. [7][8][9]

Natural materials such as silk and chitosan or polymers extracted from other biological systems or compounds of the native ECM (collagen, elastin and glycosaminoglycans) have been recognized as an attractive choice for tissue engineering application. Natural materials are biocompatible and mechanical and biological properties consistent with *in vivo* features but the limitations are short supply, expensive, batch-to-batch variation, and are susceptible to cross-contamination. [10]

A number of groups have attempted to combine ceramics with polymer-based scaffolds while others have combined synthetic polymers with natural polymers in order to enhance their biological capacity. While composite scaffolds such as these have shown some promise, each consists of at least one phase which is not found naturally in the body and they all have associated problems with biocompatibility, biodegradability or both.

[11][12]

Protein-based materials have excellent advantages such as control over their structure, high biocompatibility and ease of functionalization making them optimal candidates for biomedical application. Extensive studies, over the last two decades, have elucidated precise structure–function relationships for many proteins; an excellent example of this is elastin, a protein that provide elasticity to a variety of tissues.

1.2 Elastin as a biomaterial

In recent years, elastin based-materials are increasly investigated as promising advanced biomaterials for their use in the field of tissue engineering. This interest is fuelled by the remarkable properties of this structural protein, such as elasticity, self-assembly, long-term stability, and biological activity. [13][14]

Elastin is an extracellular matrix (ECM) protein that provide elasticity to connective tissues or organs, especially where elasticity and resilience is of major importance as for example in blood vessels, elastic ligaments, in lung and skin. Tropoelastin is the main precursor of elastin and is amongst the most elastic of all known natural proteins, with an ability to stretch eight times its resting molecular length and recoil without damage to the protein. In humans, there is only one tropoelastin gene and its expression occurs before birth and in the first few years of life when the cells of elastic

tissues produce the elastin required for the body to develop. The elastin formation process consists in the association of many tropoelastin molecules that are subsequently cross-linked or connected. [15][16] In the event of damage to the elastin such as injury, burns, sun damage or, simply as a result of aging due to the low level of elastin production in adult aging, the damage cannot be efficiently repaired and the skin gradually loses its elasticity. Researchers have for many years pursued elastin-based materials which may be useful in the repair or regeneration of elastic tissues. Such materials have evolved from fragments of elastin isolated from animal tissue through to synthetic proteins which mimic the elastic nature of tropoelastin.

Elastin can be applied as a biomaterial in various forms such as insoluble elastin fibres, hydrolysed soluble elastin, recombinant tropoelastin (fragments), repeats of synthetic peptide sequences and as block copolymers of elastin, possibly in combination with other (bio) polymers. [17]

There are different forms of elastin applied as biomaterials such as elastin in autografts, allografts and xenografts; decellularized tissue and hydrolysed elastin. Recent improvements in recombinant DNA technology allows to design and manufacture materials that lead to the production of repeated elastin-like sequences reaching complex

composition. However, this method is the most efficacious as is characterized by several advantages compared to the techniques mentioned above. [18] There are other biomaterials combined with elastin such as silk elastin-like recombinamers (SELRs) that include repetition of silk domain. They have been deeply studied as scaffolds for tissue engineering as well as for the generation of nanoparticle system for application in drug delivery. [19]

1.3. Elastin-like recombinamers (ELRs)

Elastin-like recombinamers (ELRs) are one of the most widely studied protein-derived materials. The more conventional terminology elastin-like polymers (ELPs), which include those first chemically synthesized materials, was replaced by elastin-like recombinamers (ELRs) due to their recombinant nature. [20]

ELRs are based on the repetitive of the most common pentapeptide (VPGXG) n, where X stands for any amino acid except proline, and n is the number of repetitions. [21]

One particular property of the ELRs is their thermally responsiveness namely are characterized by a transition temperature (*T*t). They undergo a reversible phase transition from a soluble to an insoluble state upon increasing or lowering the temperature above a specific threshold. Below a given “critical” temperature, the polymer chains remain relatively

extended and hydrated mainly by hydrophobic hydration and thus are soluble in aqueous solution. This hydration around its hydrophobic moiety is characterized by the existence of ordered caged-like, clathrate water structures surrounding the moieties of the polymer and stabilized by hydrogen bonding among them. When the temperature increase, the polymer chain hydrophobically folds and aggregates to other polymer chains by formation of intra- and inter-chain hydrophobic contacts. In this state, the polymer adopts a dynamic, regular, non-random structure, called β-spiral, formed by concatenation of adjacent type II β-turns and stabilized by intra-spiral, inter-turn and inter-spiral hydrophobic contacts. This is the product of the ITT in which the folded and associated state is maintained by loss of the ordered water structures of hydrophobic hydration. The T_t of the ELRs could be extensively manipulated by the amino acid at the Xaa position and resulted in a dependency on e.g. temperature, pH, and electrochemical potential. [22][23]

Using protein engineering, many different parameters of elastin-like recombinamers can be controlled: including amino acid sequence, peptide length, namely the length and number of the blocks.

The possibility to incorporate specific sequences that have cell biological effects lead to the obtainment of biomaterials with advanced functionalities (stimulating characteristics of ECM) in a simple way which

can be used for specific applications such as enhancement interaction with the cells like adhesion, proliferation, migration and differentiation. [24] For example, the fusion of the tripeptide Arginine-Glycine-Aspartic (RGD), present in fibronectin and in other extracellular matrix proteins, would enhance cell adhesion to ELRs in multiple cell types, preferably via integrins of the type α5β1 and α5β3. [25] Another example is REDV sequence, (arginine–glutamic acid–aspartic acid–valine), which is a specific adhesive sequence for endothelial cells found in the alternatively-spliced IIICS-5 domain of human plasma fibronectin. This motif mediates cell adhesion and spreading via α4β1 integrin in endothelial cells, but not in smooth muscle cells or fibroblasts.[26]

Similarly, the inclusion of enzymatic degradation sequences, such as those recognized by elastase, which contain the L-Valine-Glycine-L-Valine-L-Alanine-L-Proline-Glycine hexapeptide (VGVAPG) would improve the biodegradability of ELRs, which should happen in parallel to the therapeutic process, such as, for example, tissue regeneration.[21] New biomaterials that provide a combination of protease sensitiveness as well as bioactive epitopes, are of particular interests in tissue repair process. Material degradation rate needs to fit the envisioned application allowing the desired ingrowth of host cells and ECM deposition. [27] ELRs are slowly degraded in vivo, and their rate of degradation could be tuned, as it

has already find out, by the explicit incorporation of specific protease recognition sites within their amino acidic sequence. In particular, ELRs with specific proteolytic sites that belong to metalloproteasis (MMP) or to plasminogen activator system have been produced with an important feature regarding their degradation rate.
Lastly, ELRs for more specific applications have been produced namely growth factors have been fused, such as bone-2 morphogenetic protein ("bone morphogenetic protein-2", BMP-2), which has demonstrated its capacity to promote the regeneration of damaged bone tissue, thus conferring osteoinductive properties to ELRs. [28]

1.4. ELR-based hydrogels and their application in tissue engineering

The first ELP-based hydrogels were described by Urry et al., a poly-VPGVG ELP, which was chemically crosslinked using γ-radiation to provide a stable matrix. Eleven tests, including mutagenicity, cytotoxicity, antigenicity, sensitization, pyrogenicity and haemolysis, amongst others, were performed to prove the biocompatibility of this family of hydrogels. [29] Since then, numerous other crosslinking methods have been reported for the formation of physical or chemical gels which differs for the forces that maintain the structure. Thus, physical hydrogels, are stabilized by weak forces such as molecular entanglements, H-bonding hydrophobic interactions or coulomb forces. Chemical crosslinking produces hydrogels

with enhanced mechanical properties and, although different options are available to chemically crosslink ELRs, almost all of them involve the amino group of the lateral chain of lysine residues. Amongst the crosslinking options, the use of chemicals is the most extended option. [30] Recently, G. de Torre et al., have developed a rapid, tuneable, biocompatible and cell-friendly crosslinking system based on a 1, 3-dipolar cycloaddition reaction, a clear example of "click chemistry". [31] [32]''Click chemistry'' was introduced by Kolb et al. in 2001, and specifically the Huisgen 1,3-dipolar cycloadition of azides and alkynes, has been shown to be stereospecific, easy to perform in aqueous solution under mild conditions and provides high reaction yields. They are stable within biological systems, and have limited side product formation. As a result of these advantages, this reaction has been widely employed in drug discovery, bioconjugation with proteins and DNA, cell surface labelling and surface modifications with ELRs, among other molecules. As an improvement to conventional ''click chemistry'', the use of activated alkyne groups, such as cyclooctyne derivatives, has allowed these reactions to be carried out without the need of a catalyst. This reaction requires the presence of azides and alkynes, which react orthogonally to form an irreversible covalent bond. [33][34][35] This rapid and biocompatible approach allows the homogeneous

encapsulation of different cell types and has proved its cytocompatibility with several cell lines and in different applications. ELR-based hydrogels have proved to be an excellent platform for cell growth and proliferation for their application in wound healing, cartilage repair, liver tissue engineering, cardiovascular applications or ocular tissue engineering. [36] These "tunable" hydrogels have proven to be extremely useful in biomedical and pharmaceutical applications due to their high water content and rubbery nature, which is similar to that of natural tissue. The structural complexity of ELRs with specific mechanical, chemical, and biological properties allows us to design specific features that make them useful for a wide variety of applications, including skin substitutes, vascular grafts, heart valves, and elastic cartilage. [37][38]

1.5 Vascularization in tissue engineering constructs

In past decades a variety of biomaterials have been deeply studied to generate engineered templates for consequent application in tissue engineering but they still present a big challenge as for example vascularization before their employement in clinical application. [39] The formation of a mature vascular network in a construct supply an adequate oxygen and nutrient diffusion ensuring a successful integration into host tissue with consequent regeneration of a mature functional tissue. Primarily, one of the most important feature of the biological constructs,

applied in tissue engineering, is their architecture and design that has a profound effect on the rate of vascularization. Specifically, pore size and their interconnectivity are the most important characteristics that determine the development of blood vessels into a construct as they influence cellular migration. [40]

Currently, in literature classical vascularization approaches have been investigated such as for example the use of angiogenic growth factors, *in vitro* and *in vivo* prevascularization.

It is well known that VEGF, bFGF, FGF 2, Ang 1 and 2, PDGF β and TGF β are the main growth factors that have a pivotal role in the formation of blood vessels stimulating the mobilization, recruitment and proliferation of different cell types that are involved in angiogenesis. Several studies reported that angiogenic growth factors such as VEGF-A, FGF-2 and PDGF β have been incorporated into the constructs or onto the surfaces of degrading beads for graduating release after implantation. However, these so-called angiogenic approaches face the problem that the growth factors have very short half-life periods in the body to sustain biological activities. Thus, it is highly necessary to contrive the dosage of growth factors for enhancing the in vivo efficacy. [41]

In vitro pre-vascularization is an alternative approach that aims to generate preformed microvascular networks inside the engineered construct prior

to their implantation. After implantation, these networks can then be rapidly perfused with blood by inosculation with the surrounding host microvasculature or by surgical anastomosis of feeding and draining blood vessels. The current prevascularization concepts are divided into two groups such as *in vitro* approaches which includes cell seeding, generation of spheroids or cell sheet technology or in situ approaches that includes angiogenic ingrowth, flap technique and AV-loop technique. These strategies contributes to the obtaining of a functional network vasculature establishing a rapid blood supply after implantation. [42]

Another approach that is getting more attention is *in vivo* pre-vascularization. This approach consists in an instantaneous perfusion of a construct after implantation decreasing dramatically the time that is needed to vascularize the implant. Namely it is characterized by two stages, firstly, a tissue-engineered construct is implanted into a region with an artery suitable for microsurgical transfer and afterwards the construct is harvested toghether with the microvascular network and the supplying artery and then implanted at the defect site. At this site, the vascular axis is connected to the local vasculature using microsurgical vascular-anastomosis techniques, which results in instantaneous perfusion of the entire construct. [43] The advantage of this technique is that after implantation at the final site, the construct becomes immediately perfused

by surgical anastomosis. However, its drawbacks are that two separate surgeries (one to implant the construct at the vascularization site and one to implant the construct at the final defect site) are necessary. In addition, a vascular axis has to be removed from the initial implantation site and, furthermore, cells might have to be reseeded before implantation at the final defect site because nutrient limitations are still likely during the vascularization period at the initial implantation site.[44] Despite impressive progress in the field, this will require additional preclinical and clinical analyses to further optimize the efficiency and safety of the different concepts. Moreover, it will be necessary to identify those approaches, which are best suited for individual therapeutic interventions, while also being cost effective and marketable. These ambitious goals can only be achieved by the close collaboration of scientists, clinicians, industrial partners and regulatory bodies. [45] [46]

1.6. Biofunctionalization of surfaces with ELRs for biomedical applications.

Surface engineering is an important tool for understanding cell– surface interactions for diverse specific biological applications. Multiple approaches involving physical and chemical modifications, such as coatings and grafts or the introduction of small biological ligands (peptides or proteins), have been developed in the surface engineering of

biomaterials. [47] These approaches allow surfaces to be functionalized with fouling-anti fouling features, specific groups for cell–material interactions, responsive behavior (stimuli or environmentally sensitive), or with micro- and nano-patterns. Surface bio-functionalization with cell-adhesion molecules has attracted significant interest as regards the design of surfaces with tailored properties, such as wettability, adhesion, and biocompatibility, which are essential for various biological evaluation such as controlling cellular response. [48] ELRs are characterized by several advantages that can be used for the development of responsive surfaces. For instance, genetic engineering allows them to be designed with extraordinary control of the sequence and with desirable properties, which means that in addition to their thermo-responsive behavior they can also respond to other stimuli such as pH, light, or ionic strength, amongst others. On the other hand, biosynthesis enables precise control of the reactive sites on the polypeptide chain for use in surface grafting. For example, the nanometric control of their position leads to a tremendous potential for self-assembly and other functionalities displayed by these systems. [49] There are several examples of surfaces functionalized with ELRs as for example Chilkoti's group has created what they have called ''thermodynamically reversible addressing of proteins'' (TRAP). This allows the reversible, spatio-temporal modulation of protein binding at a

solid-liquid interface and can be applied in different systems for bio-analytical devices. [50] Other techniques used for ELRs include layer-by-layer deposition of alternating ELR-polyelectrolytes, which is a simple technique to generate bioactive surfaces. These ultra-thin nanoscale coatings promote cell adhesion and proliferation and the results show that the thickness and mechanical integrity of the multilayer assembly modulates the cell response. Costa et al., for example, have developed thermo-responsive thin coatings using electrostatic self-assembly (ESA). A recombinant ELR containing the cell attachment sequence RGD has been deposited onto chitosan and has been found to show enhanced cell adhesion in comparison with the original chitosan monolayers or glass substrates. These examples open up the field of polymeric coatings that include specific biofunctional responses. [51]

For example, the possibility to change the ELR amino acid composition lead to the production of surfaces which can be used as cellular biosensors or to develop tissue engineering constructs that require an organized structure with a specific placement of cells obtaining in this way a spatial cellular adhesion. This technique consists in creating specific areas in an artificial substrate where cells can be adhered or have resistant areas (non-adhesive zones) or even more have selective areas where only specific cells can adhere. Spatial arrangement of cells is a new tool for cell biology

that allows an improved control over cell behaviour and has a wide application in fundamental cell biology and biomedical engineering. [52] [53] In such a way, for the attachment of the cells on a solid substrate is necessary an interaction with specific surface-bound ligands that in vivo are allowed by the extracellular matrix (ECM): proteins such as collagen, fibronectin, elastin and laminin. The integrins are able to link the cell cytoskeleton to a material surface via these proteins present on the artificial substrate. [54]

ELRs have grown in popularity in the field of protein-inspired biomimetic materials. In this sense, these materials are playing an increasingly important role in a diverse range of applications such as drug delivery, tissue engineering, biosensors, and a wide variety of “smart” systems. [55]

MATERIALS AND METHODS

2. Materials and Methods

2.1 Materials

The reagents used in this thesis are reported in Table 1.

Table 1. Reagents used in this thesis.

Reactive and abbreviation	Brand
Chloridric acid	Fisher Scientific
Ethylenediaminetetraacetic acid (EDTA)	Sigma-Aldrich
Acrylamide/Bis-acrylamide	Amresco
AEBSF	Apollo Scientific
Agar	BD
Agarose Seakem	Cambrex
Ultrapure water (MilliQ)	Millipore
Antifoam 204	Sigma-Aldrich
Ampicillin	Apollo Scientific
Bromophenol Blue	Sigma-Aldrich
Copper cloride	Sigma-Aldrich
Sodium chloride (NaCl)	Fisher Scientific
Dimethyl sulfoxide (DMSO)	Sigma-Aldrich
Sodium dodecyl sulfate (SDS)	Sigma-Aldrich
E-64	Apollo Scientific

Restriction enzymes (*Sap*I, *Ear*I, *Eco*RI, *Dpn*I) y other enzymes (T4 DNA ligasa, FastAP, SAP)	Thermo Scientific
Ethanol	Panreac
Phenyl methyl sulfonyl fluoride (PMSF)	Apollo Scientific
Gentamicin/Amphotericin	Gibco
Glicerol	Fisher Scientific
Glycine	Sigma-Aldrich
Glucose	Panreac
Hematoxylin-eosin	Sigma-Aldrich
Sodium hydroxide (NaOH)	Fisher Scientific
Plasmid purification Kit "NucleoSpin Plasmid"	Macherey-Nagel
DNA extraction kit in agarose gels "PureLink Quick Gel Extraction"	Invitrogen
Leupeptine	Apollo Scientific
DNA marker 1kb Plus Ladder	Invitrogen
Protein marker "Pierce Unstained"	Thermo Scientific
Auto-induction culture medium "Terrific" (TB)	Formedium
Bacterial Culture medium (Luria Bertani, LB)	Conda
Cell culture medium (DMEM 1g/L glucosa, Medium 200)	Gibco

Paraffin	Sigma-Aldrich
Paraformaaldehyde	Sigma-Aldrich
Penicillin/Streptomycin	Gibco
Pepstatin A	Apollo Scientific
Ammonium persulfate	Sigma-Aldrich
Bovine serum albumin (FBS)	Gibco
Ammonium sulphate	Fisher Scientific
Growth supplement with low serum (LSGS)	Gibco
Phosfate buffered saline (PBS)	Gibco
Tetramethylethylenediamine (TEMED)	Sigma-Aldrich
DNA staining "SimplySafe"	Eurx
Trypsin/EDTA 0.05%	Gibco
Tris (hydroxymethyl) aminomethane (Tris)	Sigma-Aldrich
Triton X-100	Sigma-Aldrich
Trypan blue	Invitrogen
Xylol	Sigma-Aldrich
β-Mercaptoethanol	Sigma-Aldrich

2.1.1 Other Materials

All disposable plastic material (pipette tips, pipettes, centrifuge tubes, microcentrifuge tubes, etc.) were washed and rinsed several times with

distilled water and sterilized on an autoclave (Selecta Autotester E-75, 20 min 120 °C 1 atmosphere). The glassware (beakers, flasks, pipettes, etc.) was suitably washed and sterilized in the same way.

2.1.2 Cell lines

- Human foreskin fibroblasts (HFF1, ATCC® SCRC-1041™). Cells between 6 and 14 passages were used.
- Human endothelial primary cells of the umbilical cord vein (HUVECs, ATCC CRL-1730). Passages between 2 and 6 were used.

2.1.3 Animal model

- Swiss C57 mice (male) provided by the University of Valladolid animal facility.

2.1.4 Elastin like recombinamers (ELRs)

The amino acid sequence of the ELRs employed in this thesis are reported in Table 2.

Table 2. ELRs used in this work, obtained in the laboratories of G.I.R. BIOFORGE of the University of Valladolid.

ELR	Amino acid sequences	MW (kDa)
CC-RGD	CC((VPGIG)$_2$(VPGKG)(VPGIG)2EEQIGHIPRGDDYHLYP (VPGIG)$_2$(VPGKG)(VPGIG)$_2$(VGVAPG)$_3$)$_{10}$	39
CCC-REDV	CCC((VPGIG)2(VPGKG)(VPGIG)2EEQIGHIPREDVDYHLYP(VPGIG)2(VPGKG)(VPGIG)2)10	59

CCC-EI	CCC[(VPGVG)$_2$VPGEG(VPGVG)2]$_{10}$(VGIPG)$_{60}$V	47
HRGD	MGSSHHHHHHSSGLVPRGSHMESLLP-{[(VPGIG)$_2$-(VPGKG)-(VPGIG)$_2$]$_2$-AVTG**RGD**SPASS-[(VPGIG)$_2$-(VPGKG)-(VPGIG)$_2$]$_2$}$_6$V	61
REDV	MESLLP{(VPGIG)2VPGKG(VPGIG)2EEIQIGHIPREDVDYHLYP (VPGIG)2VPGKG(VPGIG)2(VGVAPG)3}10	80
GTAR	MESLLPV (((VPGIG)$_2$ VPGKG (VPGIG)$_2$)$_2$YAVTG GTAR SASPASSA ((VPGIG)$_2$ VPGKG (VPGIG)$_2$)$_2$V)$_4$	41
DRIR	MESLLPV (((VPGIG)$_2$ VPGKG (VPGIG)$_2$)$_2$YAVTG DRIR SASPASSA ((VPGIG)$_2$ VPGKG (VPGIG)$_2$)$_2$V)$_4$	41
VKV	MESLLPV VPGVG [VPGKG(VPGVG)5]23 VPGKG VPGVG VPGVG VPGVG VPGVG	60

2.2. Methods

2.2.1 Synthesis of the ELRs

All the genes encoding the ELRs used in this work were obtained by genetic engineering techniques described in literature. [56] The GTAR-ELR and DRIR-ELR have been synthetized esclusively for the development of this thesis. Briefly, the genes encoding the monomer peptides of the ELRs or the bioactive sequences were synthesized by NZYTech Company, Portugal. They were subsequently cloned in the plasmid pDriveAll, which had been mutated deleting the endogenous restriction site for *SapI* and adapting the poly-linker of pDm to the seamless iterative-recursive to obtain multimers. [24] The restriction

enzymes used for cloning are *EarI* and *SapI* as they have endonuclease activity on a contiguous sequence to the recognition. Once the final gene construct is obtained, it is extracted from the cloning plasmid and a subcloning is carried out in the expression plasmid pET7RARE, resulting from different modifications on the commercial vector pET-25b (+). Afterwards, this plasmid is used to transform expression strains of *E.Coli,* in particular BL21 Star (DE3) strain (Novagen), which are cultured in a 15 L bioreactor (Applikon Biotechnology) under controlled conditions of pH, temperature, agitation and O_2 concentration. Lastely, after the mechanical breakdown of the cell wall and the bacterial membrane by disruption (model TS 0.75KW, Constant Systems), the recombinamers are purified taking advantage of their thermosensitive characteristic through successive cooling and heating cycles which is called, "Inverse Transition Cycling", ITC, followed by centrifugation at each step. Thus, finally, a pure product is obtained that is dialysed against MQ water and subsequently lyophilized (FreeZone 1, LABCONCO) for a better preservation of the product.

2.2.2 Physicochemical characterization of the ELRs

2.2.2.1 Sodium Dodecyl Sulphate - PolyAcrylamide Gel Electrophoresis (SDS PAGE Electrophoresis)

Polyacrylamide gel electrophoresis with SDS is a technique used to separate molecules basing on their molecular weight (Mw). The SDS molecules are negatively charged able to bind to proteins providing a uniform charge-to-mass ratio. By binding to proteins, the detergent destroys to secondary, tertiary and/or quaternary structure denaturating them and turning them into negatively charged linear polypeptide chains. In this work, the vertical electrophoresis system "MiniVE" of Hoefer (Amersham Pharmacia Biotec) was used. The resulting polyacrylamide gels were stained with copper chloride or commassie brilliant blue. Copper staining is a negative stain, which does not stain the proteins, but the copper interacts electrostatically with the SDS that contains the gel itself, leaving the areas that contain unstained proteins, being observed, therefore, as dark bands. On the other hand, the Coomassie dye binds to proteins through ionic interactions between sulfonic acid groups and positive protein amine groups through Van der Waals attractions. The images of the gels in both cases were taken with the Gel Logic 100 Imaging System (Eastman Kodak) and analyzed with the Kodak 1D Image Analysis program (Eastman Kodak).

2.2.2.2 Matrix-assisted laser desorption/ionization-Time-of-flight (MALDI TOF)

Mass spectrometry of the type "Matrix-assisted laser desorption / ionization-Time-of-flight" (MALDI-TOF) allows to know exactly the Mw, so it can be considered complementary to the SDS-PAGE technique. This technique has been carried out in the Laboratory of Instrumental Techniques (LTI) of the University of Valladolid (UVa) in the MALDI-TOF Voyager STR (Applied Biosystems).

2.2.2.3 High-Performance Liquid Chromatography (HPLC)

The analysis of ELR samples previously hydrolyzed by "High-Performance Liquid Chromatography" (HPLC) allows to know the amino acid composition of the ELRs. This method was carried out in the LTI of the UVa with the Waters 600 gradient HPLC equipment coupled to a Waters 2487 UV detector (Waters).

2.2.2.4 Differential scanning calorimetry (DSC)

Differential scanning calorimetry (DSC) is a thermoanalytical technique, where sample and reference are subjected to the same temperature program and the amount of heat needed to fulfill such program is monitored and compared to that of the reference.
In our case, this technique was accomplished to study the inverse transition temperature of ELRs when temperature changes were applied. For this work, Mettler Toledo 822e equipment was used with refrigeration using

liquid nitrogen. Samples were dissolved in PBS at a concentration of 50 mg /mL. Afterwards, 20µL was loaded into a standard aluminium pan and sealed hermetically. As reference, 20µL of the solvent, in this case PBS, was placed in another pan. Both temperature and enthalpy were calibrated using a standard sample of indium. The experiments consisted of a first isothermal stage at 0 ° C for 5 minutes, followed by a heating step, from 0 to 60 ° C, at a rate of 5 ° C / min.

2.2.2.5 Nuclear magnetic resonance (^{1}H-NMR)

Nuclear magnetic resonance spectroscopy (^{1}H-NMR) studies the behavior of certain atomic nuclei (those with non-zero nuclear spin) in the presence of an external magnetic field. The applied magnetic field produces a split of the degenerated energy levels of the nuclear spin, so that transitions between them can be induced because of absorption of the adequate electromagnetic radiation. The arrangement of energy levels is a property of both the nuclei of a molecule and their electronic environment and interactions between them. Thus, the intensity, shape and position of the signals in the spectrum of a given nucleus are closely related to their molecule structure, and the whole NMR spectrum of a molecule can be considered as a fingerprint of it. In this work, NMR analysis was performed routinely with each batch of recombinamer to verify the purity of the material. The equipment used was NMR 500 (Agilent

Technologies), belonging to "Laboratorio de Técnicas Instrumentales (University of Valladolid)". The peak areas corresponding to three kind of hydrogen, namely -NH2, -CH3 and -CH- of chain, were electronically integrated and compared to the calculated theorical values.

2.2.2.6 Fourier transform infrared spectroscopy (FTIR)

Fourier Transform Infrared is the spectroscopy that deals with the infrared region of the electromagnetic spectrum. Infrared spectroscopy exploits the fact that molecules absorb specific frequencies that are characteristic of their structure. The infrared spectrum of a sample is recorded by passing a beam of infrared light through the sample. When the frequency of the IR is the same as the vibrational frequency of a bond, absorption occurs. Examination of the transmitted light reveals how much energy was absorbed at each frequency (or wavelength) revealing the presence of a certain chemical structure.

Fourier Transform Infrared (FTIR) spectroscopy was performed by attenuated total reflectance equipment (ATR-FTIR) using a Bruker Tensor27. For baseline correction and data acquisition, 256 scans were performed with a 4 cm^{-1} resolution. Briefly, freeze-dried sample is placed in the ATR equipment and compressed against the ATR crystal, until a good signal-to-noise ratio was achieved. Subsequently acquisition scans

were performed. Spectral calculations were performed by the OPUS (version 4.2) software (MATTSON INSTRUMENT, INC.).

2.2.3 Contact angle

This technique quantifies the wettability of a solid surface calculates by Young equation. The measurements were performed using the sessile drop method with Data Physics OCA20 system instrument where the images are recorded using CCD video camera. The needle is located in close proximity to the sample, so that the tip of the needle is embedded in the water drop. All the measurement were performed at 37°C.

2.2.4 X-ray photoelectron spectroscopy (XPS)

X-ray photoelectron spectroscopy (XPS) is a surface analysis technique that provide quantitative and chemical state information from the surface of the material being studied. This technique has been carried out in the Servicio de Espectroscopia UPS-XPS y Espectrometria SNMS of the University of Malaga using a Physical Electronics (PHI) 5500 spectrometer equipped with a monochromatic X-ray source (Al Kaline with an energy of 1486.6 eV and 350 W).

2.2.5 Quartz crystal microbalance with dissipation (QCM-D)

Quartz crystal microbalance with dissipation (Q-CMD) is a real-time nanoscale technique for analysing surface phenomena including thin film formation, interactions and reactions. In our case, this technique was

accomplished to study the physical parameters of the thin film of ELRs adsorbed on the gold surface. For this work a Q-Sense Explorer System equipment was used. The three samples were dissolved in PBS at a concentration of 5mg/mL. Afterwards, using a peristaltic pump (50µL/min) the solutions have been passed on an AT-cut 5 MHz quartz crystal coated with gold sensors for about 20 minutes. The frequency and dissipation changes were recorded up to 13^{th} overtone number. All data were analysed with a software provided from Biolin Scientific called Q-sense Dfind.

2.2.6 Atomic force microscopy (AFM)

Atomic force microscopy (AFM) is a type of high-resolution scanning probe microscope which can be used to form an image of the three dimensional shape of a sample surface at a high resolution. This is achieved by raster scanning the position of the sample with respect to the tip and recording the height of the probe that corresponds to a constant probe-sample interaction. This technique has been carried out in the Unidad de Microscopia de Fuerza Atomica y µRamand of the University of Malaga by a Nanoscope IV controller system (Digital Instruments) in tapping mode using V-shaped Si3N4 tips (OMCL TR400PSA, Olympus, Japan).

2.2.7 Laser ablation

Laser ablation process consist on removing material from a solid surface when irradiated by a laser beam. Usually, laser ablation refers to removing material with a pulsed laser, but it is possible to ablate material with a continuous wave laser beam if the laser intensity is high enough. This technique has been carried out in Center of Omic Science, Reus (Barcelona) using a smart beam MALDI laser in a MALDI TOF/TOF UltrafleXtrem instrument from Bruker.

2.2.8 Scanning electron microscopy (SEM)

Scanning electron microscopy (SEM) was used to investigate the surface morphology of the first chapter of this thesis and the morphology of the ELR-based hydrogels. Micrographs were obtained by SEM (JEOL, JSM-820) in low vacuum mode at 3keV. Morphological details were evaluated quantitatively using the ZEN (Blue Edition, 2012) software package (Carl Zeiss Microscopy).

2.2.9 Chemical modification of the ELRs

Chemical modification of the ELRs (HRGD, REDV, GTAR, DRIR, and VKV) was carried out according to the procedure described in literature. [57] Summarizing, the ε-amino group at the lateral chain of the lysines of each ELR was modified, specifically an azide or a cyclooctyne group was added. These groups form a covalent bond with each other when mixing, allowing the formation of hydrogels via click chemistry under

physiological conditions (aqueous solvent) and without releasing any intermediate product with a cytotoxic activity.

2.2.10 Porosity studies

The porosity of the ELR-based hydrogels was studied following this equation: $\frac{((W1-W2)/d\ water)*100}{V\ hydrogel}$

where W1 and W2 are the weight of the swollen and lyophilized gels, respectively, d_{water} is the density of pure water and $V_{hydrogel}$ is the measured volume of the gel in the swollen state. Three replicas were measured for each condition.

2.2.11 Mechanical characterization of ELR-based hydrogels by rheological measurements

Rheology is a branch of physics that studies the ability of materials to flow and deform. Therefore, this technique can be used to study the viscoelastic behavior (viscous and elastic properties in response to a deformation) of the hydrogels, obtaining a measure of their rigidity / hardness. In this work, a controlled stress rheometer was used (AR200ex, TA Instruments), equipped with a Peltier plate to control the temperature. A geometry of parallel plates of 12 mm diameter was used and a gap of about 1000 between the plates was adjusted. The samples were previously formed using a specific mold as they are chemical hydrogels. All the

measurements were conducted at 37°C with a frequency sweep between 0.01- 50 Hz at a fixed strain.

2.2.12 *In vitro* studies

In this thesis, two types of cell lines were used.

Human umbilical vein endothelial cells (HUVEC) were cultured at 37°C and 5% CO_2 in MED200 culture medium supplemented with 100U/100mg/ mL penicillin/streptomycin and low serum growth supplement kit (LSGS) or EGM-2 medium supplemented with EGM-2 Single Quot Kit Suppl. & Growth Factor. HUVEC between passages 2 and 6 were used in all experiments.

Human foreskin fibroblasts (HFF1) were cultured in DMEM medium supplemented with 15% FBS and 100U/ 100mg/mL penicillin/streptomycin at 37°C and 10% CO2. Fibroblasts between passages 6 and 10 were used in all experiments. All cell types were cultured up to 80-90% confluence, at which time they were trypsinized for passage. In addition, media were changed every 2 days in all cases.

2.2.13 *In vivo* studies

For the *in vivo* studies Swiss C57 mice were used for all the experiments performed in this thesis.

2.2.13.1 Intramuscularly injection of ELR-based hydrogels

ELRs were dissolved in PBS at a concentration of 50 mg/mL and subsequently were mixed in an eppendorf with a final volume of 30 µL. Animals were anesthetized by inalation of isofluorano at 3%. A 20G syringe was used to inject the hydrogels intramuscularly in a hind limb zone. After each time point the animals were euthanized by cervical dislocation. All the procedures were carried out under sterile conditions in rooms with positive pressure and equipped with laminar flow hoods.

2.2.13.2 Subcutaneous implantation of ELR-based hydrogels

Subcutaneous implantation was made performing a small incision on the dorsal area forming a skin pocket using surgical scissors. Afterwards, the wound was closed using absorbable sutures. Animals were anesthetized using ketamine and diazepam at a concentration of 100mg/mL and 5mg/ml, respectively. Different time points were analysed and after each time point the samples were analysed by histology and immunohistochemistry.

2.2.14 Histological and immunohistochemistry analysis

Once extracted the samples, they were fixed with paraformaldehyde at 4% for at least 24 hours at 4°C. Subsequently, a dehydratation by immersion in ethanol solutions of increasing concentration was performed ending with a final step in xylol. Finally, all the samples were included in paraffin

for about six hours and were cut with a thickness of 6 µm using a rotatory microtome. Each slide was rehydrated by immersion in xylene and subsequently in decreasing concentrations of ethanol and finally in distilled water. Hematoxylin-eosin staining was carried out following methods described in the literature. [58] The images of the cuts were obtained with a light-field optical microscope (Nikon Eclipse 80i) equipped with a color camera (Nikon Digital Sight DS-Fi1).

Immunofluorescence staining were performed on micro-sections, previously deparaffinised and subsequently incubated for 1 hour in 10% donkey blocking serum. After several washing steps in PBS 1X, all the samples were incubated O/N at 4°C with a donkey polyclonal primary PECAM antibody at a concentration of 1µg/mL in 1% with the blocking serum. Subsequently, samples were washed three times with PBS 1X for five minutes each and incubated for 2 hours with goat anti-mouse fluorescein-conjugated secondary antibodies at a concentration of 1 µg/mL with 1.5% normal blocking serum.A vectashield HardSet Antifade Mounting Medium with DAPI (Vector Laboratories, USA) was used to stain the nuclei of the cells. All images were acquired with a fluorescent microscope.

2.2.15 Statistical analysis

The data presented in this thesis is presented as the mean ± standard deviation. The statistical analysis was carried out using a one-way variance analysis with the post-hoc Holm-Sidak test. A p-value less than 0.05 has been considered significant. The significant differences are shown as follows: (*) $p < 0.05$; (**) $p < 0.01$; (***) $p < 0.001$; $p > 0.05$ indicates absence of significant differences ("no significant differences", n.s.d).

3. References

[1] Khan, Ferdous, and Masaru Tanaka. "Designing smart biomaterials for tissue engineering." *International journal of molecular sciences* 19.1 (2018): 17.

[2] Huebsch, Nathaniel, and David J. Mooney. "Inspiration and application in the evolution of biomaterials." *Nature* 462.7272 (2009): 426.

[3] O'brien, Fergal J. "Biomaterials & scaffolds for tissue engineering." *Materials today* 14.3 (2011): 88-95.

[4] Rahmati, Maryam, et al. "Biomaterials for Regenerative Medicine: Historical Perspectives and Current Trends." *Cell Biology and Translational Medicine, Volume 4*. Springer, Cham, 2018. 1-19.

[5] Reis, Rui L., et al. *Natural-based polymers for biomedical applications*. Elsevier, 2008.

[6] Hardy, John G., Jae Y. Lee, and Christine E. Schmidt. "Biomimetic conducting polymer-based tissue scaffolds." *Current opinion in biotechnology* 24.5 (2013): 847-854.

[7] Cheung, Hoi-Yan, et al. "A critical review on polymer-based bio-engineered materials for scaffold development." *Composites Part B: Engineering* 38.3 (2007): 291-300.

[8] Stevens, Molly M. "Biomaterials for bone tissue engineering." *Materials today* 11.5 (2008): 18-25.

[9] Ma, Peter X. "Biomimetic materials for tissue engineering." *Advanced drug delivery reviews* 60.2 (2008): 184-198.

[10] Stratton, Scott, et al. "Bioactive polymeric scaffolds for tissue engineering." *Bioactive materials* 1.2 (2016): 93-108.

[11] Gloria, Antonio, Roberto De Santis, and Luigi Ambrosio. "Polymer-based composite scaffolds for tissue engineering." *Journal of Applied Biomaterials and Biomechanics* 8.2 (2010): 57-67.

[12] Almine, Jessica F., et al. "Elastin-based materials." *Chemical Society Reviews* 39.9 (2010): 3371-3379.

[13] Wise, Steven G., Suzanne M. Mithieux, and Anthony S. Weiss. "Engineered tropoelastin and elastin-based biomaterials." *Advances in protein chemistry and structural biology*. Vol. 78. Academic Press, 2009. 1-24.

[14] Vrhovski, Bernadette, and Anthony S. Weiss. "Biochemistry of tropoelastin." *European Journal of Biochemistry* 258.1 (1998): 1-18.

[15] Wise, Steven G., and Anthony S. Weiss. "Tropoelastin." *The international journal of biochemistry & cell biology* 41.3 (2009): 494-497.

[16] Daamen, Wilhelmina Francisca, et al. "Elastin as a biomaterial for tissue engineering." *Biomaterials* 28.30 (2007): 4378-4398.

[17] Gregory, Kenton W. "Elastin and elastin-based materials." U.S. Patent No. 6,110,212. 29 Aug. 2000.

[18] Rodríguez-Cabello, José Carlos, et al. "Elastin-like polypeptides in drug delivery." *Advanced drug delivery reviews* 97 (2016): 85-100.

[19] Rodríguez-Cabello, J. Carlos, et al. "“Recombinamers” as advanced materials for the post-oil age." *Polymer* 50.22 (2009): 5159-5169.

[20] Nettles, Dana L., Ashutosh Chilkoti, and Lori A. Setton. "Applications of elastin-like polypeptides in tissue engineering." *Advanced drug delivery reviews* 62.15 (2010): 1479-1485.

[21] Meyer, Dan E., and Ashutosh Chilkoti. "Quantification of the effects of chain length and concentration on the thermal behavior of elastin-like polypeptides." *Biomacromolecules* 5.3 (2004): 846-851.

[22] Ribeiro, Artur, et al. "Influence of the amino-acid sequence on the inverse temperature transition of elastin-like polymers." *Biophysical journal* 97.1 (2009): 312-320.

[23] Girotti, Alessandra, et al. "Elastin-like recombinamers: Biosynthetic strategies and biotechnological applications." *Biotechnology journal* 6.10 (2011): 1174-1186.

[24] Ruoslahti, Erkki. "RGD and other recognition sequences for integrins." *Annual review of cell and developmental biology* 12.1 (1996): 697-715.

[25] Humphries, Martin J. "Peptide recognition motifs involved in the binding of integrins to their ligands." *Kidney international* 41.3 (1992): 645-649.

[26] Tan, Huaping, and Kacey G. Marra. "Injectable, biodegradable hydrogels for tissue engineering applications." *Materials* 3.3 (2010): 1746-1767.

[27] Coletta, Dante J., et al. "Bone regeneration mediated by a bioactive and biodegradable extracellular matrix-like hydrogel based on elastin-like recombinamers." *Tissue Engineering Part A* 23.23-24 (2017): 1361-1371.

[28] Urry, Dan W., et al. "Biocompatibility of the bioelastic materials, poly (GVGVP) and its γ-irradiation cross-linked matrix: summary of generic biological test results." *Journal of Bioactive and Compatible Polymers* 6.3 (1991): 263-282.

[29] Sallach, Rory E., et al. "Elastin-mimetic protein polymers capable of physical and chemical crosslinking." *Biomaterials* 30.3 (2009): 409-422.

[30] Testera, Ana M., et al. "Biocompatible elastin-like click gels: design, synthesis and characterization." *Journal of Materials Science: Materials in Medicine* 26.2 (2015): 105.

[31] de Torre, Israel González, et al. "Random and oriented electrospun fibers based on a multicomponent, in situ clickable elastin-like recombinamer system for dermal tissue engineering." *Acta biomaterialia* 72 (2018): 137-149.

[32] Huisgen, Rolf. "1, 3-dipolar cycloadditions. Past and future." *Angewandte Chemie International Edition in English* 2.10 (1963): 565-598.

[33] Baskin, Jeremy M., et al. "Copper-free click chemistry for dynamic in vivo imaging." *Proceedings of the National Academy of Sciences* 104.43 (2007): 16793-16797.

[34] Wenge, Ulrike, Thomas Ehrenschwender, and Hans-Achim Wagenknecht. "Synthesis of 2′-O-propargyl nucleoside triphosphates for enzymatic oligonucleotide preparation and “click” modification of DNA with nile red as fluorescent probe." *Bioconjugate chemistry* 24.3 (2013): 301-304.

[35] Rodríguez-Cabello, J. Carlos, et al. "Bioactive scaffolds based on elastin-like materials for wound healing." *Advanced drug delivery reviews* 129 (2018): 118-133.

[36] de Torre, Israel González, et al. "Elastin-like recombinamer-covered stents: Towards a fully biocompatible and non-thrombogenic device for cardiovascular diseases." *Acta biomaterialia* 12 (2015): 146-155.

[37] Mahara, Atsushi, Kristi L. Kiick, and Tetsuji Yamaoka. "In vivo guided vascular regeneration with a non-porous elastin-like polypeptide hydrogel tubular scaffold." *Journal of Biomedical Materials Research Part A* 105.6 (2017): 1746-1755.

[38] Brey, Eric M., ed. *Vascularization: regenerative medicine and tissue engineering*. CRC Press, 2014.

[39] Rouwkema, Jeroen, Nicolas C. Rivron, and Clemens A. van Blitterswijk. "Vascularization in tissue engineering." *Trends in biotechnology* 26.8 (2008): 434-441.

[40] Serbo, Janna V., and Sharon Gerecht. "Vascular tissue engineering: biodegradable scaffold platforms to promote angiogenesis." *Stem cell research & therapy* 4.1 (2013): 8.

[41] Mitchell, Geraldine M., and Wayne A. Morrison. "In vitro and in vivo approaches for pre-vascularization of 3-dimensional engineered tissues." *Vascularization for Tissue Engineering and Regenerative Medicine* (2017): 1-27.

[42] Laschke, Matthias W., and Michael D. Menger. "Prevascularization in tissue engineering: current concepts and future directions." *Biotechnology advances* 34.2 (2016): 112-121.

[43] Lovett, Michael, et al. "Vascularization strategies for tissue engineering." *Tissue Engineering Part B: Reviews* 15.3 (2009): 353-370.

[44] West, Jennifer L., and James J. Moon. "Vascularization of engineered tissues: approaches to promote angiogenesis in biomaterials." *Current topics in medicinal chemistry* 8.4 (2008): 300-310.

[45] Kim, Joseph J., Luqia Hou, and Ngan F. Huang. "Vascularization of three-dimensional engineered tissues for regenerative medicine applications." *Acta biomaterialia* 41 (2016): 17-26.

[46] Balani, Kantesh, Roger Narayan, and Arvind Agarwal. "Surface engineering and modification for biomedical applications." *Biosurfaces: A Materials Science and Engineering Perspective* (2015): 201.

[47] Tampieri, Anna, and Simone Sprio, eds. *Bio-Inspired Regenerative Medicine: Materials, Processes, and Clinical Applications*. CRC Press, 2016.

[48] Nyanhongo, Gibson Stephen, Walter Steiner, and Georg M. Gübitz, eds. *Biofunctionalization of Polymers and their Applications*. Vol. 125. Springer

Science & Business Media, 2011.

[49] Frey, Wolfgang, Dan E. Meyer, and Ashutosh Chilkoti. "Thermodynamically reversible addressing of a stimuli responsive fusion protein onto a patterned surface template." *Langmuir* 19.5 (2003): 1641-1653.

[50] Costa, Rui R., et al. "Stimuli-responsive thin coatings using elastin-like polymers for biomedical applications." *Advanced Functional Materials* 19.20 (2009): 3210-3218.

[51] Ekerdt, Barbara L., Rachel A. Segalman, and David V. Schaffer. "Spatial organization of cell-adhesive ligands for advanced cell culture." *Biotechnology journal* 8.12 (2013): 1411-1423.

[52] Li, Linying, et al. "Creating cellular patterns using genetically engineered, gold- and cell-binding polypeptides." *Biointerphases*11.2 (2016): 021009.

[53] García-Arévalo, Carmen, et al. "A comparative study of cell behavior on different energetic and bioactive polymeric surfaces made from elastin-like recombinamers." *Soft Matter* 8.11 (2012): 3239-3249.

[54] Rodríguez-Cabello, J. Carlos, et al. "Emerging applications of multifunctional elastin-like recombinamers." *Nanomedicine* 6.1 (2011): 111-122.

CHAPTER 1

SPATIAL CONTROL AND CELL ADHESION SELECTIVITY ON MODEL GOLD SURFACES GRAFTED WITH ELASTIN-LIKE RECOMBINAMERS

Tatjana Flora, [1] Israel González de Torre, [2] Luis Quintanilla, [1] Matilde Alonso, [1] José Carlos Rodríguez-Cabello[1]

[1]BIOFORGE, CIBER-BBN, University of Valladolid, Spain

[2]Technical Proteinn Nanotechnology (TPNBT S.L), Valladolid, Spain

Flora, T., de Torre, I. G., Quintanilla, L., Alonso, M., & Rodríguez-Cabello, J. C. (2018). Spatial control and cell adhesion selectivity on model gold surfaces grafted with elastin-like recombinamers. *European Polymer Journal*, *106*, 19-29.

Abstract

A simple system for cell selectivity and spatially controlled cell adhesion has been developed using model gold surfaces grafted with a combination of two ELRs containing into their backbone cell-adhesion domains such as RGD and REDV. Grafting onto gold was achieved via redox reaction through thiol groups present in amino terminal cysteine tails of the ELRs. The correlation among contact angle, SEM micrographs, AFM, XPS and QCMD have been carried out. After in-depth adhesion studies, a mixture of 75% ELR-REDV and 25% ELR-RGD was found to exhibit high selectivity for endothelial cells, promoting strong adhesion thereof. Consequently, certain areas of gold surfaces (strips) were cleaned by laser ablation and functionalized with the mixture 75% ELR-REDV – 25% ELR-RGD leading to a spatial segregation of the co-culture made of HUVEC and HFF1 cells. This platform therefore exhibits selective spatial control over cell adhesion associated with the bioactive epitopes (RGD and REDV) contained in the ELR sequence, since each functionalized surface (including strips) have similar topographic and hydrophobic characteristics and mechanical properties are in the same order of magnitude.

1. Introduction

Spatial cellular adhesion control plays a pivotal role in the production of novel cellular biosensors as well as in the development of tissue engineering constructs that require an organized structure with a specific placement of cells [1, 2]. This technique consists in creating specific areas in an artificial substrate where cells can be adhered or have resistant areas (non-adhesive zones) or even more have selective areas where only specific cells can adhere. Spatial arragement of cells is a new tool for cell biology that allows an improved control over cell behaviour and has a wide application in fundamental cell biology and biomedical engineering [3, 4]. In such a way, for the attachment of the cells on a solid substrate is necessary an interaction with specific surface-bound ligands that in vivo are allowed by the extracellular matrix (ECM): proteins such as collagen, fibronectin, elastin and laminin. The integrins are able to link the cell cytoskeleton to a material surface via these proteins present on the artificial substrate [5]. Surface bio-functionalization with cell-adhesion molecules has attracted significant interest as regards the design of surfaces with tailored properties, such as wettability, adhesion, and biocompatibility, which are essential for various biological evaluation such as controlling cellular response [6]. Currently, recombinant proteins such as elastin-like recombinamers (ELRs) are excellent candidates for the

development of smart surfaces as, together with their extensive potential to self-assemble, their sequence, functionality and bioactivity can be closely controlled using recombinant technologies [7–9]. ELRs are based on the repetition of certain sequences derived from natural elastin, specifically the pentapeptide (VPGXG), where X can stand for any amino acid except Lproline. This sequence confers elastic properties on the resulting recombinamer along with many other of their most striking properties, such as high biocompatibility and lower critical solution temperature behavior [10–12]. They are produced by recombinant techniques, thus allowing total control over the amino-acid sequence and a completely tailored design of the polypeptide chain at the gene level [13]. Thanks to their recombinant nature, ELRs allow the inclusion of bioactive domains such as REDV or RGD promoting in this way cell adhesion and cell spreading via its receptor [14]. REDV (arginine–glutamic acid–aspartic acid–valine) is a specific adhesive sequence for endothelial cells found in the alternatively-spliced IIICS-5 domain of human plasma fibronectin [15]. This motif mediates cell adhesion and spreading via α4β1 integrin in endothelial cells, but not in smooth muscle cells or fibroblasts [16]. On the other hand, RGD is a universal cell adhesive sequence within fibronectin that mediates cell attachment, and present in numerous proteins such as integrins [17, 18]. A subset of integrins recognize the RGD motif

within their ligands, the binding of which mediates both cell-substrate and cell-cell interactions [19]. Both REDV and RGD have been considered in this work, thus leading to the selective adhesion of endothelial cells due to their high specificity [20]. Moreover, amino terminal cysteines (Cys, Cblock) have been incorporated into the ELRs employed in this work (CC-RGD and CCC-REDV) in order to allow grafting to gold surfaces via a redox reaction. There are numerous characteristics of gold that make it a good choice as a substrate to study biological events. Firstly, gold is an inert metal, easy to obtain, compatible with cells, namely cells can adhere and proliferate without evidence of toxicity and lastly is easy to pattern by a combination of lithographic tools [21, 22]. Currently, several methods have been used, to produce protein patterns with a desired spatial resolution on surfaces, such as photolithography and photochemistry, laser lithography, ablation and vapor deposition, microwriting, ion implantation and soft lithography [23, 24]. All these methods lead to the generation of a two-dimensional control over the surface chemistry, in other words, production of regions that support protein adsorption and regions that reduce protein surface interaction where no cell attachment is desired [25]. Furthermore, surface chemistry and topography are important features that affect protein adsorption and them interaction with a biological environment such as cell cultures [26]. Laser ablation technique generate

a high precision surface topography for the self-organized and direct fabrication of nano- and microstructures on a surface. This technique has many advantages over other methods such as low surface contamination, low mechanical damage, and controllable surface structuring of three dimensional components [27]. It is characterized by a great recent progress due to its ability to control not only physical, but also chemical surface features and will continue to be developed into a more standardized research tool in biology [28, 29] Selective laser ablation is applied where individual layers have to be ablated without significantly damaging the layers or substrates below leaving the surfaces of conducting core material undamaged and without process marks such as cracks like at minimal heat input [30,31]. A prominent analytical technique, namely matrix assisted laser desorption/ionization (MALDI), provides a means of ejecting intact molecules—even large biomolecules—into the gas phase. The kinetic energies of ablated particles are typically high enough to promote surface diffusion, but not so high as to induce bulk damage [24, 32, 33]. Ultrashort pulse laser ablation is very beneficial given the large variety of structures that can be fabricated, the limited number of heat-affected zones that cannot be transferred to the surrounding material, and its high precision and reproducibility [34]. These findings suggest the possibility of producing biomaterial interfaces for electronic devices and widespread use

in the majority of biological applications [35]. This work describes the development of an efficient system in which the selective adhesion of a co-culture made of HUVECs and HFF-1 cells is spatially controlled due to the use of two ELRs that have a complementary bioactivity (CC-RGD and CCC-REDV) and include cysteines at the amino terminal region to promote a covalent linkage to gold surfaces. We will demonstrate that an optimal composition of 75% CCCREDV and 25% CC-RGD leads to the selective adhesion of endothelial cells in the co-culture system. To achieve this goal, whole model gold surfaces (Fig. 1a) were initially bio-functionalized with the ELR including CC-RGD (Fig. 1b). Strips cleaned by laser ablation (Fig. 1c), were afterward grafted with a previously optimized proportion of a mixture of two ELRs (25%CC-RGD and 75% CCC-REDV) (Fig. 1d). Finally, a co-culture of cells was employed and spatially controlled cell adhesion was obtained (Fig. 1e–f). The synergy between two different bioactivities, which produces an enhanced cell selectivity effect, is clearly demonstrated.

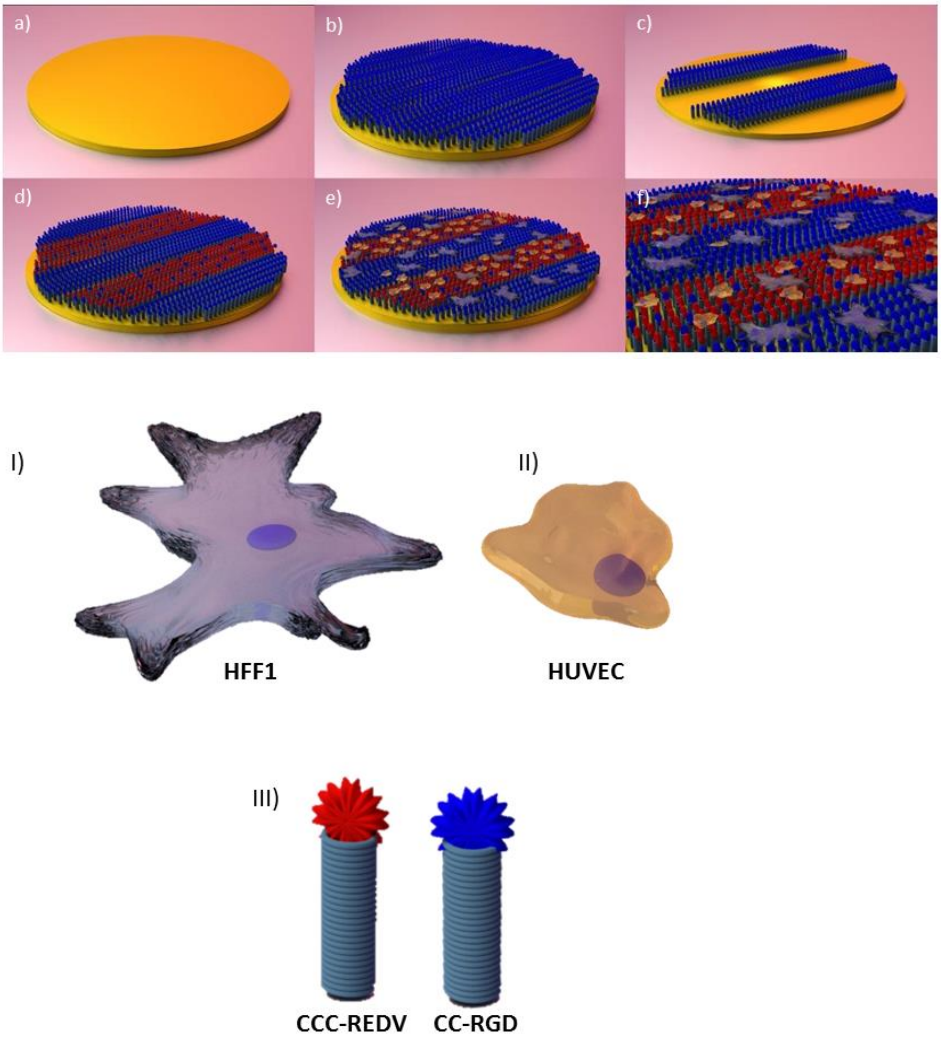

Fig. 1. Schematic representation of the bio-functionalized surface: (a) non-functionalized gold surface; (b) gold surface functionalized with CC-RGD recombinamer; (c) gold surface ablated with MALDI TOF/TOF laser; (d) ablated strips functionalized with 75% CCC-REDV/25% CC-RGD; e) adhesion of HUVEC and HFF1 cells; (f) magnification of adhered cells. (I) fibroblast cells (HFF1); (II) endothelial cells (HUVEC); (III) CCC-REDV (red color), and CC-RGD (blue color) recombinamers beyond the transition temperature. (For interpretation of the references to color in this figure legend, the reader is referred to the web version of this article.)

2. Materials and methods

2.1 Materials

2.1.1 Gold surfaces

Gold surfaces (glass coverslips with a thickness of 0.13–0.16mm were coated with a gold layer) were purchased from AMSBIO Company (Madrid, Spain). A diameter of 1 cm was coated with gold with a thickness of 10 nm. The thin gold film was deposited onto a supporting substrate by sputtering (the material to be deposited is ejected from a source by plasma discharge and then deposited onto the substrates).

2.1.2 Elastin-like recombinamers

The ELRs were constructed using standard genetic engineering techniques [13]. The bio-produced recombinamers were purified by a series of centrifugations under and above their transition temperature (Tt) and were dialyzed against ultrapure water (MilliQ) before being lyophilized. Three different ELRs containing the cysteines required for surface immobilization at the amino terminal region were produced. The first one (CC-RGD) contains a cell-adhesive RGD (Arg-Gly-Asp) sequence and includes two C-blocks; the second one (CCC-REDV) contains REDV (Arg-Glu-Asp-Val) and includes three C-blocks, and the last one (CCC-EI) was synthesized as a control recombinamer in cell cocultures with no

bioactive sequence, which showed antifouling behavior. The sequences of the three ELRs used in this work are:

REDV:CCC((VPGIG)2(VPGKG)(VPGIG)2EEQIGHIPREDVDYHLYP(VPGIG)2(VPGKG)(VPGIG)2)10

RGD:CC((VPGIG)2(VPGKG)(VPGIG)2EEQIGHIPRGDDYHLYP(VPGIG)2(VPGKG)(VPGIG)2(VGVAPG)3)10

EI: CCC[(VPGVG)2VPGEG(VPGVG)2]10(VGIPG)60V

The purity and molecular weight of the ELRs were verified by sodium dodecyl sulfate–polyacrylamide gel electrophoresis and matrixassisted laser desorption/ionization time-of-flight (MALDI-TOF) mass spectrometry. An amino acid composition analysis was also performed. Additional characterization of the ELRs was accomplished by infrared spectroscopy, differential scanning calorimetry (DSC) and nuclear magnetic resonance (NMR) techniques. The characterization results for the ELRs are provided in Supporting Information (see Figs. S1–S5 in Supporting Information). The corresponding ELR transition temperatures are: 31 ℃ (CC-RGD), 29 ℃ (CCC-REDV), and 30 ℃ (CCC-EI) (see Fig. S2 in Supporting Information). CC-RGD was designed with two cysteines in order to improve its production yield. Different number of cysteines does not affect the efficiency of grafting [36, 14].

2.1.3 Cell culture

Human umbilical vein endothelial cells (HUVEC) were purchased from Life Technologies S.A. (Madrid, Spain). These cells were cultured at 37 °C and 5% CO2 in MED200 culture medium (M200500, Life Technologies S.A, Madrid, Spain) supplemented with 100 U/100 mg/ Ml penicillin/streptomycin (15140-122, Invitrogen Corporation, Madrid, Spain). HUVEC between passages 2 and 6 were used in all experiments. Human foreskin fibroblasts (HFF1) were purchased from Life Technologies S.A. (Madrid, Spain) and were cultured in DMEM medium supplemented with 15% FBS and 100 U/100 mg/mL penicillin/streptomycin at 37 °C and 10% CO2. Fibroblasts between passages 6 and 10 were used in all experiments.

2.2. Methods

2.2.1. Surface cleaning/activation

The surfaces were treated with Plasma Cleaner (Sterilizer PDC-002, Harrick Scientific Corporation, USA) using Argon plasma for 20 min at a high power setting (30W applied to the RF coil) in order to etch the surface before each experiment.

2.2.2. Surface functionalization

After cleaning/activation by plasma treatment, the surfaces were immersed in ELR solutions with a concentration of 5 mg/mL for 6 h. Although

several ELR concentrations were considered, a value 5 mg/mL was selected due to the homogeneous coverage obtained analyzed by SEM. Subsequently, several washing steps with milliQ water were performed in order to remove remnants of ELRs not grafted to the surfaces. Finally, the surfaces were dried under a nitrogen flow and submitted to several treatments reported below.

2.2.3. Contact angle

Contact angle measurements were performed using the sessile drop method with a Data Physics OCA20 system instrument. The drop profile images during micro-syringe dispensation were recorded using an adapted CCD video camera. The stainless-steel needle tip was always kept at the top of the sessile drop and immersion of the needle into the drop was avoided during the measurements to prevent distortion of the drop shape by the needle. Ten measurements at 37 °C from different locations on each surface were measured to ensure a representative value of the contact angle.

2.2.4. X-ray photoelectron spectroscopy (XPS)

XPS experiments were carried out using a Physical Electronics (PHI) 5500 spectrometer equipped with a monochromatic X-ray source (Al Ka line with an energy of 1486.6 eV and 350 W). The pressure inside the analysis chamber was 10−7 Pa. All measurements were performed at an angle of

45° with respect to both the X-ray source and analyzer. Survey scans were taken in the range 0–1100 eV and high resolution scans were obtained for the C1s, N1s, O1s and Au peaks. The elemental surface composition was estimated from the area of the different photoemission peaks taken from the survey scans modified by their corresponding sensitivity factors. The signal coming from a circular spot area of 100 μm of radius has been collected. Different areas of each surface were analyzed and the average signal is calculated.

2.2.5. Scanning electron microscopy (SEM)

Scanning electron microscopy (SEM) was used to investigate the surface morphology. Thus, the surfaces were immersed in recombinamer solutions with a concentration of 5 mg/mL for 6 h. After several washing steps with MilliQ water, the surfaces were dried with gaseous nitrogen. Micrographs were obtained using a scanning electron microscope (FEI Quanta 200 FEG) in low vacuum mode at 3 keV. Morphological details were evaluated quantitatively using the ZEN (Blue Edition, 2012) software package (Carl Zeiss Microscopy).

2.2.6. Atomic force microscopy (AFM)

AFM measurements were performed using a Dimension 3100 microscope controlled by a Nanoscope IV controller system (Digital Instruments) in tapping mode using V-shaped Si3N4 tips (OMCL TR400PSA, Olympus,

Japan). AFM images were taken from PBS immersed samples, with a nominal spring constant of 0.32 N/m. The scan area was 10 μm×10 μm and the root-mean-square (RMS) roughness of the surfaces was evaluated for regions of 1 μm×1μm. Surface roughness quantifies the vertical variations of a real surface from its ideal form. One of the most common parameters used to describe the degree of roughness of a surface is the root mean square (RMS) roughness, Rq, which is defined as:

$$Rq = \sqrt{\frac{\sum_{n=1}^{N}(Z_n - \bar{z})^2}{N}} \qquad \text{Equation 1}$$

where "Zn" corresponds to the vertical height for a given point, ⟨z⟩ corresponds to the mean value of the surface height and N to the number of points in the sample area. Five randomized sections were created for each image to determine the surface roughness of the polymeric surfaces.

2.2.7. Quartz crystal microbalance with dissipation

The QCM-D technique was applied in order to estimate the physical parameters representing the ELR thin film adsorbed on the surface [37, 38]. This technique allows simultaneous measurements of both frequency and energy dissipation changes. A Q-Sense Explorer System equipment (Biolin Scientific, Sweden) was used, with a peristaltic pump pumping every solution through the circular flow-through circuit at a flow rate of 50 μL/min. An AT-cut 5 MHz quartz crystal coated with gold (Biolin

Scientific) was used as sensor, and the frequency and dissipation changes were recorded up to the 13th overtone number. The following sequence of flows (or events) was allowed to occur in each QCM-D measurement. First, since PBS was used as buffer for the polymer solutions, a flow of PBS at 23 °C was injected for 3 min to define a stable baseline, followed by the flow of the polymer solution under study at 23 °C for 20 min; next, a buffer rinse at 23 °C for 10 min. was accomplished; the last event corresponded to a buffer rinse at 37 °C for 15 min. Pure CC-RGD and pure CCC-REDV have been measured. Based on preliminary co-culture cellular assays that showed better performance with this ratio, a mixture of 75% REDV/ 25% RGD has been also measured. QCM-D measurements where the temperature of all the events (both polymer deposition and flows of PBS) is 37 °C have been also carried out. Three replicates were performed for each measurement. The QCM-D experimental data were numerically fitted to the Voigt (continuous) viscoelastic model using Dantzig's Simplex algorithm as implemented in the software from Biolin Scientific (Q-Sense Dfind) [39, 40]. An explicit consideration of the frequency dependence of viscoelastic properties was assumed according to a power law. A descending incremental fitting was used, with the quality of the fitting being determined by the parameter $\chi 2$ (lower $\chi 2$ values

indicate a better fitting). Only fits providing fitting without jumps between solutions in the resulting physical parameters have been considered.

2.2.8. Laser ablation

After functionalization of the whole surface with 100% CC-RGD, some regions (width: 200 μm) were ablated using a smart beam MALDI laser in a MALDI TOF/TOF UltrafleXtrem instrument from Bruker (Center for Omic Sciences, Reus, Spain). Smartbeam technology combines the speed of a solid-state laser with the wide range of applications associated with nitrogen lasers. The new UltrafleXtreme, with a 1000 Hz smartbeam-II laser, enables laser focus diameters down to 10 μm for high spatial resolution imaging without pixel overlap. The Smartbeam MALDI laser was used at low intensity by preparing 500 shots/raster spots at 20% laser intensity and a large smartbeam.

2.2.9. *In vitro* cellular studies

A reference standard cell adhesion curve for each cell type was created to convert sample fluorescence values into cell numbers per unit well area. HUVEC and HFF1 cells were labeled following the protocols for the PKH67 Fluorescent Cell Linker Kit and PKH26 Red Fluorescent Cell Linker Kit respectively, which were purchased from Sigma-Aldrich Quimica S.L. (Madrid, Spain). A range from 500 to 4000 cells were seeded on the functionalized surfaces and subsequently were incubated for 4 h at

37 ºC in a 5% CO2 atmosphere with the corresponding medium without adding FBS in either in order to avoid the interaction of serum proteins with the cell adhesive domains of the coatings. A fluorescence microplate reader with appropriate filters (490 nm excitation, and 502 nm emission for green fluorescence; 551 nm excitation, and 567 nm emission for red fluorescence) was used to measure the sample fluorescence. After the determination of the standard adhesion curves, cell adhesion studies were performed co-seeding onto the surfaces HUVEC and HFF1 cells previously labeled with PKH67 and PKH26 Red Fluorescent Cell Linker Kit, with a 1:1 ratio. Both of them were seeded at a density of 5 · 103 cells/surface using MED200 culture medium for the co-culture supplemented exclusively with 100 U/100 mg/mL penicillin/streptomycin. After 4 h of culture, the medium was removed and the functionalized surfaces were washed with DPBS (Dulbecco's Phosphate- Buffered Saline, Life Technologies, Madrid, Spain). Adhesion was evaluated by measuring the fluorescence with a photometer plate reader. Fluorescence images were also used to count the HUVEC and HFF1 cells adhered to the strips using ImageJ software.

2.2.10. Statistical analysis

Data are reported as mean±SD (n=3). Statistical analysis was evaluated by one-way analysis of variance using the Holm–Sidak method. A p value

of<0.05 was considered to be statistically significant. (**) $p < 0.001$, (*) $p < 0.05$, and $p > 0.05$ indicates no significant differences (n.s.d.).

3. Results

3.1. Contact angle

The functionalization of gold surfaces were characterized by contact angle measurements (Fig. 2). Thus, non-functionalized and non-activated (control) surfaces exhibited average contact angles of 57°, whereas after functionalization these values increased to around 92°. The contact angle for activated control surfaces was small enough to be measured under our experimental conditions (< 8°). As expected, the contact angle was significantly affected by functionalization, with the high value of the contact angle corresponding to a high surface hydrophobicity. No significant differences were found for the three samples functionalized with ELRs. Even after vigorous rinsing with MilliQ water, a layer of recombinamers remains grafted to the surface.

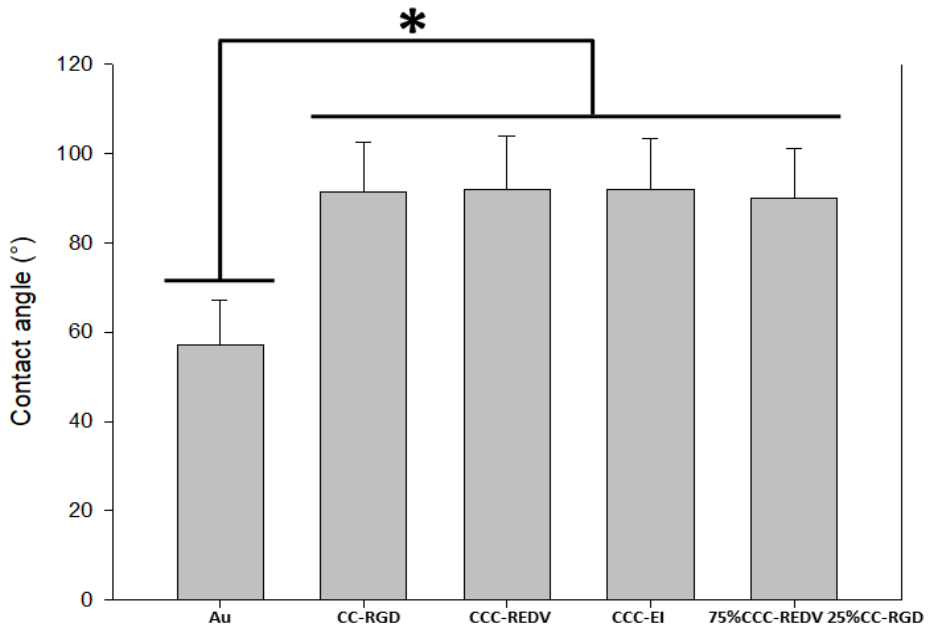

Fig 2. Contact angle for a non-functionalized and non-activated surface (Au), surface functionalized with CC-RGD, surface functionalized with CCC-REDV and surface functionalized with CCC-EI. Data are reported as mean ± SD (n=3). Statistical analysis was evaluated by analysis of variance using the Holm–Sidak method. *p<0.05; n.s.d., no significant differences.

3.2. X-Ray photoelectron microscopy (XPS)

XPS is the most widely used surface-analysis technique as it can be applied to a broad range of materials and provides valuable quantitative and chemical information about the surface of the material being studied. Detailed XPS spectra of some fundamental elements can be found in the Supporting Information (Fig. S6). Table 1 shows the atomic percentage for some significant surface atoms for the functionalized surfaces, control sample and the strip ablated and subsequently functionalized with 75%

CCC-REDV/25% CC-RGD. The orbitals used to calculate concentrations were C1s, O1s, N1s, Au4f and Au4d. The atomic ratios of the most significant elements on the gold surfaces (C, O, N, and Au) were examined. Thus, whereas a marked variation in the percentage of the most representative atoms for each surface with respect to the control Au surface was observed, no significant differences are observed between the different functionalized surfaces and the strip. The Au4f percentage decreases and the proportion of carbon and nitrogen (typical atoms in ELRs) increases. The high level of carbon is mainly due to extrinsic hydrocarbon deposition on the surfaces since these samples were exposed to air prior to the XPS analysis. The Au4f percentage decrease indicates coating of the Au surface with the ELR-based thin film since the peak intensity undergoes an exponential attenuation with the electron path length travelled. In additions, the similar Au4f percentage obtained for functionalized surfaces (Table 1) suggests ELR coatings with similar thicknesses.

Table 1. Atomic percentages for C, O, N and Au4f in control (Au) and functionalized surfaces.

	C1s (%)	*N1s (%)*	*O1s (%)*	*Au4f (%)*
Au (control)	30.11	0.99	12.31	56.59
CCC-REDV	57.77	12.33	14.52	15.39
CC-RGD	51	9.4	30	14.22
CCC-EI	59.82	15.77	15.14	9.27
STRIP (75%CCC-REDV-25% CC-RGD)	66.01	13.04	18.01	12.52

3.3. Scanning electron microscopy (SEM)

SEM morphological analysis allowed high-resolution imaging of the gold surfaces before (Fig. 3a) and after functionalization with the three recombinamers used in this work (Fig. 3b–d). This technique allow us to have a first sight of the surfaces before and after functionalization. Au clusters, formed as a result of sputtering deposition of gold on the glass surface, can clearly be seen in Fig. 3a. The size of these clusters depends on the deposition rate and the different probability of gold atom capture on the bare glass substrate [41, 42]. An initial study of the coating effectiveness shows a uniform coverage of the surfaces (see Fig. 3b–d) as the gold clusters have been smoothed with the applied coating. Ablated strip micrographs (Fig. 4a and b) show an absence of damage and marks on the surface. This morphology agrees with that of the control surface

(Fig. 4c), which consists of Au clusters formed during the Au sputtering deposition process.

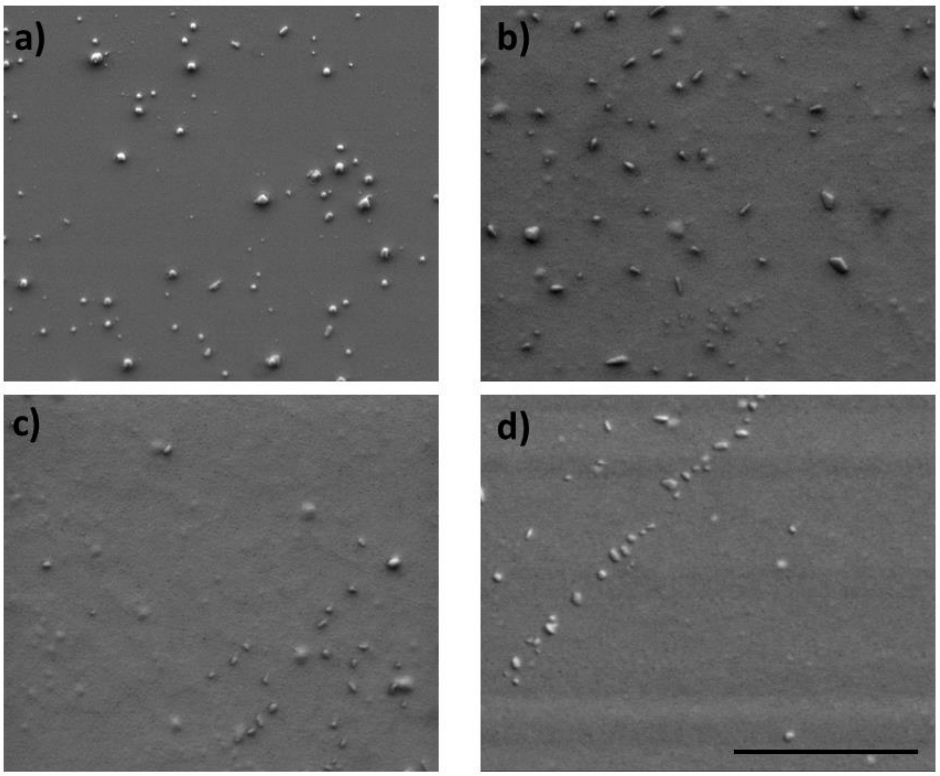

Fig 3. SEM micrographs of: a) non-functionalized gold surfaces (control); b) a gold surface functionalized with CC-RGD; c) a gold surface functionalized with CCC-REDV; d) a gold surface functionalized with CCC-EI. Scale bar: 4 μm.

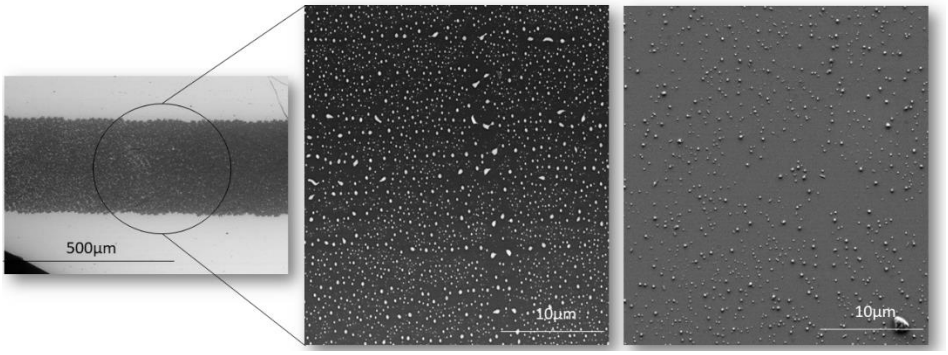

Fig. 4. SEM micrographs of (a) the strip ablated with MALDI TOF/TOF UltrafleXtrem (b) magnification of the ablated strip, and (c) non-functionalized (control) surface.

3.4. Atomic force microscopy (AFM)

The morphology and roughness of the surfaces were assessed by AFM, comparing the functionalized surfaces with the non-functionalized one (Fig. 5). Clear changes in surface topography can be seen after functionalization. In agreement with the morphology observed in the SEM micrographs, although gold clusters can clearly be seen in the nonfunctionalized sample, the coating process gives rise to a granular surface where these clusters have been covered. The average RMS roughness of the bare gold surface (4.79 ± 0.2 nm) is significantly reduced when the polymer is coated onto the whole Au surface (REDV: 0.40 ± 0.02 nm; RGD: 0.46 ± 0.07 nm; and EI: 0.81 ± 0.1 nm). As can be seen, a low average RMS roughness value is found (lower than 1 nm for every polymer coating). Moreover, the low standard deviation indicates a

uniform coating of the surface. The roughness of the strips was analyzed by AFM. After functionalization, the RMS roughness is 0.9 ± 0.2 nm, which is lower than the roughness for bare gold, thus meaning that the mixture of recombinamers has been deposited onto the strips (Fig. 5e).

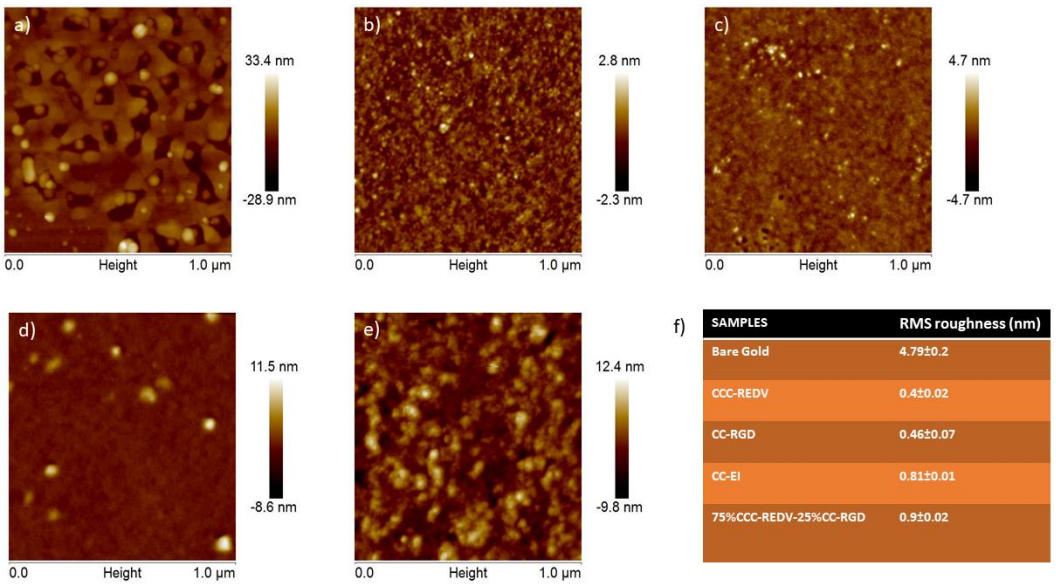

Fig. 5. Different nano-topographies visualized using AFM technique: a) the-non-functionalized (control) surface, b) CCC-REDV, c) CC-RGD, d) CCC-EI and e) 75% CCC-REDV/25% CC-RGD. Scanned area: 1x1 μm^2.

3.5. Quartz crystal microbalance with dissipation

To complete the physical characterization of the surfaces functionalized with the ELRs, quartz crystal microbalance (QCM-D) was used as it allows to determine the thickness as well as layer's softness of a film

deposited in a liquid environment. Before making the QCM-D measurements, the viscous penetration depth, δ, corresponding to our buffer (PBS) was estimated. [43] This parameter indicates the decay rate of the oscillating wave with the distance from the sensor surface and is defined in Eq. (2).

$$\delta=\sqrt{\frac{2\eta}{\rho\omega}}$$

where η and ρ are the viscosity and density, respectively, of the buffer used in the QCM-D measurement and ω is the oscillation frequency. For PBS (η=0.92 mPa.s and ρ=1.005 g/cm3), δ is about 140 nm for 15 MHz (third overtone, n=3). QCM-D measurements were initially carried out at 37 °C, namely, all the events are at 37 °C. The evolution of the frequency and dissipation change with time are shown in Supporting Information for the mixture 75% CCC-REDV-25% CC-RGD (Fig. S7). As can be seen, some harmonics cannot be detected during the measurement in a systematic and repetitive way. After applying modeling to the experimental truncated data, a film thickness roughly of 250 nm was obtained. Thus, the film thickness is larger (around twofold) than the viscous penetration depth.

Since the QCM-D signal is exponentially attenuated, the signal coming from some overtones cannot be measured. Moreover, a highly nonlinear response of the QCM in the thick film regime (where, nevertheless, the

Voigt model is still useful) has been previously reported [44–46]. Yet, when the deposition event is accomplished at 23 °C no signal loss is found (Fig. 6). This different behavior with temperature is associated with the ELR transition temperature, Tt, where a conformational reorganization at the molecular level occurs, determining the deposition characteristics during the QCM measurement. The simultaneously measured shifts in frequency (normalized to the corresponding overtone, n), $\Delta fn/n$ (Fig. 6a), and in energy dissipation, ΔDn (Fig. 6b), obtained at n=3 (15 MHz) are displayed as a function of time. Although measurements were carried out up to the 13th overtone (65 MHz) under our experimental conditions, only the third harmonic is shown for clarity. The frequency change at the fundamental frequency is not generally analyzed since this is affected by the flow of the bulk solution and is prone to more pronounced instabilities than the overtones [47–49]. Thus, only overtones are used for further quantitative analysis. Four events can be distinguished in the transient evolution: (i) flow of pure PBS at 23 °C to establish the baseline, (ii) flow of the polymer solution at 23 °C, (iii) pure buffer rinse at 23 °C, followed by (iv) a final pure buffer rinse at 37 °C to determine the impact of the conformational transition on the properties of the deposited thin film. At this point we will focus our attention on the results obtained for pure CCC-REDV and pure CC-RGD (Fig. 6). Upon exposure to the polymer solution,

the decrease in frequency indicates adsorption on the side of the sensor. A higher frequency change was observed for CCCREDV (around −53 Hz, n=3) than for CC-RGD (around −35 Hz, n=3). This mass uptake is accompanied by a strong increase in dissipation for both CCC-REDV and CC-RGD (up to 10×10−6, n=3; 7×10−6, n=3, respectively). Next event in the QCM-D experiment corresponds to rinsing with pure PBS solution at 23 ºC to stabilize and eliminate any material accumulated on the surface. Thus, along with fairly small variations are found in the frequency changes, a similar dissipation for both ELRs is observed (at saturation, 3×10−6, n=3). The final stage corresponds to a PBS rinse at 37 °C. As can be seen, significant frequency and dissipation changes are found with respect to the PBS rinse at 23 °C. These experimental results suggest that a thin film stabilization occurs, more noticeable for the conformation at 37 ºC. The frequency dependence observed for the three overtones in Supporting Information Fig. S8, and the high energy dissipation, indicate that the simple Sauerbrey model is not valid and therefore that a viscoelastic model is required. In this case, a Voigt viscoelastic model based on a single layer was used [39, 50, 40]. The adsorbed film is represented by a lateral homogeneous film with uniform thickness and density which, in our case, was estimated at 1.1 g/cm3 (corresponding to a hydrated protein) [51]. This film is situated between the sensor surface

and on its other side is in contact with a semi-infinite bulk solution (in our case, PBS) that was assumed to be Newtonian, with a viscosity and density of 0.92 mPa.s and 1.005 g/cm3, respectively. No significant impact of surface roughness on the QCM experimental values is expected since, given the average RMS roughness obtained by AFM (< 1 nm for each polymer coating), the coated QCM sensor can be regarded as flat [37]. Moreover, within the resolution of the AFM images (Fig. 5) the thin film can be considered to be laterally homogeneous. Subsequent characterization of the adsorbed thin film was based on the QCM-raw data. Several sets of raw experimental data and the corresponding fitted curves can be found in the Supporting Information (Fig. S8). At the end of the third and four event, the Voigt model provides the parameters that characterize the stabilized thin film. The corresponding values for CC-RGD, CCC-REDV and the mixture are summarized in Table 2. It should be pointed out that the rheological parameters are measured in the MHz frequency range, whereas rheological characterization is usually accomplished in the Hz-kHz range. It should also be noted that, during QCM measurements, liquid or solvent molecules may couple as an additional mass via direct hydration, viscous drag, or entrapment in cavities in the adsorbed film [38]. For both polymers after the PBS rinse at 37 °C, the conformational transformation gives rise to a decrease of the

thickness. As can be seen, when the deposition event is carried out at 23 °C, film thickness are clearly lower than the viscous penetration depth around 140 nm and, therefore, the microbalance response become linear.

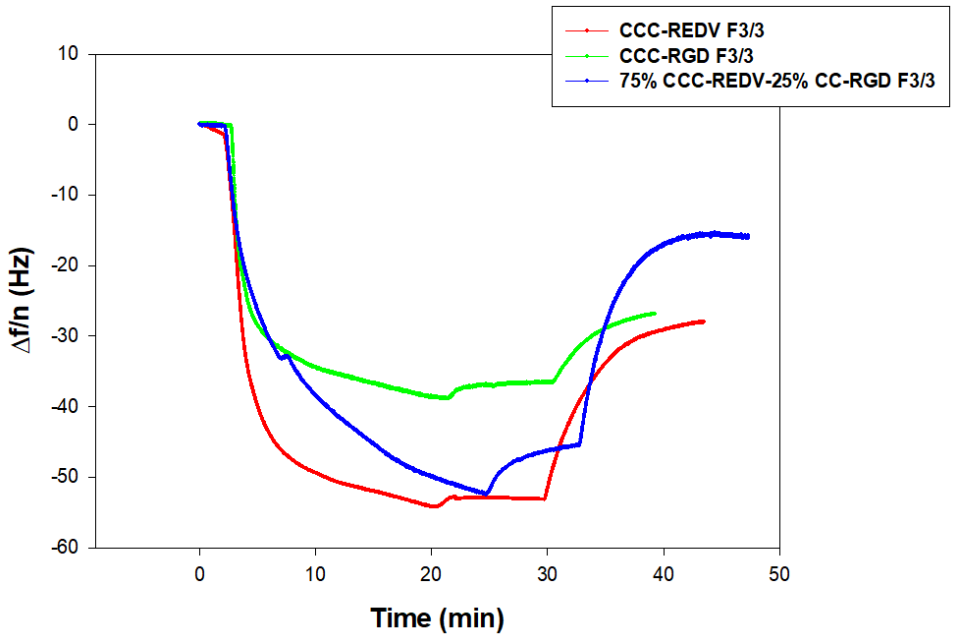

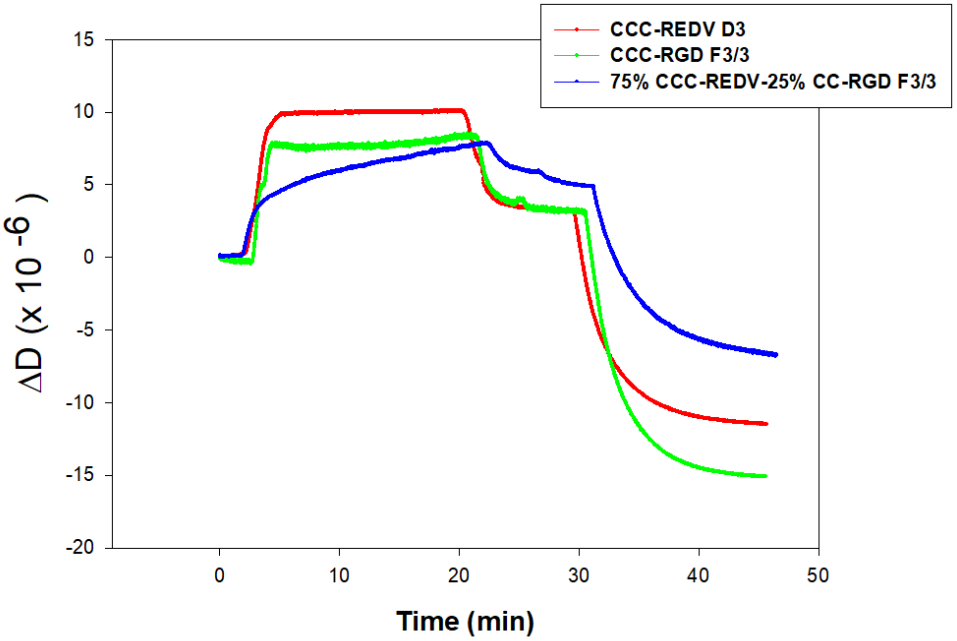

Fig. 6. Normalized frequency (a) and energy dissipation shifts (b) measured at the third (n=3) overtone for CCC-REDV, CC-RGD and the mixture 75% REDV/25% RGD. Four events are distinguished: first, pure buffer (PBS) solution at 23 °C for 3 min; second, exposure to ELR solution at 23 °C for 20 min; third, pure buffer solution at 23 °C for 10 min., and finally, pure buffer solution at 37 °C for 15 min.

3.6. Selective cell adhesion on ELR-bio functionalized model gold surfaces

The next step in this work consisted in determining the optimum mixture of CC-RGD and CCC-REDV in order to obtain selective adhesion of endothelial cells. A co-culture of HUVEC and HFF1 cells was used to that end. Adhesion was carried out under serum-free conditions in order to avoid the interference of soluble extracellular matrix (ECM) proteins

found in the serum with the observed behavior. To achieve this goal, whole gold surfaces were functionalized with ELR mixtures comprising varying percentages of each ELR: a) 100% CCRGD, b) 25% CCC-REDV/75% CC-RGD, c) 50% CCC-REDV/50% CCRGD, d) 75% CCC-REDV/25% CC-RGD, and e) 100% CCC-REDV. A surface functionalized with CCC EI, which does not contain any bioactive sequence, was used as a negative control. In Fig. 7 the adhesion of HUVEC (green) and HFF1 (red) on each functionalized surface with different percentages of the recombinamer mixture can be seen from top to bottom: phase contrast (A1-A6), FITC channel (B1-B6, only the HUVEC cells are visualized), G-2A channel (C1-C6, for HFF1 visualization) and, finally, all channels merged (D1-D6). For HUVEC cells, there was no significant difference in adhesion on surfaces functionalized with 0%, 25% and 100% CCC-REDV, although a relatively minor increase in adhesion of these cells was observed on surfaces functionalized with 50% CCC-REDV. In contrast, a significant increase in the adhesion of HUVECs on surfaces functionalized with 75% CCC-REDV and 25% CC-RGD was observed. The quantity of cells adhered onto one square centimeter of various surfaces can be seen in Fig. 8. It can clearly be seen that the presence of the REDV sequence minimizes HFF1 adhesion. Thus, as the percentage of CCC-REDV recombinamer increases, the number of HFF1 cells adhered decreases

considerably, thereby highlighting the significance of the REDV ligand for selective adhesion of endothelial cells on model gold surfaces. The presence of this motif provides an unfavorable environment for this cell type. In light of the above, we decided to use the mixture 75% CCCREDV/ 25% CC-RGD as the optimal mixture for our spatially selective cell cultures given the enhanced adhesion of endothelial cells.

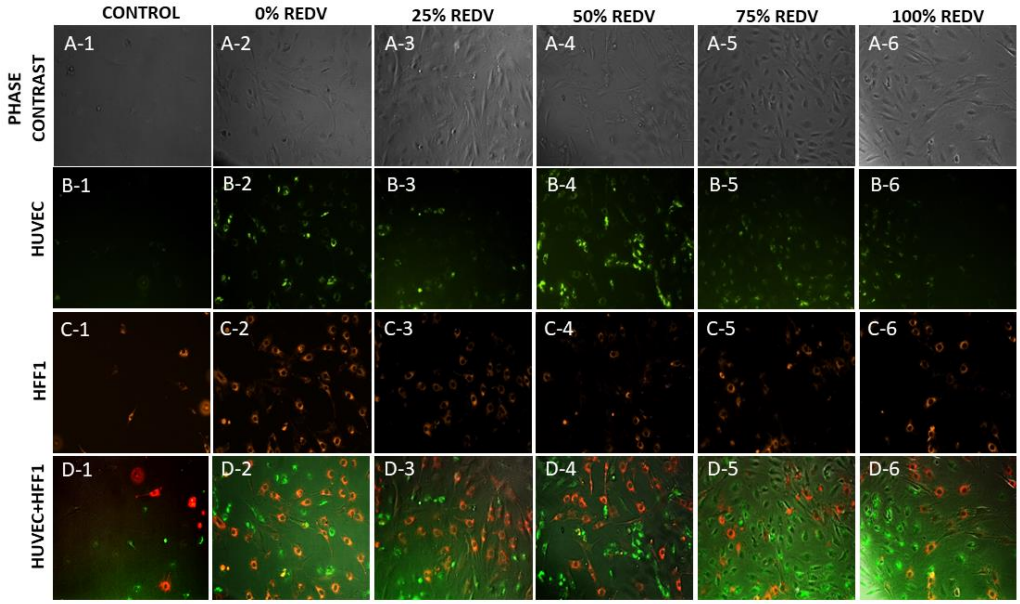

Fig. 7. HUVEC (membrane labeled with PKH67 Green Fluorescent Cell Linker Kit) and HFF1 (membrane labeled with PKH26 Red Fluorescent Cell Linker Kit) adhered to surfaces functionalized with 0% CCC-REDV, 25% CCC-REDV, 50% CCC-REDV, 75% CCC-REDV and 100% CCC-REDV, respectively. From top to bottom: image A shows the phase contrast for each percentage functionalization; image B the FITC channel to visualize HUVEC cells; image C the G-2A channel to visualize HFF1, and finally, all channels are merged in image D. Scale bar: 50 μm.

3.7. Spatial control of endothelial cell behaviour

Once the optimal percentage for selective adhesion of endothelial cells and the protocol for cleaning gold strips by laser ablation had been established, the next step was the selective functionalization of these strips. Thus, the strips were functionalized with the mixture of 75% CCC-REDV and 25% CC-RGD. This functionalization only takes place on those strips where a bare gold surface is available as the rest of the surface has been previously functionalized with the CC-RGD recombinamer. These surfaces were submitted to a co-culture of endothelial and HFF1 cells for 48 h in order to demonstrate a maximal cell selective confluence onto the strips. Cells were counted using ImageJ software. Interestingly, we observed a considerable increase of endothelial cells on the strips functionalized with 75% CCC-REDV/25% CC-RGD when compared with the other areas functionalized with 100% CC-RGD. Indeed, Fig. 9 clearly shows that the number of endothelial cells (green1) (Fig. 9c) onto the surfaces is higher than that for HFF1 (red) (Fig. 9b). Specifically, the number of endothelial cells present onto the strips is 520 ± 35, while the value for HFF1 cells is 175 ± 20. A noticeable spatial control of HUVEC adherence on the strip is therefore demonstrated. This result suggests that surface bio-functionalized with REDV or RGD-related peptides would likely promote

preferential adherence of cell types with the appropriate cell-surface ligand.

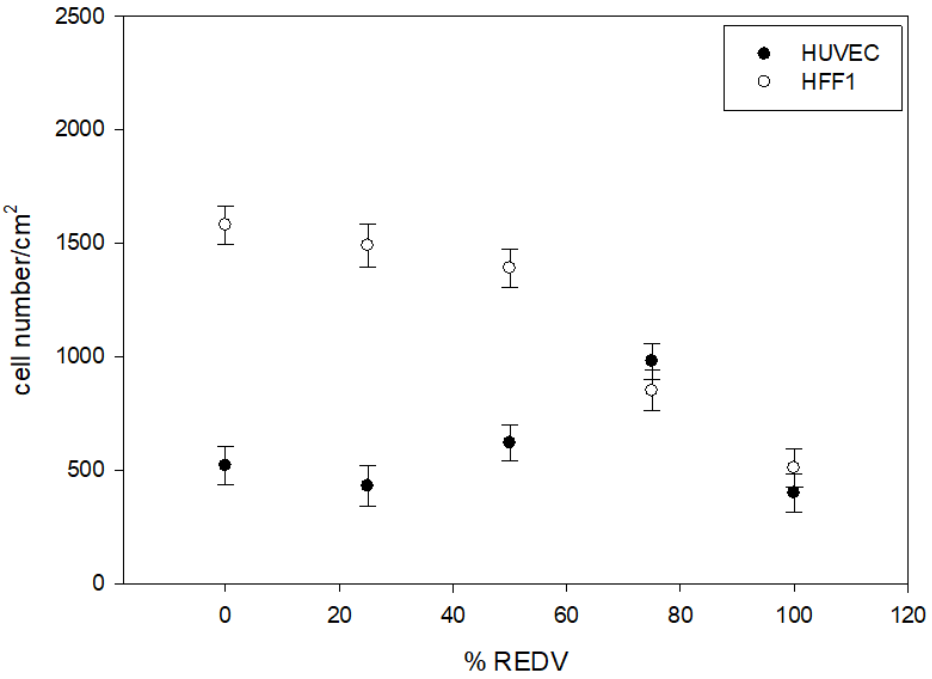

Fig. 8. Number of HUVEC (black) and HFF1 cells (white) adhered onto surfaces functionalized with different percentages of ELR (100% CC-RGD, 25% CCCREDV/ 75% CC-RGD, 50% CCC-REDV/50% CC-RGD, 75% CCC-REDV/25% CCRGD and 100% CCC-REDV).

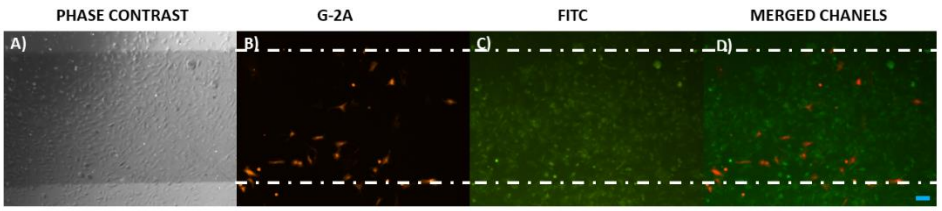

Fig. 9. From left to right: image a shows the phase contrast of the strip ; image b the G-2A channel to visualize HFF1 present onto the strip; image c the FITC channel to visualize HUVEC cells, and finally all channels have been merged in image d. Scale bar: 100 μm.

4. Discussion

REDV sequence plays a critical role in the adhesion of endothelial cells while exhibits better cell-type selectivity due to its receptor in their membrane which is only expressed in limited cell-lines [15,52]. Although, this sequence is considered highly selective for endothelial cells, when present on its own it promotes only poor and weak adhesion despite its selectivity [15]. This validates the results obtained to date, namely that the presence of the RGD sequence in the mixture used to functionalize the surfaces is necessary to facilitate the adhesion of endothelial cells. Overall, we have demonstrated that the REDV sequence is a selective bioactive domain for endothelial cells by increasing their adhesion to a model gold surface. This selectivity towards endothelial cells in the presence of the REDV sequence further underlies the crucial bioactivity and, more importantly, selectivity provided by this ligand in cell adhesion and allowed us to demonstrate that adhesion of endothelial cells is markedly enhanced on those surfaces functionalized with 75% CCCREDV and 25% CC-RGD. The adhesion ratio of endothelial cells was significantly higher than for HFF1 cells, thus indicating a selective adhesion with respect to endothelial cells. In addition of cell adhesion sequences such as REDV and RGD, the ELRs contain cysteines at the amino-terminal region of their backbone as these are essential for grafting onto gold and avoid the use of

intermediates such as alkane thiols. As reported in literature there are considerable limitation on using chemical approaches like biocompatibility, applicability to only a limited number of surfaces, high costs, low yield and stability that are overcome with the use of genetically engineered recombinamers [50]. Apart from potential receptor-mediated interactions, physical and chemical factors, including surface chemistry, topography and hydrophilicity, are key to the long-term viability and proliferation of cells. Protein grafting on model gold surfaces was assessed using several techniques, such as contact angle, XPS, SEM, AFM, and QCM-D. The contact angle values highlighted an increase in hydrophobicity with no significant differences in the functionalized surfaces. As can be seen from the literature, this results confirm that clean gold is hydrophilic and deposition of a recombinamer monolayer renders it hydrophobic [39]. The chemical composition of the surfaces was studied by XPS, which showed a clear variation in atomic levels at the surface. Both the significant increase in the percentage of C1s and N1s and the marked reduction in the intensity of Au in comparison with the non-functionalized surface indicate the effective coating of gold surface with a similar thickness for every functionalized surface on which covalent Au-S bonding occurs. The Au4f7/2 peak typically appears at around 83–84 eV for Au (0) in the XPS spectrum [53–56]. When Au (I) thiolates are formed,

a positive shift in binding energy of about 0.2–1.0 eV has been reported [54]. In accordance with this, our XPS spectra (see Fig. S6 in Supporting Information) show a positive shift of around 0.3 eV, thus indicating Au-S covalent bonding in the thin ELR film. Following with the characterization, the morphology and nano-topography of the surfaces were studied in more detail by SEM microscopy and AFM, respectively, thereby offering an initial insight into the grafting effectiveness and showing homogenous coverage of the surface topography. The RMS roughness decrease when gold surfaces are functionalized with the recombinamers having similar values lower than 1 nm. Numerical fitting of the QCM-D experimental data to a Voigt viscoelastic model indicated a stabilization of the adsorbed film after the PBS rinse. QCM characterization of the thin film based on the mixture of both ELRs was then carried out (see Fig. 6) and its parameters are included in Table 2. Similar to pure ELRs, the PBS rinse at 37 °C gives rise to a decrease of the mixture film thickness. On the whole these results therefore suggest that the ELRs are grafted onto the surfaces giving rise to functionalized surfaces. Specific regions of the surfaces (strips) were cleaned by laser ablation without altering their bulk properties and were subsequently characterized by SEM and AFM confirming that gold had not been removed. A comparison of the SEM micrographs for the as-received gold

surface and ablated strips showed no major differences. Consequently, these strips were functionalized with the optimized mixture (75% CCCREDV- 25% CC-RGD). No topographic differences has been found among the functionalized surfaces and the re-functionalized strips. The results demonstrated that spatially controlled selective cell adhesion was bio-specific on strips functionalized with the optimized mixture of recombinamers, which showed a better ability to promote endothelial cell adhesion due to the presence of the REDV motif [57, 58]. Since no significant differences in topography and hydrophobicity are observed and mechanical properties are in the same order of magnitude in each functionalized surface (including strips), the cell selectivity and spatially controlled cell adhesion is related to the presence of the bioactive sequences existing into the backbone of the ELRs [59]. The ability to spatially control cell adhesion and multicellular organization is critical to many biomedical and tissue-engineering applications and has become increasingly important for the development of cellular biosensor technology and tissue engineering applications.

5. Conclusions

In this study we developed an efficient system for spatial control of cell adhesion for further applications in various research fields. It could be applied in different fields, such as drug discovery, biomedical engineering,

and intercellular applications, as well as to the study of fundamental cell biology and the production of cell-based biosensors and diagnostic devices. Our method is extremely simple and cheap, and is compatible with standard cell culture substrates. Moreover, the presence of bioactive sequences encoded into the backbone of the recombinamers helped us to mimic ligands that allow them interaction when grafted onto a solid substrate. It provides a reliable and accessible tool with sufficient flexibility to address a wide range of biological and engineering problems that require control over the spatial and temporal organization of cells. This two approach provides theoretical cues for futures studies involving the use of other bioactive sequences or growth factors.

6. Acknowledgments

The authors are grateful for the funding from the European Commission (NMP-2014-646075, MSCA-ITN-2014-642687), MINECO of the Spanish Government (PCIN-2015-010, MAT2015-68901-R, MAT2016-78903-R and MAT2016-79435-R), Junta de Castilla y León (VA015U16) and Centro en Red de Medicina Regenerativa y Terapia Celular de Castilla y León.

7. References

[1] S.H. Ku, J.S. Lee, C.B. Park, Spatial control of cell adhesion and patterning throughmussel-inspired surface modification by polydopamine, Langmuir 26 (2010) 15104–15108.

[2] K. von der Mark, J. Park, S. Bauer, P. Schmuki, Nanoscale engineering of biomimetic surfaces: cues from the extracellular matrix, Cell. Tissue. Res. 339 (2010) 131.

[3] H. Shin, S. Jo, A.G. Mikos, Biomimetic materials for tissue engineering, Biomaterials 24 (2003) 4353–4364.

[4] W.F. Liu, C.S. Chen, Cellular and multicellular form and function, Adv. Drug Delivery Rev. 59 (2007) 1319–1328.

[5] F.T. Bosman, I. Stamenkovic, Functional structure and composition of the extracellular matrix, J. Pathol. 200 (2003) 423–428.

[6] B.L. Frey, C.E. Jordan, S. Kornguth, R.M. Corn, Control of the specific adsorption of proteins onto gold surfaces with poly (l-lysine) monolayers, Anal. Chem. 67 (1995) 4452–4457.

[7] J.C. Rodríguez-Cabello, L. Martín, A. Girotti, C. García-Arévalo, F.J. Arias, M. Alonso, Emerging applications of multifunctional elastin-like recombinamers, Nanomedicine 6 (2011) 111–122.

[8] J.C. Rodríguez-Cabello, A. Girotti, A. Ribeiro, F.J. Arias, Synthesis of genetically engineered protein polymers (recombinamers) as an example of advanced self-assembled smart materials, Nanotechnology in Regenerative Medicine, Springer, 2012, pp. 17–38.

[9] A. Ibáñez-Fonseca, T.L. Ramos, I. González de Torre, L.I. Sánchez-Abarca, S. Muntión, F.J. Arias, et al., Biocompatibility of two model elastin-like recombinamer-based hydrogels formed through physical or chemical cross-linking for various applications in tissue engineering and regenerative medicine, J. Tissue Eng. Regen. Med. 12 (2018) e1450–e1460.

[10] R. Machado, A.J. Ribeiro, J. Padrão, D. Silva, A. Nobre, J. Teixeira, et al., Exploiting the sequence of naturally occurring elastin: construction, production and characterization of a recombinant thermoplastic protein based polymer, J. Nano Res. Trans. Tech. Pub. (2009) 133–145.

[11] D.W. Urry, D.C. Gowda, T.M. Parker, C.H. Luan, M.C. Reid, C.M. Harris, et al., Hydrophobicity scale for proteins based on inverse temperature transitions, Biopolym. Original Res. Biomol. 32 (1992) 1243–1250.

[12] I.G. de Torre, A. Ibáñez-Fonseca, L. Quintanilla, M. Alonso, J.-C. Rodríguez-Cabello, Random and oriented electrospun fibers based on a multicomponent, in situ clickable elastin-like recombinamer system for dermal tissue engineering, Acta Biomater. (2018).

[13] A. Girotti, A. Fernández-Colino, I.M. López, J.C. Rodríguez-Cabello, F.J. Arias, Elastin-like recombinamers: biosynthetic strategies and biotechnological applications, Biotechnol. J. 6 (2011) 1174–1186.

[14] M. Pierna, M. Santos, F.J. Arias, M. Alonso, J.C. Rodríguez-Cabello, Efficient cell and cell-sheet harvesting based on smart surfaces coated with a multifunctional and self-organizing elastin-like recombinamer, Biomacromolecules 14 (2013) 1893–1903.

[15] S.C. Heilshorn, K.A. DiZio, E.R. Welsh, D.A. Tirrell, Endothelial cell adhesion to the fibronectin CS5 domain in artificial extracellular matrix proteins, Biomaterials 24 (2003) 4245–4252.

[16] A. Girotti, J. Reguera, J.C. Rodríguez-Cabello, F.J. Arias, M. Alonso, A.M. Testera, Design and bioproduction of a recombinant multi (bio) functional elastin-like protein polymer containing cell adhesion sequences for tissue engineering purposes, J. Mater. Sci. Mater. Med. 15 (2004) 479–484.

[17] A. Mould, A. Komoriya, K. Yamada, M. Humphries, The CS5 peptide is a second site in the IIICS region of fibronectin recognized by the integrin alpha 4 beta 1. Inhibition of alpha 4 beta 1 function by RGD peptide homologues, J. Biolog. Chem. 266 (1991) 3579–3585.

[18] U. Hersel, C. Dahmen, H. Kessler, RGD modified polymers: biomaterials for stimulated cell adhesion and beyond, Biomaterials 24 (2003) 4385–4415.

[19] S.E. D'Souza, M.H. Ginsberg, E.F. Plow, Arginyl-glycyl-aspartic acid (RGD): a cell adhesion motif, Trends Biochem. Sci. 16 (1991) 246–250.

[20] C. García-Arévalo, M. Pierna, A. Girotti, F.J. Arias, J.C. Rodríguez-Cabello, A comparative study of cell behavior on different energetic and bioactive polymeric surfaces made from elastin-like recombinamers, Soft Matter 8 (2012) 3239–3249.

[21] E.T. Demann, P.S. Stein, J.E. Haubenreich, Gold as an implant in medicine and dentistry, J. Long-term Effects Med. Imp. 15 (2005).

[22] E. Pensa, E. Cortés, G. Corthey, P. Carro, C. Vericat, M.H. Fonticelli, et al., The chemistry of the sulfur–gold interface: in search of a unified model, Acc. Chem. Res. 45 (2012) 1183–1192.

[23] D. Qin, Y. Xia, G.M. Whitesides, Soft lithography for micro-and nanoscale patterning, Nature Protocols 5 (2010) 491.

[24] L. Wen-Wen, C. Zhen-Ling, X.-Y. Jiang, Methods for cell micropatterning on twodimensional surfaces and their applications in biology, Chin. J. Anal. Chem. 37 (2009) 943–949.

[25] R.S. Kane, S. Takayama, E. Ostuni, D.E. Ingber, G.M. Whitesides, Patterning proteins and cells using soft lithography, Biomaterials: Silver Jubilee Compendium, Elsevier, 2006, pp. 161–174.

[26] B. Kasemo, Biolog. Surf. Sci. Surf. Sci. 500 (2002) 656–677.

[27] R.E. Russo, X. Mao, J.J. Gonzalez, V. Zorba, J. Yoo, Laser ablation in analytical chemistry, ACS Pub. (2013).

[28] C. Momma, S. Nolte, Chichkov BN, Alvensleben Fv, Tünnermann A. Precise laser ablation with ultrashort pulses, Appl. Surf. Sci. 109 (1997) 15–19.

[29] X. Liu, D. Du, G. Mourou, Laser ablation and micromachining with ultrashort laser pulses, IEEE J. Quant. Elect. 33 (1997) 1706–1716.

[30] J. Yeh, Laser ablation of polymers, J. Vac. Sci. Tech. A Vac. Surf. Films 4 (1986) 653–658.

[31] B.N. Chichkov, C. Momma, S. Nolte, F. Von Alvensleben, A. Tünnermann, Femtosecond, picosecond and nanosecond laser ablation of solids, Appl. Phys. A 63 (1996) 109–115.

[32] A. Vogel, V. Venugopalan, Mechanisms of pulsed laser ablation of biological tissues, Chem. Rev. 103 (2003) 577–644.

[33] M.E. Marques, A.A. Mansur, H.S. Mansur, Chemical functionalization of surfaces for building three-dimensional engineered biosensors, Appl. Surf. Sci. 275 (2013) 347–360.

[34] C. Momma, B.N. Chichkov, S. Nolte, F. von Alvensleben, A. Tünnermann, H. Welling, et al., Short-pulse laser ablation of solid targets, Optics Commun. 129 (1996) 134–142.

[35] M. Shirk, P. Molian, A review of ultrashort pulsed laser ablation of materials, J. Laser Appl. 10 (1998) 18–28.

[36] H. Häkkinen, The gold–sulfur interface at the nanoscale, Nat. Chem. 4 (2012) 443.

[37] K. Rechendorff, M.B. Hovgaard, M. Foss, F. Besenbacher, Influence of surface roughness on quartz crystal microbalance measurements in liquids, J. Appl. phys. 101 (2007) 114502.

[38] F. Höök, B. Kasemo, T. Nylander, C. Fant, K. Sott, H. Elwing, Variations in coupled water, viscoelastic properties, and film thickness of a Mefp-1 protein film during adsorption and cross-linking: a quartz crystal microbalance with dissipation monitoring, ellipsometry, and surface plasmon resonance study, Anal. Chem. 73 (2001) 5796–5804.

[39] T. Smith, The hydrophilic nature of a clean gold surface, J. Coll. Interf. Sci. 75 (1980) 51–55.

[40] B. Crist, A Review of XPS Data-Banks XPS Reports 2007//XPS Reports.–1 (2007) 1–52.

[41] M. Schwartzkopf, A. Hinz, O. Polonskyi, T. Strunskus, F.C. Löhrer, V. Körstgens, et al., Role of sputter deposition rate in tailoring nanogranular gold structures on polymer surfaces, ACS Appl. Mater. Interf. 9 (2017) 5629–5637.
[42] P. Malinský, P. Slepička, V. Hnatowicz, V. Švorčík, Early stages of growth of gold layers sputter deposited on glass and silicon substrates, Nanoscale Res. Lett. 7 (2012) 241.

[43] K.K. Kanazawa, J.G. Gordon, Frequency of a quartz microbalance in contact with liquid, Anal. Chem. 57 (1985) 1770–1771.

[44] G. Dunér, E. Thormann, A. Dėdinaitė, Quartz Crystal Microbalance with Dissipation (QCM-D) studies of the viscoelastic response from a continuously growing grafted polyelectrolyte layer, J. Collid Interf. Sci. 408 (2013) 229–234.

[45] A. Granéli, M. Edvardsson, F. Höök, DNA-Based Formation of a Supported, Three-Dimensional Lipid Vesicle Matrix Probed by QCM-D and SPR, ChemPhysChem 5 (2004) 729–733.

[46] M. Rodahl, B. Kasemo, On the measurement of thin liquid overlayers with the quartz-crystal microbalance, Sens. Actuat. A Phys. 54 (1996) 448–456.

[47] A. Mechler, S. Praporski, K. Atmuri, M. Boland, F. Separovic, L.L. Martin, Specific and selective peptide-membrane interactions revealed using quartz crystal microbalance, Biophys. J. 93 (2007) 3907–3916.

[48] C.M. Bailey, E. Kamaloo, K.L. Waterman, K.F. Wang, R. Nagarajan, T.A. Camesano, Size dependence of gold nanoparticle interactions with a supported lipid bilayer: A QCM-D study, Biophys. Chem 203 (2015) 51–61.

[49] S.B. Nielsen, D.E. Otzen, Quartz Crystal Microbalances as Tools for Probing Protein- Membrane Interactions, Lipid-Protein Interactions, Springer, 2013, pp. 1–21.

[50] T. Kacar, M.T. Zin, C. So, B. Wilson, H. Ma, N. Gul-Karaguler, et al., Directed selfimmobilization of alkaline phosphatase on micro-patterned substrates via genetically fused metal-binding peptide, Biotechnol. Bioeng. 103 (2009) 696–705.

[51] J. Malmström, H. Agheli, P. Kingshott, D.S. Sutherland, Viscoelastic modeling of highly hydrated laminin layers at homogeneous and nanostructured surfaces: quantification of protein layer properties using QCM-D and SPR, Langmuir 23 (2007) 9760–9768.
[52] S.P. Massia, J.A. Hubbell, Vascular endothelial cell adhesion and spreading promoted by the peptide REDV of the IIICS region of plasma fibronectin is mediated by integrin alpha 4 beta 1, J. Biolog. Chem. 267 (1992) 14019–14026.

[53] B.V. Crist, A review of XPS data-banks, XPS Reports 1 (2007).

[54] M.-C. Bourg, A. Badia, R.B. Lennox, Gold− sulfur bonding in 2D and 3D self-assembled monolayers: XPS characterization, J. Phys. Chem. B 104 (2000) 6562–6567.

[55] M.L. Yola, N. Atar, A novel voltammetric sensor based on gold nanoparticles involved in p-aminothiophenol functionalized multi-walled carbon nanotubes: application to the simultaneous determination of quercetin and rutin, Electrochim. Acta 119 (2014) 24–31.

[56] J.R. Reimers, M.J. Ford, S.M. Marcuccio, J. Ulstrup, N.S. Hush, Competition of van der Waals and chemical forces on gold–sulfur surfaces and nanoparticles, Nature Rev. Chem. 1 (2017) 0017.

[57] M.J. Humphries, S.K. Akiyama, A. Komoriya, K. Olden, K.M. Yamada, Identification of an alternatively spliced site in human plasma fibronectin that mediates cell typespecific adhesion, J. Cell Biol. 103 (1986) 2637–2647.

[58] N. Faucheux, R. Schweiss, K. Lützow, C. Werner, T. Groth, Self-assembled monolayers with different terminating groups as model substrates for cell adhesion studies,Biomaterials 25 (2004) 2721–2730.

[59] Y. Lu, S. Chen, Micro and nano-fabrication of biodegradable polymers for drug delivery, Adv. Drug Delivery Rev. 56 (2004) 1621–1633.

8. Supporting Information

Characterization of materials

1. SDS-PAGE electrophoresis

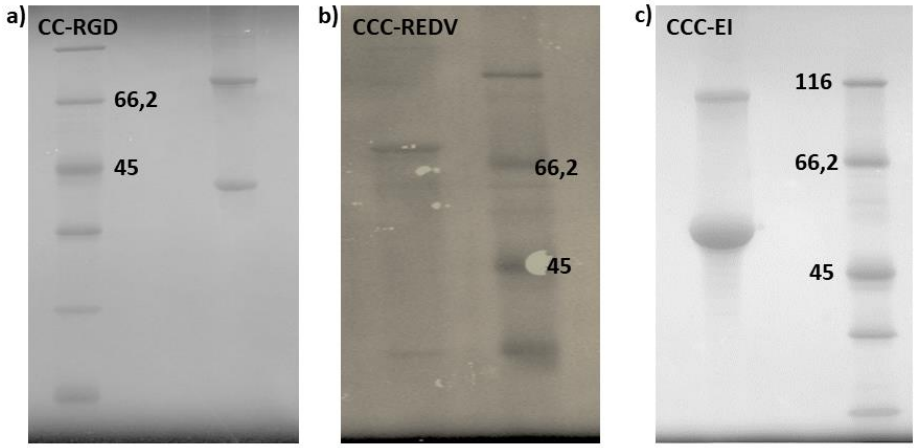

Figure S1. SDS PAGE electrophoresis of a) CC-RGD b) CCC-REDV c) CCC-EI

2. Amino acid analysis

CCC-REDV			CCC-EI		CC-RGD	
AA	Experimental	Teoric	Experimental	Teoric	Experimental	Teoric
D	25.81	25			6.53	6
E	50.28	50	11.31	10	2.64	3
S					11.33	12
H	15.82	16				
G	213.51	210	225.43	224	168.90	168
T					4.96	4
R	10.55	10			4.61	4

A					**10.58**	**11**
Y	**19.98**	**20**				
C	**3.20**	**3**	**3**	**3**	**3.39**	**3**
V	**110.27**	**111**	**149.31**	**150**	**78.77**	**80**
M	**0.4**	**1**	**0.39**	**1**	**0.25**	**1**
I	**95.49**	**100**	**59.82**	**60**	**64.39**	**64**
L	**9.75**	**10**			**3.70**	**4**
K	**11.51**	**12**			**16.86**	**16**
P	**119.86**	**120**	**109.09**	**110**	**85.71**	**85**

Table S1. Aminoacidic composition of CCC-REDV, CCC-EI and CC-RGD

3. Differential scanning calorimetry (DSC)

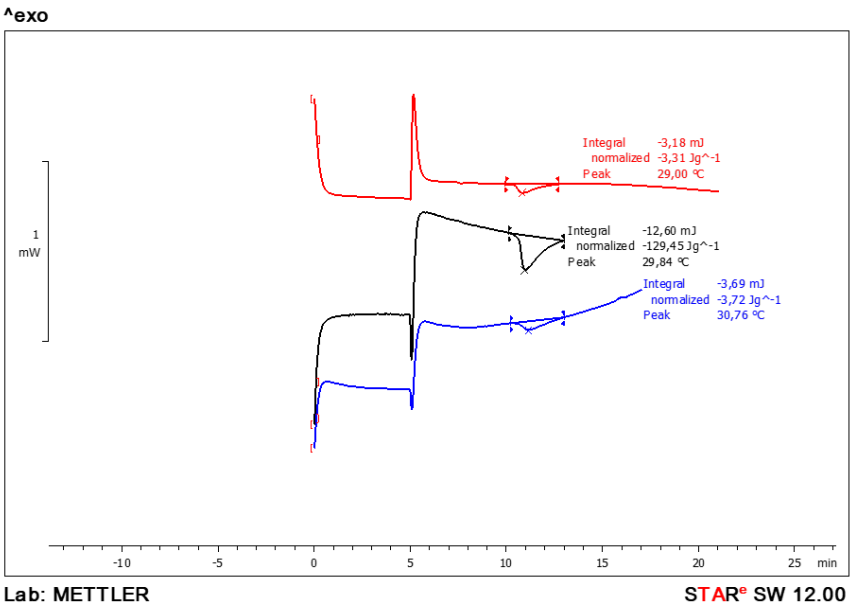

Figure S2. DSC thermograms of the solutions in PBS of CCC-REDV, CCC-EI and CC-RGD (from top to bottom).

4. Fourier transformation infrared spectroscopy (FTIR)

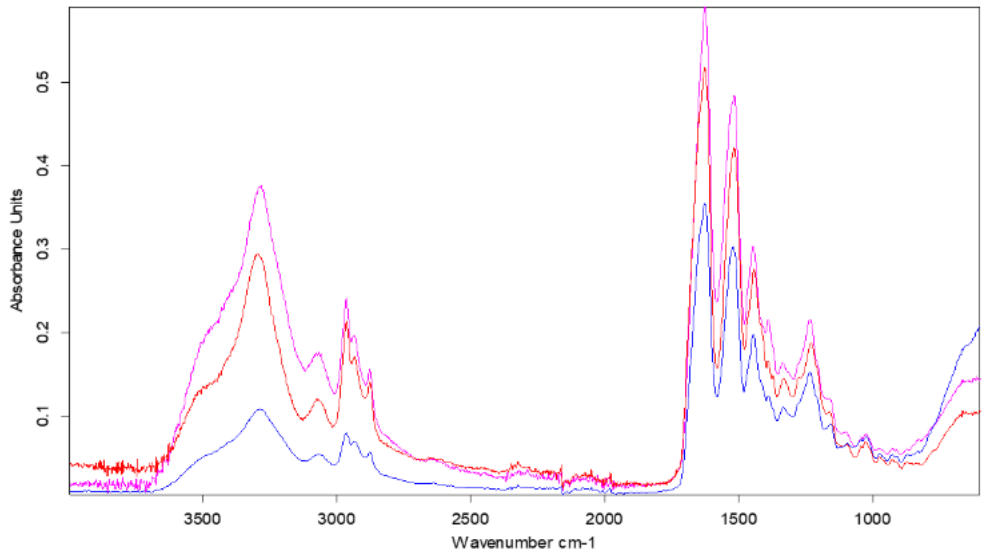

Figure S4. FTIR spectrum of a) CC-RGD b) CCC-REDV c) CCC-EI

5. Matrix-assisted Laser Desorption/Ionization Time-of-flight (MALDI TOF)

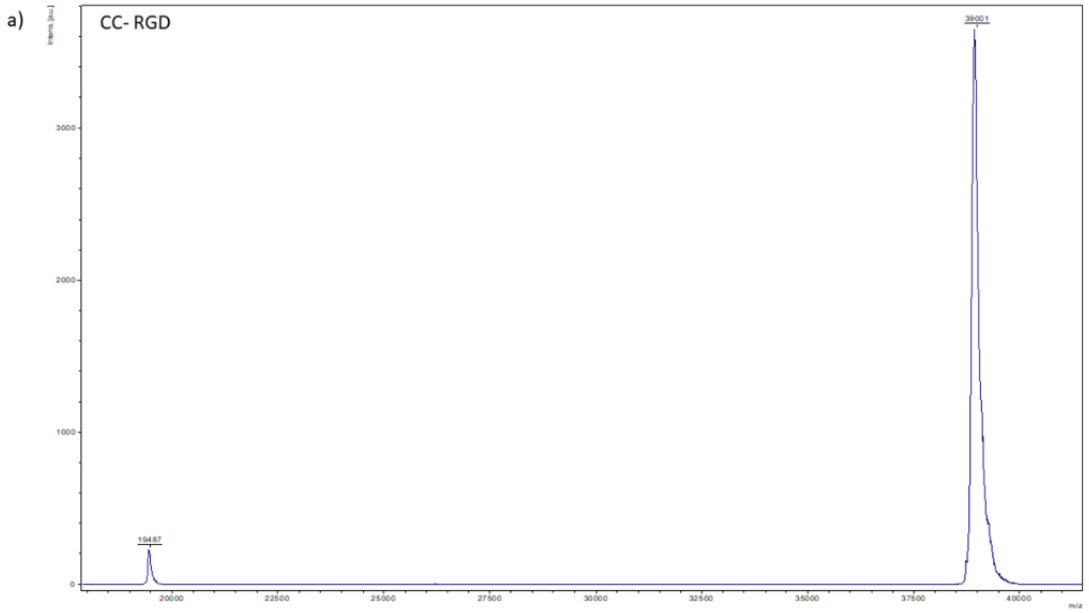

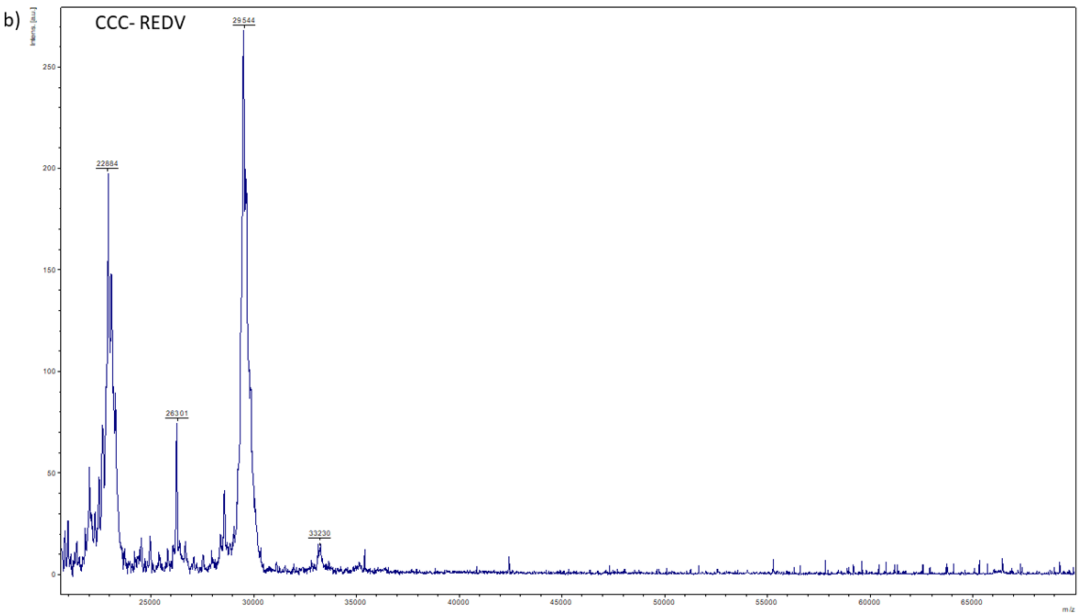

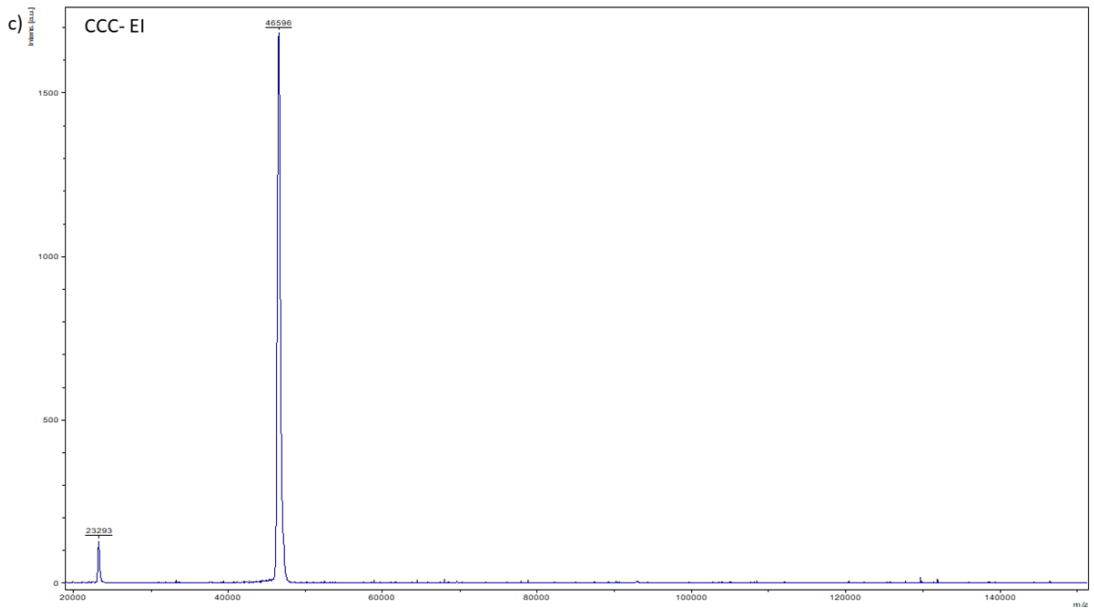

Figure S5. MALDI TOF spectrum of a) CC-RGD b) CCC-REDV c) CCC-EI

6. Nuclear magnetic resonance (NMR)

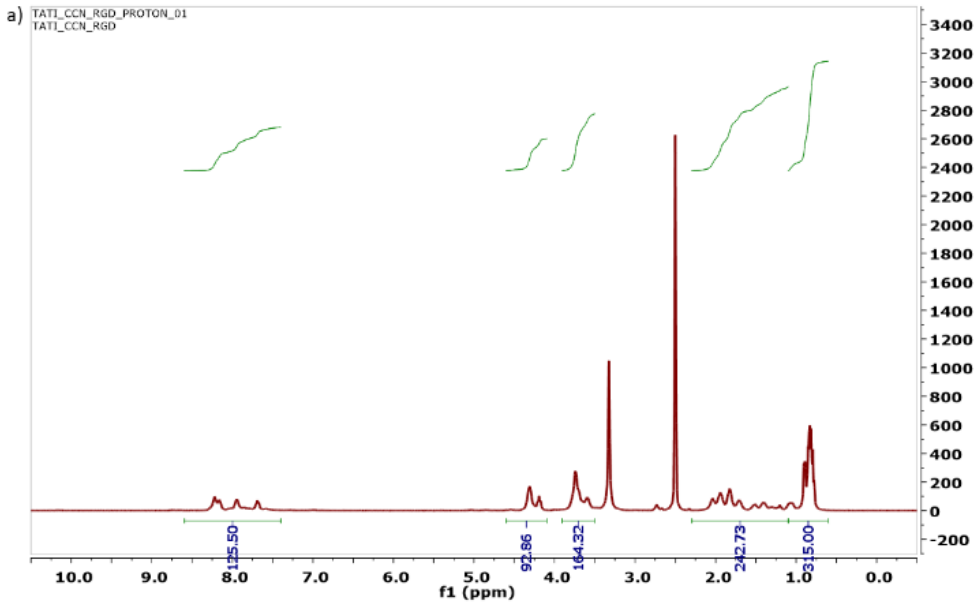

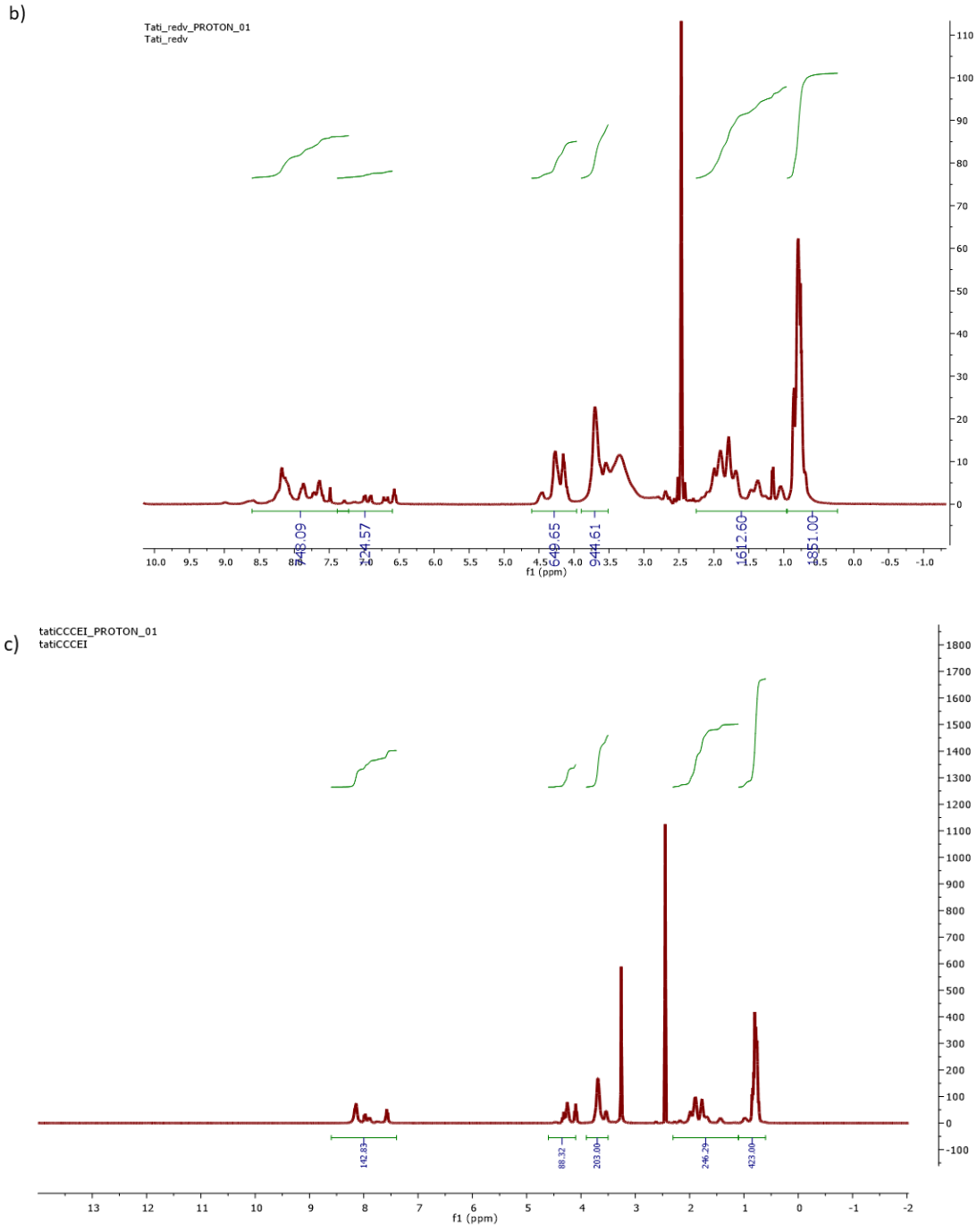

Figure S5. NMR spectrum of a) CC-RGD b) CCC-REDV c) CCC-EI

7. X-Ray photoelectron spectroscopy (XPS)

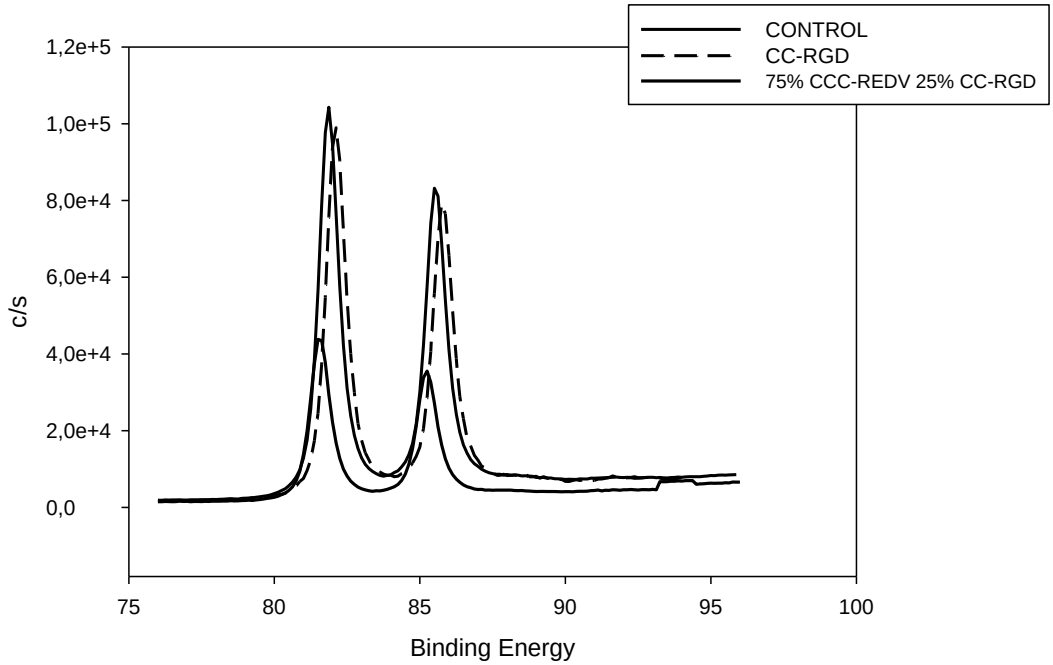

Figure S6. XPS spectrum of bare Au, 100% CC-RGD and 75% CCC-REDV 25% CC-RGD.

8. Quartz crystal microbalance with dissipation (QCM-D)

a)

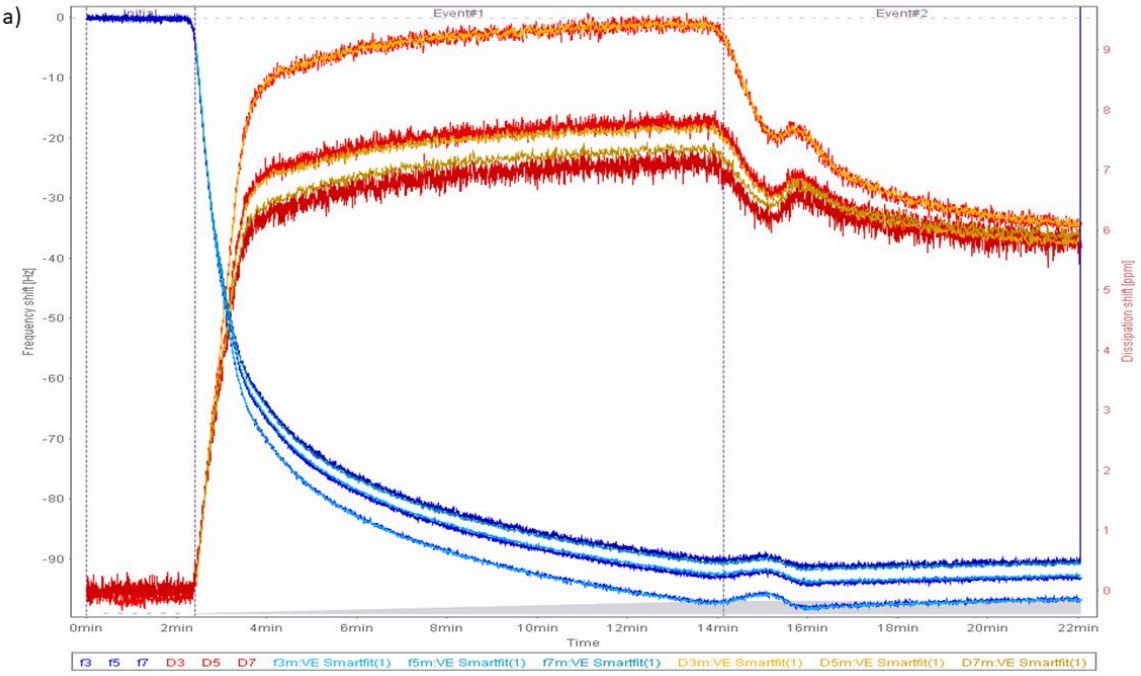

b)

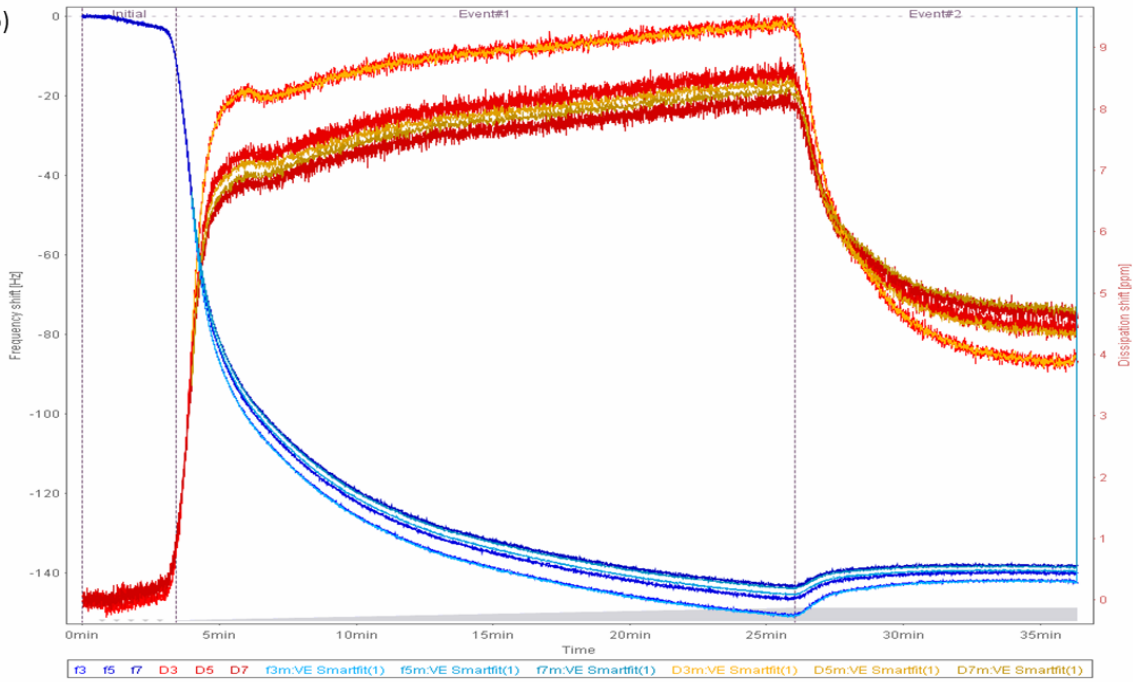

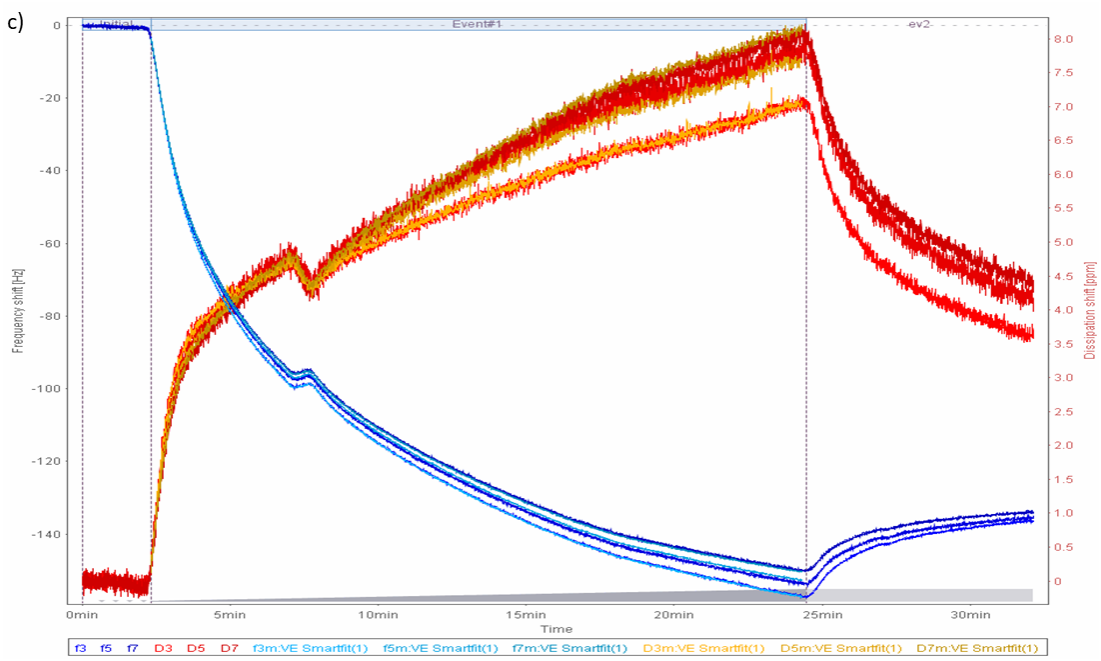

Figure. S7. QCM-D measurements. Dependence of the frequency and energy dissipation changes on the time (flow of the polymer solution: 20 min.). Both the raw (frequency, blue: f3, f5, and f7; dissipation, red: D3, D5, and D7) and Voight viscoelastic model fitted (VE Smartfit) data are shown. Only the overtones corresponding to n = 3, 5, and 7 are displayed for clarity, but the overall fitting includes all the harmonic up to the 13rd. a) Pure CC RGD ($\chi^2 < 4$), b) pure CCC REDV ($\chi^2 < 4$), and c) 75%REDV-25%RGD ($\chi^2 < 2$).

CHAPTER 2

TETHERING QK PEPTIDE TO ENHANCE ANGIOGENESIS IN ELASTIN-LIKE RECOMBINAMER (ELR) HYDROGELS

Tatjana Flora, [1] Israel González de Torre, [2] Matilde Alonso, [1] José Carlos Rodríguez-Cabello,[1]

[1] BIOFORGE, CIBER-BBN, Universidad de Valladolid, Spain

[2] Technical Proteins NanoBioTechnology (TPNBT) S.L., Valladolid, Spain

Flora, Tatjana, et al. "Tethering QK peptide to enhance angiogenesis in elastin-like recombinamer (ELR) hydrogels." *Journal of Materials Science: Materials in Medicine* 30.2 (2019): 30.

Abstract

The development of new capillary networks in engineered constructs is essential for their survival and their integration with the host tissue. It has recently been demonstrated that ELR-based hydrogels encoding different bioactivities are able to modulate their interaction with the host after injection or implantation, as indicated by an increase in cell adhesion and the ability to trigger vascularization processes. Accordingly, the aim of this study was to increase their angiogenic ability both *in vitro* and *in vivo* using a small VEGF mimetic peptide named QK, which was tethered chemically to ELR-based hydrogels containing cell-adhesion sequences in their backbone, such as REDV and RGD, as well as a proteolytic site (VGVAPG). *In vitro* studies were performed using a co-culture of endothelial and fibroblast cells encapsulated into the ELR-based hydrogels in order to determine cell proliferation after 21 days of culture, as well as the number of cell-cell interactions. It was found that although the presence of this peptide does not influence the morphological and rheological properties of these hydrogels, it has an effect on cell behaviour, inducing an increase in cell proliferation and the formation of endothelial cell clusters. *In vivo* studies demonstrate that the QK peptide enhances the formation of prominent functional capillaries at three weeks post-injection, as confirmed by H&E staining and CD31

immunohistochemistry. The newly formed functional microvasculature ensures perfusion and connection with surrounding tissues. These results show that ELR-QK hydrogels increase capillary network formation and are therefore attractive candidates for application in tissue regeneration, for example for the treatment of cardiovascular diseases such as myocardial infarction or ischemia.

1. Introduction

Tissue engineering is an interdisciplinary therapeutic field that aims to repair or even replace damaged tissues and organs, thus resulting in the recovery of their integrity and functionality. This discipline meets tissue- and organ-related medical needs by developing engineered constructs that are able to restore or enhance tissue or organ function. [1] Scaffolds for use in vascular tissue engineering, for example hydrogels, simulate most of the required properties for these tissues, thus making them ideal supports for the promotion of tissue regeneration. [2, 3] The presence of a network of vessel-like structures is essential in engineered constructs for the diffusion of nutrients and oxygen, thus providing a pro-angiogenic environment suitable for cell survival and tissue growth. [4] Neovascularization is obtained as a result of marked cell infiltration into the hydrogels, which can be facilitated by the presence of adhesion sequences that increase the quantity of cells, specifically endothelial cells in this case, along with proteolytic target sequences. These latter sequences are particularly important as they allow enzymatic degradation of the scaffold, thus favouring an adequate space to support extensive angiogenesis. [5]

Elastin-like recombinamer (ELR)-based hydrogels are the most recent engineered constructs to have found a use in biomedicine and biotechnology as a result of their potential angiogenic properties. [6] [7] The presence of distinct bioactivities encoded into their backbone results in an increase in cell adhesion, thus contributing to an enhanced release of angiogenic factors and subsequent endothelial cell organization. [8] Moreover, these systems are characterized by other important properties, such as excellent biocompatibility, non-immunogenicity, optimal biomechanical properties and an ability to respond to different stimuli. [9] They also mimic the elastic properties of natural tissues due to the presence of elastin, which is crucial in tissue regeneration since it is one of the main components of the extracellular matrix (ECM). [10] [11]

ELRs are obtained using recombinant DNA technologies that allow a clear-cut, complex and absolute control of the sequences, thus providing an ability to include different bioactive sequences, such as those guiding cell adhesion, differentiation and protease sensitivity. They are characterized by a self-assembly behaviour associated with a conformational re-organization at the molecular level. Thus, whereas the polymer chains are soluble in water below a transition temperature, above this temperature they self-assemble into nano- and micro-aggregates and become insoluble. This process is completely reversible. [12] [13, 14]

In this work, the bioactivity of the ELR-based hydrogels was enhanced using two cell-adhesion sequences, namely RGD (arginine-glycine-aspartate) and REDV (arginine-glutamic-aspartate-valine), which were coded into their amino acid sequences. Various studies have shown that the RGD sequence promotes the attachment of different cell types and is the principal integrin-binding domain present within ECM proteins such as fibronectin, vitronectin, fibrinogen, osteopontin, and bone sialoprotein. [8] [15] [16-18] In contrast, the REDV sequence, which is derived from fibronectin, binds to endothelial cells selectively via integrin a4b1 and is well known to promote endothelial cell adhesion and migration when immobilized to a wide variety of biomaterials. [19] [20]

Furthermore, the proteolytic site VGVAPG (valine-glycine-valine-alanine-proline-glycine), which is coded into one of the ELRs employed in this work, is known for its chemotactic activity with respect to various cell types, such as monocytes or fibroblasts, and it also upregulates metalloproteinases and is sensitive to proteolysis by elastolytic enzymes. [21]

Various approaches are currently used to achieve better vascularization in scaffolds, such as implanting scaffolds with endothelial cells, the use of growth factors and the provision of a *vascularized* tissue. [22] [23] [24] Vascular endothelial growth factor (VEGF) is the main regulator of

neovascularization and, specifically, $VEGF_{165}$ is known to stimulate vascularization both *in vitro* and *in vivo*. [25] Several studies have demonstrated that the use of growth factor proteins has several inherent disadvantages, such as immunogenicity, lower stability and loss of bioactivity, therefore the use of shorter bioactive peptide sequences derived from a growth factor protein that confer the same bioactivity and cellular response is becoming increasingly common. [26]

A vascular mimetic peptide known as QK has been widely studied as a promising candidate for the promotion and control of angiogenesis in tissue-engineering constructs. Indeed, it has been shown to possess a similar biological activity to VEGF as regards its ability to induce capillary formation and organization. In this regard, D'Andrea et al. designed and synthesized QK peptide and demonstrated that this peptide has a stable helical conformation in aqueous solution and that an alpha helix conformation to bind the ligand-receptor site is necessary for its functionality. QK is a synthetic 15-amino acid peptide based on the 17-25 alpha region of $VEGF_{165}$ that binds to the main VEGF receptors, such as VEGFR-1 and VEGFR-2, and is required for the cell signalling pathway step in VEGF-R modulated angiogenesis. [27] [28] [29]

Although initially used only as a locally delivered soluble factor, QK peptide has demonstrated promising therapeutic outcomes. Furthermore,

it has been immobilized to hydrogels and been shown to retain its bioactivity under all conditions tested. [30, 31] [32] This peptide provides different advantages, especially a smaller size, ease of use in chemical reactions, lesser likelihood of triggering an immune response, and an ability to be more easily modified to include variations that allow the tuning of a biomimetic matrix system.

The current study aims to demonstrate enhancement of the angiogenic activity of ELR-based hydrogels bearing a VEGF-mimetic peptide (QK peptide) both *in vitro* and *in vivo*, thus providing an alternative to the use of growth factor proteins in angiogenic signalling. Moreover, the inclusion of bioactive sequences such as RGD and REDV favours cell adhesion and the proteolytic site VGVAPG favours a customised cell biodegradation, which is an essential pre-requisite for hydrogels in tissue-engineering applications. Cell behaviour was initially studied *in vitro* employing a co-culture of human umbilical vein endothelial cells (HUVEC) and human foreskin fibroblasts (HFF1), comparing the biological activity of hydrogels with a tethered QK peptide (ELR-QK) with that of hydrogels with soluble VEGF (ELR-VEGF) and with control hydrogels, in this case a factor-free ELR hydrogel (ELR).

Subsequent *in vivo* studies were performed in mice by injecting cell-free ELR-based hydrogels (factor-free ELR and ELR-QK hydrogel)

intramuscularly into a hind limb region in order to determine if the presence of this pro-angiogenic peptide enhances the formation of new functional capillaries within the hydrogels, which were detected by immunofluorescence staining with CD31.

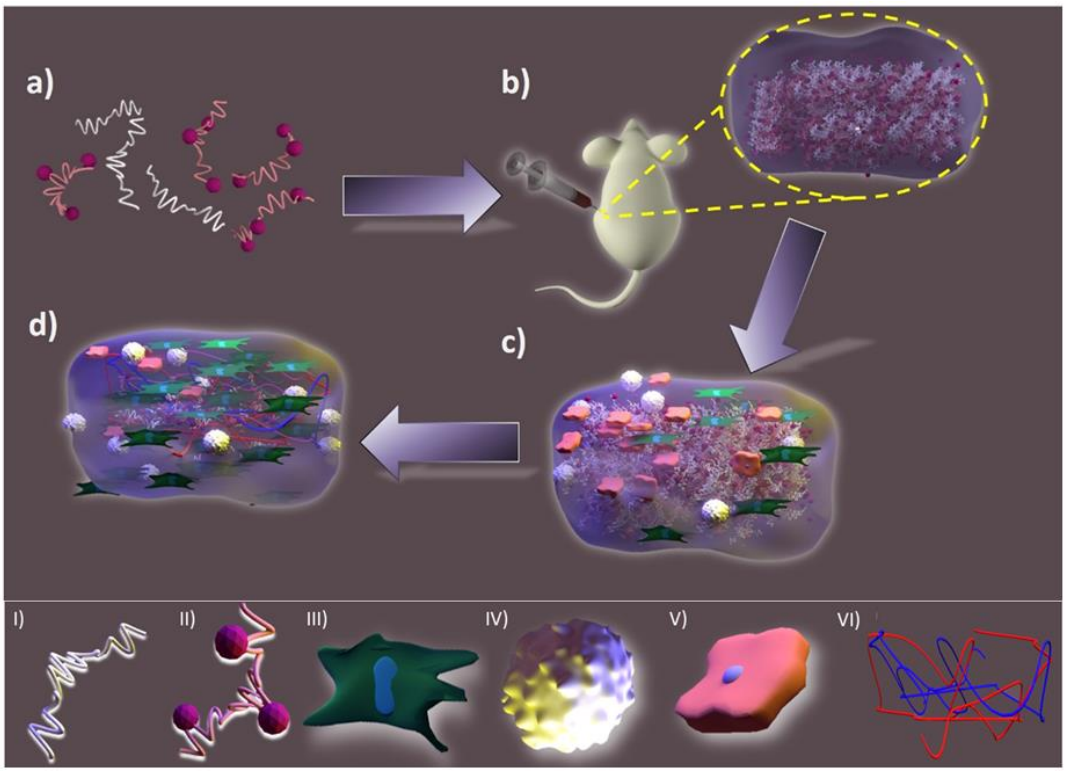

Figure 1. Schematic representation of a) composition of ELR-based hydrogel (REDV-ELR + RGD-QK ELR) b) ELR-QK hydrogel injected in mice c) ELR-QK hydrogel invaded by different cell type d) formation of new capillaries into the hydrogel

I) REDV-ELR II) RGD-QK ELR III) fibroblast cells IV) immune cells V) HUVEC cells VI) capillaries

2. Materials and Methods

2.1 ELR bio-production, modification and characterization

The ELRs used in this work have been previously described elsewhere. [33, 34] Briefly, they were produced using a 15-L bioreactor and purified using a process known as Inverse Transition Cycling (ITC), which involves several cycles of precipitation (heating) and resuspension (cooling) of the supernatant. The final product obtained was dialysed against deionized water with several changes and freeze-dried prior to storage. The ELRs obtained were characterized by SDS-PAGE electrophoresis, HNMR and FTIR spectroscopy and DSC. Two different ELRs, namely HRGD and REDV, were employed in this study. Chemical modification of these ELRs was achieved using click chemistry and their degree of modification confirmed by NMR and FTIR spectroscopy, respectively. (Figure S5-S6, Supporting Information)

2.2 QK peptide and recombinant human $VEGF_{165}$

QK peptide (KLTWQELYQLKYKGI) was purchased from BACHEM (Switzerland) as a white powder. This peptide presents an azide group in the amino terminal region (5-Azido-pentanoyl-Lys-Lys-Leu-Thr-Trp-Gln-Glu-Leu-Tyr-Gln-Leu-Lys-Tyr-Lys-Gly-Ile-OH), which can be reacted with RGD-ELR previously modified with a cyclootyne group via a click reaction. The resulting recombinamer, known as RGD-QK, was

characterized by NMR and FTIR spectroscopy, DSC and MALDI-TOF, thus confirming that QK peptide was correctly bound to the recombinamer (Figure S1-S4, Supporting Information). Recombinant Human Vascular Endothelial Growth Factor ($VEGF_{165}$) was purchased from Lonza (Madrid) in a soluble form.

2.4 Mechanical and morphological properties of ELR-based hydrogels

The chemically modified ELRs were crosslinked for subsequent formation of the hydrogels via a click reaction. Thus, the recombinamers, with a concentration of 50 mg/mL, were dissolved in PBS 1X and mixed at 4 °C. Specific molds were used to form the hydrogels, and the reaction mixture was maintained at 4 °C for 20 minutes to allow crosslinking. The VEGF hydrogels (ELR-VEGF) were prepared in an identical manner, with the sole difference that the human recombinant $VEGF_{165}$ was added to the endothelial cell growth medium at a concentration of 10 ng/mL, as per the literature. [35]

The elastic modulus of the hydrogels was measured using a TA Instruments AR2000 stress-controlled rheometer equipped with a 12 mm diameter load plate, at 1% strain and 37 °C. The hydrogels were kept in PBS to avoid sample shrinking below the diameter of the plate upon heating. Oscillatory experiments were performed within the linear

viscoelasticity region, where storage (G') and loss (G'') moduli are independent of the stress magnitude. Three different hydrogels were tested (n = 3).

Scanning electron microscopy (SEM) was used to investigate their morphology. Thus, hydrogels with a concentration of 50 mg/mL were dropped into liquid nitrogen, physically fractured, and subsequently freeze-dried. Micrographs were obtained using a scanning electron microscope (FEI Quanta 200 FEG) in low vacuum mode at 3 keV. Morphological details were evaluated quantitatively using the ZEN (Blue Edition, 2012) software package (Carl Zeiss Microscopy).

2.4 Cell cultures

Human umbilical vein endothelial cells (HUVEC) were purchased from Lonza (Madrid, Spain) and were cultured in EGM-2 medium (M200500, Life Technologies S.A, Madrid, Spain) supplemented with EGM-2 Single Quot Kit Suppl. & Growth Factor (Lonza, Madrid, Spain) at 37 °C and 5% CO_2. Human foreskin fibroblast (HFF1) were purchased from Life Technologies S.A. (Madrid, Spain) and were cultured in DMEM medium supplemented with 15% FBS and 100 U/100 mg/mL penicillin/streptomycin at 37 °C and 10% CO_2. Cells between passages 2 and 4 were used in all experiments.

2.5 *In vitro* 3D proliferation tests and histological analysis

For *in vitro* studies, recombinamers with a concentration of 50 mg/mL were dissolved in EGM-2 medium and mixed at 4 °C. $10*10^6$/mL of HUVEC and $3*10^6$/mL of HFF1 cells were added to previously prepared ELR hydrogels. The hydrogels were formed in 96-well plates, with 45 µL of each recombinamer being mixed and kept at 4 °C for 20 minutes to allow crosslinking prior to subsequent addition of basal medium for the QK-hydrogels and with recombinant human $VEGF_{165}$ for the VEGF-hydrogels. The 96-well plate containing the hydrogels was incubated at 37 °C and 5% CO_2 for 21 days. All measurements were carried out in triplicate. Media were replaced every day for all the hydrogels. After incubation for 21 days, the hydrogels were fixed in 10% formalin for 4 hours, then dehydrated by immersion in ethanol solutions of increasing concentration, and then in xylene solution. Finally, they were immersed in paraffin for 3 hours and stored at -20 °C overnight. All samples were sliced on a microtome and stained with Haematoxylin-Eosin following a general protocol. [36]

2.6 Ethical approval

Experimental procedures involving the use of animals were approved by the Animal Care and Use Committee of the University of Valladolid in

accordance with Directive 2010/63/EU of the European Union and Spanish Royal Decree RD 53/2013.

2.7 *In vivo* studies

Swiss C57 mice (male) were used for intramuscular injection of the hydrogels. They were anesthetized by inhalation of isoflurane at 3%. The ELRs were mixed in an eppendorf immediately prior to injection, and were injected cell-free using a 1 mL syringe with a 20G needle. Animals were sacrificed at 21 days post-injection.

2.8 Histological analysis of *in vivo* studies

After 21 days, the presence of ELR-based hydrogels was confirmed by the existence of a solid material at the injection site. They were extracted and processed for histological analysis. Specimens were fixed in 10% formalin at 4 °C for 24 h and subsequently dehydrated by immersion in ethanol solutions from 70% to 100%, finishing with two changes in xylene solution. The hydrogels were subsequently embedded in paraffin for 6 h and cut with a microtome. The resulting specimens were placed on slides and deparaffinised, with subsequent immersion in xylene, ethanol solutions of decreasing concentration and, finally, in distilled water. Samples were evaluated by H&E staining to get a general overview of cellular invasion.

2.9 Immunohistochemistry

Specimens were immunostained using a goat polyclonal primary PECAM antibody (Santa Cruz Biotechnology, USA) at a concentration of 1 µg/mL in 1% blocking serum (donkey serum) and with a donkey anti-goat fluorescein-conjugated secondary antibody (Santa Cruz Biotechnology, USA). During each step, the samples were washed three times with PBS 0.1 M for three minutes each. A vectashield HardSet Antifade Mounting Medium with DAPI (Vector Laboratories, USA) was used to stain cell nuclei. All images were acquired using a fluorescent microscope.

2.10 Statistical Analysis

Results are reported as means ± standard error of the mean (n = 3). Data were evaluated statistically using a one-way analysis of variance, applying the Holm–Sidak method. A p value of less than 0.05 was considered statistically significant. n.s.d indicates no significant differences.

3. Results

3.1 Morphological and rheological properties

Variation of the linear viscoelastic range due to the presence of growth factors was measured rheologically in hydrogels at a concentration of 50 mg/mL. Three samples, namely factor-free hydrogel (ELR), ELR-VEGF, and ELR-QK hydrogels were tested in this study. The strain sweep was evaluated in the range 0.6–10 Pa and was found to remain independent of the strain amplitude up to values of about 7-8%. Figure 2 shows the trend in complex modulus for all hydrogels at a frequency of 1 Hz, with 1% strain and at a temperature of 37 °C. No significant differences were found between the samples, all of which exhibit a similar complex modulus of around 1100 Pa.

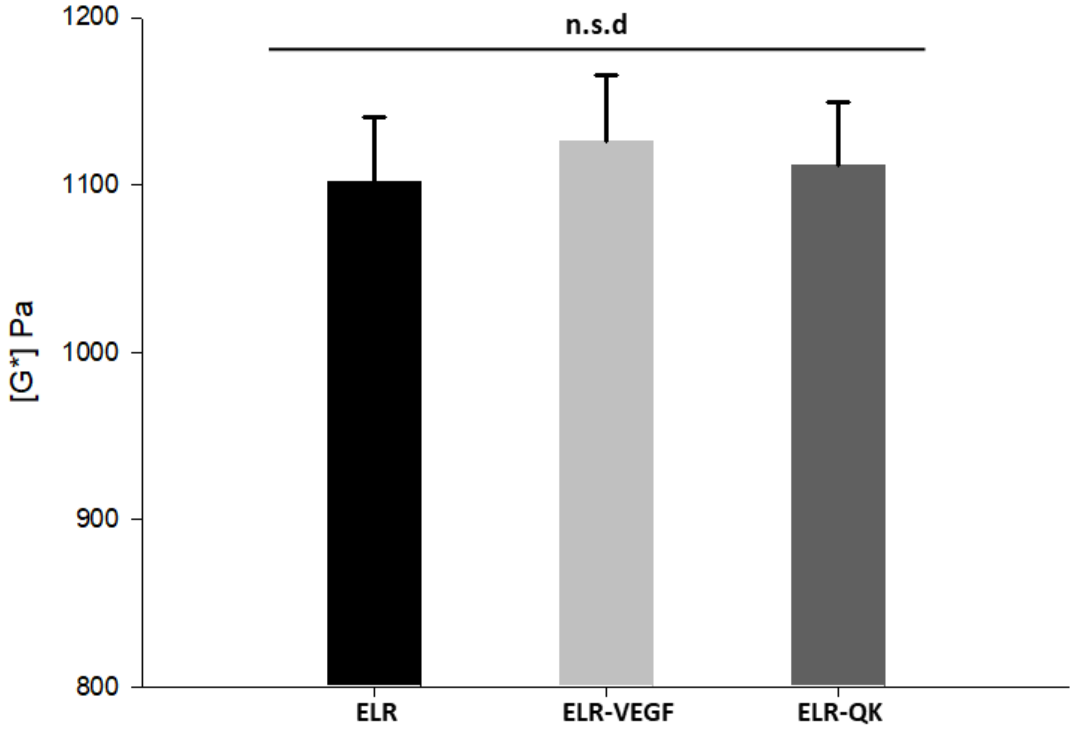

Figure 2. Graphical representation of the complex elastic modulus [G*] for: factor-free ELR hydrogel (ELR); ELR hydrogel with soluble VEGF protein (ELR-VEGF) and ELR hydrogel with QK peptide tethered chemically (ELR-QK). Statistical analysis was carried out by performing an analysis of variance using the Holm–Sidak method. *p<0.05; n.s.d no significant differences.

SEM micrographs for the factor-free hydrogel (ELR) (a), ELR-VEGF (b) and ELR-QK (c) hydrogels can be found in Figure 3. These structures exhibit high porosity and well-interconnected pore networks with a pore size of between 12 and 15 µm. These results demonstrated that the

presence of the peptide and growth factor do not affect their morphology. Similar experimental results have been reported in a previous study of ELR-based catalyst-free click hydrogels. [33] [37, 38]

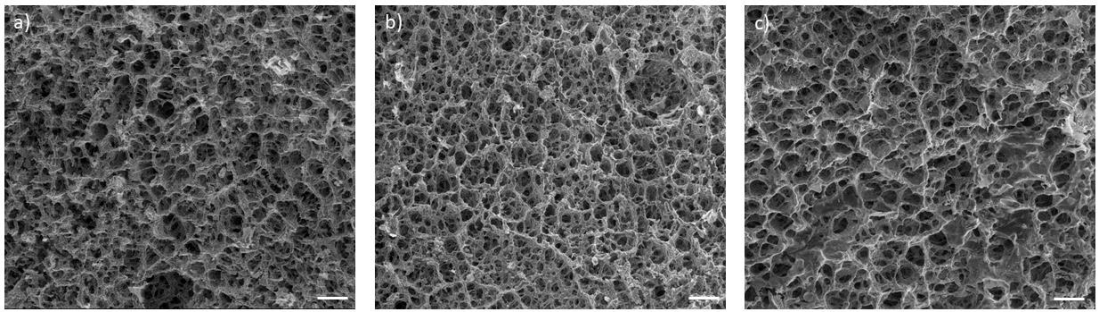

Figure 3. Representative SEM images for freeze-dried cross-sectional sections of: a) factor-free ELR hydrogel; b) ELR-VEGF and c) ELR-QK hydrogel. Scale bar: 50μm.

3.2 *In vitro* 3D cell proliferation assay

In accordance with the literature, the pro-angiogenic activity of QK peptide was evaluated *in vitro* employing endothelial cells and fibroblasts encapsulated into the hydrogels in a proportion of 3:1, respectively. [39] Figure 4 shows H&E staining images for factor-free hydrogel (ELR) (a1), ELR-VEGF (a2) and ELR-QK hydrogel (a3) after culture for 21 days. These images demonstrate that all hydrogels exhibit good cytocompatibility at three weeks given the number of cells present. It is also clear that they exhibit different trends in terms of cell proliferation,

with the factor-free ELR hydrogel containing a lower number of cells than for the ELR-VEGF and ELR-QK hydrogels. These latter two samples exhibit similar trends in terms of cell proliferation, with only a minor difference between the ELR-QK and ELR-VEGF hydrogels. The number of cells/cm^2 was quantified for each sample by applying Image J to the H&E staining images. Specifically, the number of cells is 245±22 for factor-free ELR hydrogel, 382±35 for ELR-VEGF and 375±29 for ELR-QK hydrogels, as shown graphically in Figure 5. As can be seen, there is no significant difference between ELR-VEGF and ELR-QK hydrogels in terms of cell proliferation, whereas the factor-free ELR hydrogel contains a much lower number of cells at three weeks.

Moreover, the ELR-VEGF and ELR-QK hydrogels exhibit various regions containing adherens junctions (indicated with a black arrow in Figure 4-b2 and Figure 4-b3, respectively). These junctions are required for correct organization of the new capillaries formed.

CD31 immunofluorescence staining was also performed to confirm the presence of endothelial cell junctions as this protein has been reported to be able to mediate cell-cell adhesion. [40] The images shown in Figure 6 (a1-a2-a3) indicate that all hydrogels exhibit marked CD31 expression, albeit with significant differences between them. Thus, CD31 expression in ELR-VEGF (Figure 6-a2) and ELR-QK hydrogels (Figure 6-a3) is

significantly higher than in factor-free ELR hydrogels (Figure 6-a1). A similar behaviour, namely that the number of cells which form clusters is higher in VEGF-ELR and QK-ELR than in factor free ELR hydrogels, the latter of which present a lower number of fused cells, was observed in samples stained with H&E.

Despite these differences, it can be seen that factor-free ELR hydrogels (Figure 6-a1) still contain CD31 expression cells due to the presence of bioactive sequences such as RGD and REDV, which enhance cell adhesion and endothelial cell organization *in vitro*. Nevertheless, the difference between this latter sample and ELR-VEGF and ELR-QK hydrogels lies in the number of endothelial cell clusters formed. Thus, in ELR-VEGF (Figure 6-a2) and ELR-QK (Figure 6-a3) hydrogels, endothelial cells form a large number of cell aggregates or clusters in unorganized assemblies of more than five cells, whereas factor-free ELR hydrogels are characterized mainly by containing single cells within the hydrogel.

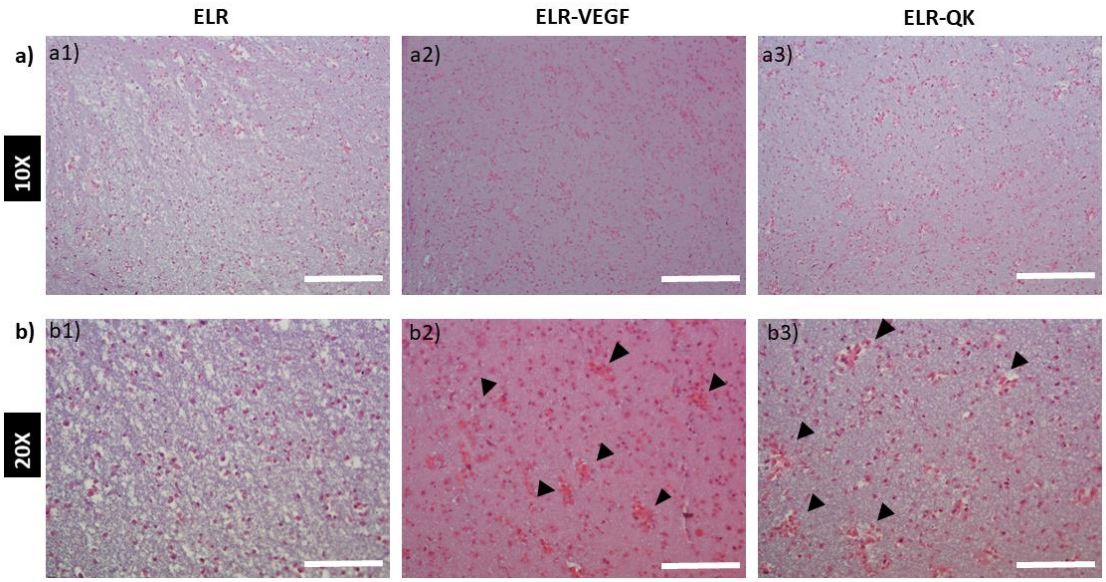

Figure 4. H&E staining with 10X magnification of: a1) factor-free ELR hydrogel (ELR); (a2) ELR-VEGF; and (a3) ELR-QK hydrogel after co-culturing HUVEC and HFF1 cells for 21 days. b) 20X Magnification of: b1) factor-free ELR hydrogel (ELR); b2) ELR-VEGF; and b3) ELR-QK hydrogels. Black arrows indicate the presence of endothelial cells clusters. Scale bar: 500µm.

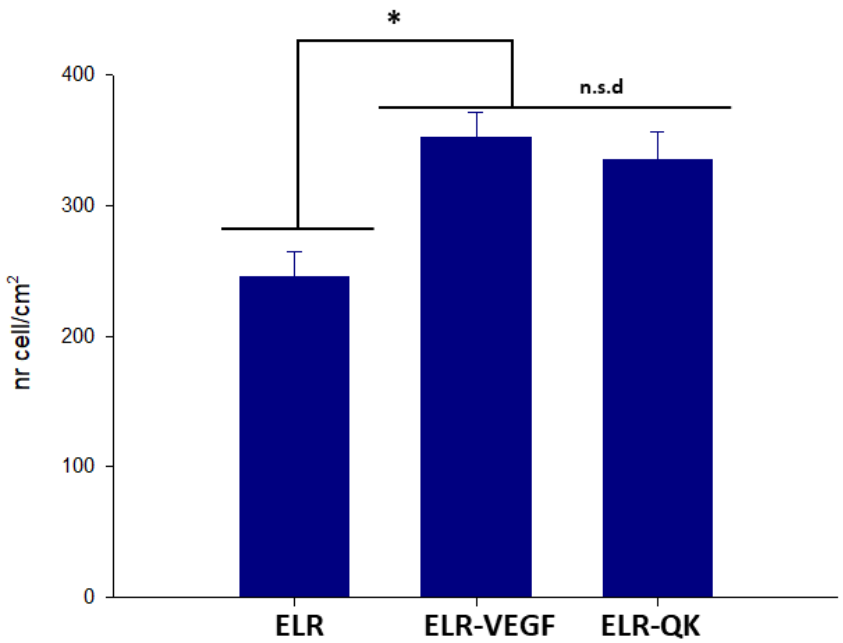

Figure 5. Graphical representation of number of cells/cm^2, as counted using Image J. Data are reported as mean ± SD (n=3). Statistical analysis was carried out by performing an analysis of variance using the Holm–Sidak method. *p<0.05; n.s.d., no significant difference.

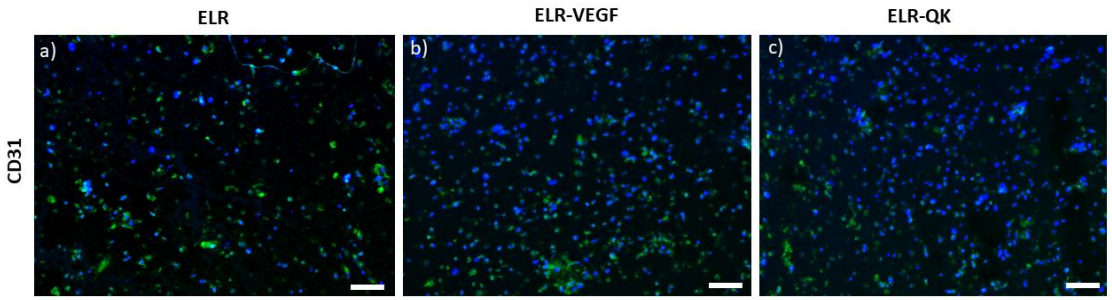

Figure 6. CD31 immunostaining of: a) factor-free ELR hydrogel (ELR); (b) ELR-VEGF; and (a3) ELR-QK hydrogel. Blue: DAPI staining. Green: CD31 expression. Scale bar: 50µm.

3.3 *In vivo* behaviour of QK peptide

The formation of new vasculature in the ELR hydrogels enhanced by QK peptide was evaluated *in vivo* using mice in which hydrogels were injected into a hind limb region. Two main samples, namely a factor-free ELR hydrogel (ELR) and ELR-QK hydrogel, were used for the *in vivo* analysis. This choice was based on the previous *in vitro* results, which demonstrated that the soluble VEGF and VEGF-mimetic peptides (QK peptide) exhibit similar biological activities.

To get an overview of cell invasion in ELR hydrogels, histological H&E staining was performed; the corresponding images are shown in Figure 7 (factor-free ELR hydrogel (7a) and ELR-QK hydrogel (7b)). ELR-hydrogels are surrounded by a discontinuous line and labelled with the letter H, whereas host tissue is indicated with a letter T. Figures 7c and 7d, which are magnifications of Figures 7a and 7b, respectively, both show good biocompatibility as the hydrogels are well infiltrated by different cell types at three weeks post-injection.

The hydrogels were entirely present up to 21 days, thus indicating early host cell infiltration, although there were clear differences between them. Thus, in ELR-QK hydrogels (Figure 7b), the cells reached the center of the hydrogel after three weeks, whereas the factor-free ELR hydrogel (Figure 7a) presented different areas that are almost intact, thus indicating

a lack of cellular infiltration. This becomes clearer in Figure 8a, which is a magnification of a non-infiltrated area.

Upon initial inspection, this difference suggests that QK peptide facilitates the recruitment of cells and tissue integration and increases the rate of cell migration.

A closer examination of the ELR-QK sample stained with H&E (Figure 7d) indicated the formation of new capillaries with a uniform distribution inside the hydrogel. These new capillaries are indicated in Figure 7d with a black arrow, and the magnification in Figure 8b shows the presence of red blood cells forming the lumen of blood vessels surrounded by endothelial cells. [X] The size of the new capillaries formed varies between 25- and 50 μm. The total number of capillaries present in the hydrogel (>30) is significantly higher than for the factor-free ELR hydrogel. Indeed, new capillaries are completely absent from the factor-free ELR hydrogel (Figure 7a). This does not mean that they cannot be formed, however, simply that more time is needed for both complete colonization and for the organization of endothelial cells.

To further confirm new capillary formation in the scaffolds, CD31 protein expression was also determined by immunohistochemical staining, which allowed us to confirm the presence of endothelial cells junction. (Figure 9) As shown in Figure 9e-9f, the new capillaries (indicated by the presence

of green florescence) are located in the ELR-QK hydrogel, which contrasts with the situation for the factor-free ELR hydrogel, Figure 9b-9c.

QK peptide therefore stimulates angiogenesis and enhances cellular migration, and therefore subsequent capillary structure formation, *in vivo*. These results agree with those obtained *in vitro* upon triggering the auto-phosphorylation of $VEGFR_2$ intracellular domains, which leads to the induction of HUVEC proliferation, survival and migration. [41]

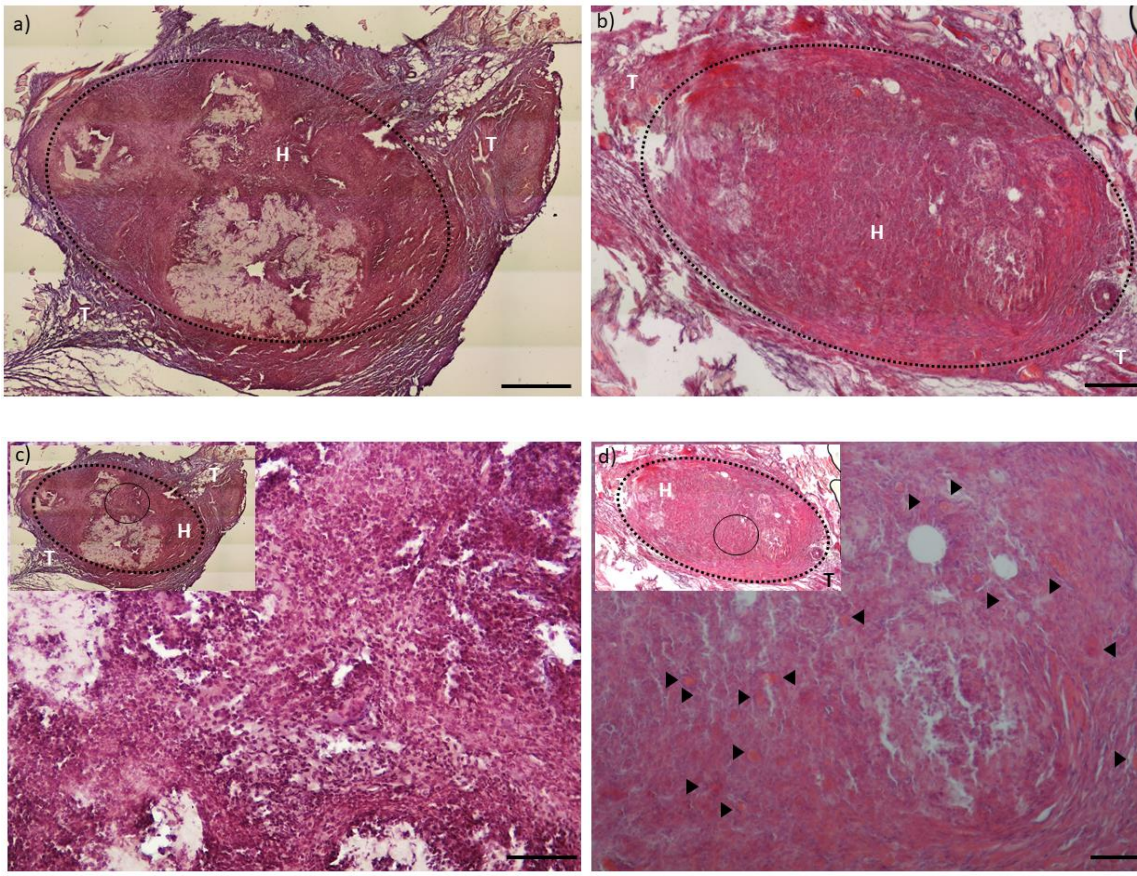

Figure 7. H&E staining images of: a) ELR factor-free hydrogel; and b) ELR-QK hydrogel; c) magnification 20X of image a); d) magnification 20X of image b). The black arrows indicate the presence of capillaries formed. Scale bar: 100µm

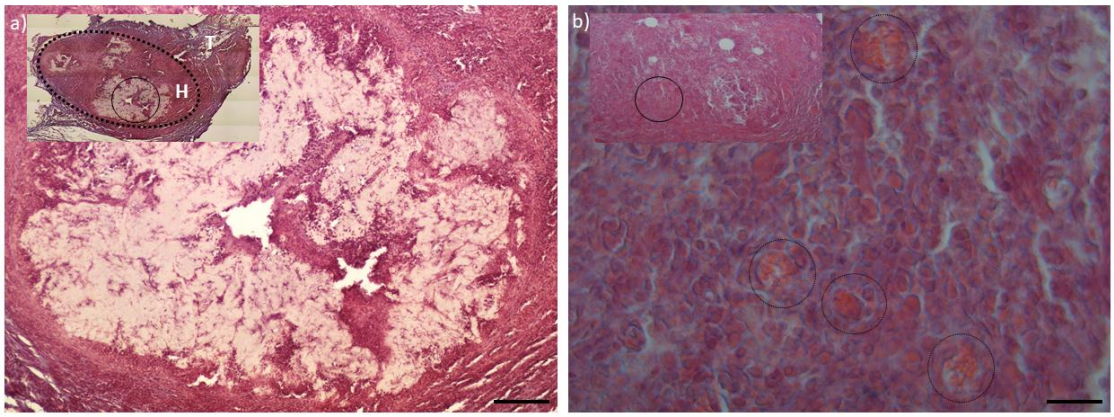

Figure 8. Magnification of H&E staining images of a non-colonized area of ELR factor-free hydrogel, which is indicated with a black circle. b) Magnification of ELR-QK hydrogel image in Figure 7b to better visualize the presence of new capillaries. Scale bar: 100µm.

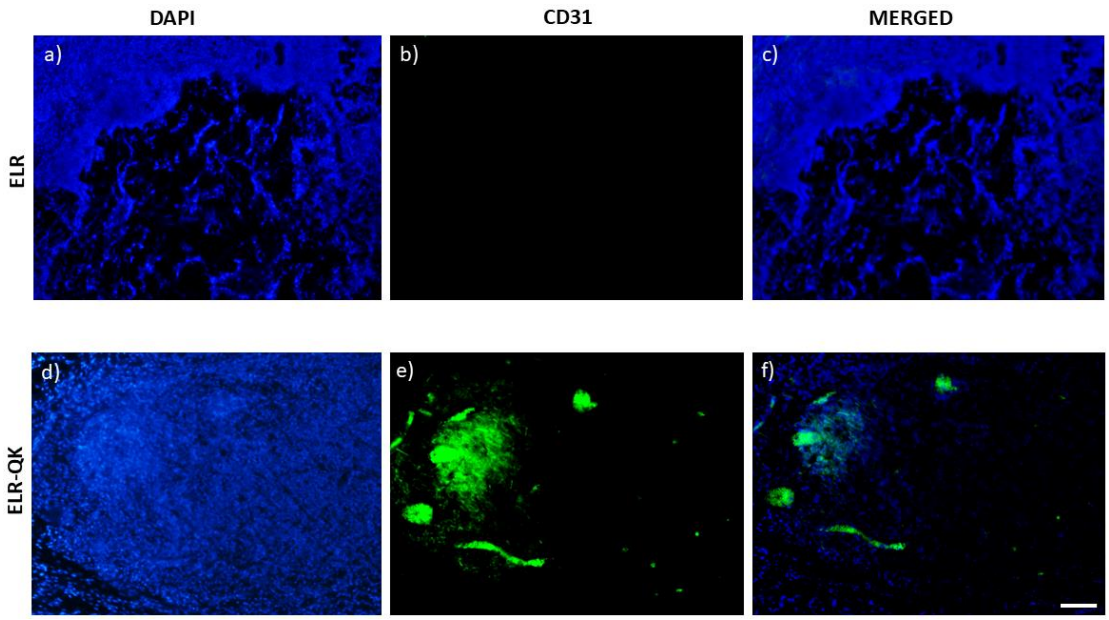

Figure 9. CD31 immunofluorescent staining images of: a-b-c) factor free ELR hydrogel (ELR) d-e-f) ELR-QK hydrogel. DAPI: nucleus staining (9a; 9d). CD31: expression of CD31 protein (9b; 9e). MERGED: merged channels (DAPI+CD31) (9c; 9f). Scale bar for all the images: 50 μm.

4. Discussion

In recent years, one of the most important efforts undertaken to achieve functional vascularization in scaffolds utilized in tissue engineering has involved modulating angiogenesis by targeting VEGF and its receptors. [22] Indeed, a VEGF mimetic peptide known as QK is commonly used to improve vascularization into 3D scaffolds as this protein has been demonstrated to exhibit pro-angiogenic activity *in vitro* and *in vivo* by binding to VEGFRs, thus initiating VEGF-induced signalling cascades and giving rise to the formation of new capillaries. [42, 43]

In this study, we proposed the use of QK peptide tethered chemically to ELR-based hydrogels via a click reaction to enhance vascularization within engineered constructs, which is also favoured by the presence of two main adhesion sequences, namely the universal cell-adhesion sequence RGD and a specific sequence for endothelial cells (REDV), encoded into their backbone. Moreover, the presence of the VGVAPG sequence codified into the recombinamer chains favours the chemotactic

ability of monocytes and facilitates biodegradation of the ELR-based hydrogels by increasing their sensitivity to elastolytic enzymes. [8]

Several previous studies reported in the literature used small peptides such as RGD and the collagen-binding CMP domain bonded chemically to PEG scaffolds to increase cell adhesion and proliferation. [44] The proteinaceous nature of ELRs results in an absolute control over the amino acid sequences, thus allowing codification of the adhesion sequences into their backbone and overcoming the limitations that may be presented by these chemically bonded peptides. [45] In addition, proteolytic biodegradation is an essential feature for promoting cellular infiltration, which subsequently induces an enhanced cellular migration into the scaffold.

It has been shown herein that the presence of QK peptide does not affect the mechanical properties of the ELR-based hydrogels or their morphological features, although it significantly alters cell behaviour, such as proliferation, in the hydrogels. In light of this, we studied its biological activity *in vitro* using a co-culture of HUVEC and HFF1 cells, demonstrating that this peptide enhances cell proliferation, which in turn gives rise to the development of cell clusters and, subsequently, the formation of capillary structures. The use of a co-culture is mandatory before *in vivo* studies to confirm the biocompatibility of the hydrogels as

well as their influence on *in vitro* angiogenesis. [46] These cell types were employed since they are the most widely used in angiogenesis assays given that the majority of ECM components produced provide support for capillary-like structure formation.

A quantitative analysis involving *in vitro* assays showed that QK peptide has a similar biological activity to the soluble VEGF used as positive control. Moreover, an estimation of cell numbers in a histological section of ELR-QK, ELR-VEGF and factor-free ELR hydrogels confirmed that the former two samples contained similar numbers of cells and demonstrated significant differences with respect to factor-free ELR hydrogels. These studies allowed us to determine that the presence of QK peptide enhances cell proliferation.

Small peptides have many benefits with respect to large proteins, such as a lack of denaturation, structural stability, ease of synthesis, absence of a need for a secondary conformation to preserve their biological activity, and they tend to be characterized by the absence of immunogenicity and toxicity. [47] Furthermore, the constant delivery of growth factors from a hydrogel to obtain the optimal concentrations and gradients required for precise spatial-temporal control remains a big challenge even though several strategies, such as covalent binding, use of carriers, electrostatic interactions, etc., have been used. [48] A major limitation of natural

growth factors is their short effective half-life, low stability, and rapid deactivation of their specialized properties by enzymes at body temperature. In this regard, our *in vitro* studies confirmed that QK peptide mimics the biological activity of VEGF when tethered chemically, inducing angiogenesis-related behaviour such as cell proliferation, cell-cell contact and the formation of capillary-like structures. The advantage of a chemically tethered peptide is that its concentration is controlled over time instead of a soluble growth factor.

Subsequent *in vivo* studies involved the intramuscular injection of hydrogels into mice. At three weeks post-injection the ELR-QK hydrogels were completely infiltrated by different cell types. Moreover, although inflammatory cells were still present at 21 days post-injection, there was no corresponding chronic inflammatory response. It has been widely demonstrated that inflammatory cells play a crucial role in restoring vascular networks as a result of reconstruction of the ECM, fusion of endothelial cells and increasing collagen synthesis. Macrophages and fibroblasts tend to degrade hydrogel networks and produce type I collagen, thus resulting in the gradual replacement of the hydrogel by regenerated tissue. In addition, the enzymatic degradation of these gels caused by the presence of proteolytic sites enhances the cellular invasion response and consequent formation of new micro-vasculature. [49]

There is a noticeable difference between the factor-free ELR and ELR-QK hydrogels. Firstly, the former was not completely invaded by cells, as demonstrated by the presence of intact regions from which cells were absent. In contrast, the entire ELR-QK hydrogel was invaded by cells and the formation of new functional blood vessels was clearly visible. To confirm the formation of new vasculature, CD31 immunostaining was performed to confirm the presence of this vasculature at the same position as observed with H&E staining.

This study therefore reveals that an angiogenic stimulus is important for the replacement of hydrogels by vascularized tissues and confirms that small peptides, such as QK peptide, behave in a similar manner as their larger VEGF counterpart, in other words by activating the canonical pathway in VEGF signalling. Combination of the *in vivo* data with the *in vitro* findings indicates that the presence of QK peptide enhances the formation of new vasculature in ELR-based hydrogels and could therefore give rise to a new design process for biomimetic cellular environments, thus highlighting their advantages compared to the use of soluble growth factors such as VEGF.

In light of the above, ELR-based hydrogels are promising constructs for future applications in tissue engineering, especially in cardiovascular disease, since they exhibit significant pro-angiogenic activity and allow

the inclusion of several functionalities that are required for the tissue-repair process and for the formation of new vasculature.

5. Conclusions

This study has demonstrated that a VEGF mimetic peptide (QK peptide), tethered chemically into ELR-based hydrogels and injected into a hind limb region in mice, enhances the formation of new capillaries within the constructs. It has also been established that QK peptide affects the biological behavior of the cells in a similar manner to VEGF, as seen from the increase in pro-angiogenic activity (endothelial cell proliferation, migration and organization) in the ELR constructs. The *in vivo* findings showed that a functional microvasculature was obtained in QK hydrogels, thus providing a pro-angiogenic environment for cell survival and tissue growth. The approach described herein provides new insights that could be applied to a wide range of cardiovascular diseases requiring a spatial-temporal control of growth factors. It also provides useful cues that could be utilized in both therapeutic angiogenesis and in other clinical models where the presence of new vasculature is essential.

6. Acknowledgement

The authors are grateful for the funding from the European Commission (NMP-2014-646075, PITN-GA-2012-317306), MINECO of the Spanish Government (PCIN-2015-010, MAT2015-68901-R, MAT2016-78903-

R), Junta de Castilla y León (VA015U16) and Centro en Red de Medicina Regenerativa y Terapia Celular de Castilla y León.

7. References

[1] Jenkins DD, Yang GP, Lorenz HP, Longaker MT, Sylvester KG. Tissue engineering and regenerative medicine. Clinics in plastic surgery. 2003;30:581-8.

[2] Place ES, Evans ND, Stevens MM. Complexity in biomaterials for tissue engineering. Nature materials. 2009;8:457.

[3] Dhandayuthapani B, Yoshida Y, Maekawa T, Kumar DS. Polymeric scaffolds in tissue engineering application: a review. International journal of polymer science. 2011;2011.

[4] Lovett M, Lee K, Edwards A, Kaplan DL. Vascularization strategies for tissue engineering. Tissue Engineering Part B: Reviews. 2009;15:353-70.

[5] West JL, Moon JJ. Vascularization of engineered tissues: approaches to promote angiogenesis in biomaterials. Current topics in medicinal chemistry. 2008;8:300-10.

[6] Javier Arias F, Santos M, Fernández-Colino A, Pinedo G, Girotti A. Recent contributions of elastin-like recombinamers to biomedicine and nanotechnology. Current topics in medicinal chemistry. 2014;14:819-36.

[7] MacEwan SR, Chilkoti A. Elastin-like polypeptides: Biomedical applications of tunable biopolymers. Peptide Science: Original Research on Biomolecules. 2010;94:60-77.

[8] Girotti A, Fernández-Colino A, López IM, Rodríguez-Cabello JC, Arias FJ. Elastin-like recombinamers: Biosynthetic strategies and biotechnological applications. Biotechnology journal. 2011;6:1174-86.

[9] Chilkoti A, Christensen T, MacKay JA. Stimulus responsive elastin biopolymers: applications in medicine and biotechnology. Current opinion in chemical biology. 2006;10:652-7.

[10] Urry DW, Parker TM, Reid MC, Gowda DC. Biocompatibility of the bioelastic materials, poly (GVGVP) and its γ-irradiation cross-linked matrix: summary of generic biological test results. Journal of Bioactive and Compatible Polymers. 1991;6:263-82.

[11] Ibáñez-Fonseca A, Ramos TL, González de Torre I, Sánchez-Abarca LI, Muntión S, Arias FJ, et al. Biocompatibility of two model elastin-like recombinamer-based hydrogels formed through physical or chemical cross-linking for various applications in tissue engineering and regenerative medicine. Journal of tissue engineering and regenerative medicine. 2018;12:e1450-e60.

[12] Urry DW. Entropic elastic processes in protein mechanisms. I. Elastic structure due to an inverse temperature transition and elasticity due to internal chain dynamics. Journal of protein chemistry. 1988;7:1-34.

[13] Urry DW, Luan CH, Parker TM, Gowda DC, Prasad KU, Reid MC, et al. Temperature of polypeptide inverse temperature transition depends on mean residue hydrophobicity. Journal of the American Chemical Society. 1991;113:4346-8.

[14] Urry DW, Gowda DC, Parker TM, Luan CH, Reid MC, Harris CM, et al. Hydrophobicity scale for proteins based on inverse temperature transitions. Biopolymers: Original Research on Biomolecules. 1992;32:1243-50.

[15] Girotti A, Reguera J, Rodríguez-Cabello JC, Arias FJ, Alonso M, Testera AM. Design and bioproduction of a recombinant multi (bio) functional elastin-like protein polymer containing cell adhesion sequences for tissue engineering purposes. Journal of Materials Science: Materials in Medicine. 2004;15:479-84.

[16] Wang F, Li Y, Shen Y, Wang A, Wang S, Xie T. The functions and applications of RGD in tumor therapy and tissue engineering. International journal of molecular sciences. 2013;14:13447-62.

[17] Ruoslahti E. RGD and other recognition sequences for integrins. Annual review of cell and developmental biology. 1996;12:697-715.

[18] D'Souza SE, Ginsberg MH, Plow EF. Arginyl-glycyl-aspartic acid (RGD): a cell adhesion motif. Trends in biochemical sciences. 1991;16:246-50.

[19] Heilshorn SC, DiZio KA, Welsh ER, Tirrell DA. Endothelial cell adhesion to the fibronectin CS5 domain in artificial extracellular matrix proteins. Biomaterials. 2003;24:4245-52.

[20] Massia SP, Hubbell JA. Vascular endothelial cell adhesion and spreading promoted by the peptide REDV of the IIICS region of plasma fibronectin is mediated by integrin alpha 4 beta 1. Journal of Biological Chemistry. 1992;267:14019-26.

[21] Hubbell JA, Massia SP, Desai NP, Drumheller PD. Endothelial cell-selective materials for tissue engineering in the vascular graft via a new receptor. Nature biotechnology. 1991;9:568.

[22] Papavasiliou G, Cheng M-H, Brey EM. Strategies for vascularization of polymer scaffolds. BMJ Publishing Group Limited; 2010.

[23] Kaully T, Kaufman-Francis K, Lesman A, Levenberg S. Vascularization—the conduit to viable engineered tissues. Tissue Engineering Part B: Reviews. 2009;15:159-69.

[24] El-Sherbiny IM, Yacoub MH. Hydrogel scaffolds for tissue engineering: Progress and challenges. Global Cardiology Science and Practice. 2013:38.

[25] Testa U, Pannitteri G, Condorelli GL. Vascular endothelial growth factors in cardiovascular medicine. Journal of Cardiovascular Medicine. 2008;9:1190-221.

[26] Lee K, Silva EA, Mooney DJ. Growth factor delivery-based tissue engineering: general approaches and a review of recent developments. Journal of the Royal Society Interface. 2011;8:153-70.

[27] D'Andrea LD, Iaccarino G, Fattorusso R, Sorriento D, Carannante C, Capasso D, et al. Targeting angiogenesis: structural characterization and biological properties of a de novo engineered VEGF mimicking peptide. Proceedings of the National Academy of Sciences. 2005;102:14215-20.

[28] Diana D, Ziaco B, Colombo G, Scarabelli G, Romanelli A, Pedone C, et al. Structural determinants of the unusual helix stability of a de novo engineered vascular endothelial growth factor (VEGF) mimicking peptide. Chemistry–A European Journal. 2008;14:4164-6.

[29] Ziaco B, Diana D, Capasso D, Palumbo R, Celentano V, Di Stasi R, et al. C-terminal truncation of Vascular Endothelial Growth Factor mimetic helical peptide preserves structural and receptor binding properties. Biochemical and biophysical research communications. 2012;424:290-4.

[30] Wang L, Zhao M, Li S, Erasquin UJ, Wang H, Ren L, et al. “Click” immobilization of a VEGF-mimetic peptide on decellularized endothelial extracellular matrix to enhance angiogenesis. ACS applied materials & interfaces. 2014;6:8401-6.

[31] Leslie-Barbick JE, Saik JE, Gould DJ, Dickinson ME, West JL. The promotion of microvasculature formation in poly (ethylene glycol) diacrylate hydrogels by an immobilized VEGF-mimetic peptide. Biomaterials. 2011;32:5782-9.

[32] Cai L, Dinh CB, Heilshorn SC. One-pot synthesis of elastin-like polypeptide hydrogels with grafted VEGF-mimetic peptides. Biomaterials science. 2014;2:757-65.

[33] de Torre IG, Santos M, Quintanilla L, Testera A, Alonso M, Cabello JCR. Elastin-like recombinamer catalyst-free click gels: characterization of poroelastic and intrinsic viscoelastic properties. Acta biomaterialia. 2014;10:2495-505.

[34] Staubli SM, Cerino G, De Torre IG, Alonso M, Oertli D, Eckstein F, et al. Control of angiogenesis and host response by modulating the cell adhesion properties of an Elastin-Like Recombinamer-based hydrogel. Biomaterials. 2017;135:30-41.

[35] Nakatsu MN, Sainson RC, Pérez-del-Pulgar S, Aoto JN, Aitkenhead M, Taylor KL, et al. VEGF 121 and VEGF 165 regulate blood vessel diameter through vascular endothelial growth factor receptor 2 in an in vitro angiogenesis model. Laboratory investigation. 2003;83:1873.

[36] Fischer AH, Jacobson KA, Rose J, Zeller R. Hematoxylin and eosin staining of tissue and cell sections. Cold Spring Harbor Protocols. 2008;2008:pdb. prot4986.

[37] Fernández-Colino A, Wolf F, Keijdener H, Rütten S, Schmitz-Rode T, Jockenhoevel S, et al. Macroporous click-elastin-like hydrogels for tissue engineering applications. Materials Science and Engineering: C. 2018;88:140-7.

[38] Testera AM, Girotti A, de Torre IG, Quintanilla L, Santos M, Alonso M, et al. Biocompatible elastin-like click gels: design, synthesis and characterization. Journal of Materials Science: Materials in Medicine. 2015;26:105.

[39] Bishop ET, Bell GT, Bloor S, Broom I, Hendry NF, Wheatley DN. An in vitro model of angiogenesis: basic features. Angiogenesis. 1999;3:335-44.

[40] Ilan N, Cheung L, Pinter E, Madri JA. Platelet-endothelial cell adhesion molecule-1 (CD31), a scaffolding molecule for selected catenin family members whose binding is mediated by different tyrosine and serine/threonine phosphorylation. Journal of Biological Chemistry. 2000;275:21435-43.

[41] Abhinand CS, Raju R, Soumya SJ, Arya PS, Sudhakaran PR. VEGF-A/VEGFR2 signaling network in endothelial cells relevant to angiogenesis. Journal of cell communication and signaling. 2016;10:347-54.

[42] D'Andrea LD, De Rosa L, Vigliotti C, Cataldi M. VEGF mimic peptides: Potential applications in central nervous system therapeutics. New Horizons in Translational Medicine. 2017;3:233-51.

[43] Finetti F, Basile A, Capasso D, Di Gaetano S, Di Stasi R, Pascale M, et al. Functional and pharmacological characterization of a VEGF mimetic peptide on reparative angiogenesis. Biochemical pharmacology. 2012;84:303-11.

[44] Chan TR, Stahl PJ, Yu SM. Matrix-Bound VEGF Mimetic Peptides: Design and Endothelial-Cell Activation in Collagen Scaffolds. Advanced functional materials. 2011;21:4252-62.

[45] Rodríguez-Cabello JC, Martín L, Alonso M, Arias FJ, Testera AM. "Recombinamers" as advanced materials for the post-oil age. Polymer. 2009;50:5159-69.

[46] Richards M, Mellor H. In vitro coculture assays of angiogenesis. Angiogenesis Protocols: Springer; 2016. p. 159-66.

[47] Raza F, Zafar H, Zhu Y, Ren Y, Ullah A, Khan AU, et al. A Review on Recent Advances in Stabilizing Peptides/Proteins upon Fabrication in Hydrogels from Biodegradable Polymers. Pharmaceutics. 2018;10:16.

[48] Martino MM, Brkic S, Bovo E, Burger M, Schaefer DJ, Wolff T, et al. Extracellular matrix and growth factor engineering for controlled angiogenesis in regenerative medicine. Frontiers in bioengineering and biotechnology. 2015;3:45.

[49] Arroyo AG, Iruela-Arispe ML. Extracellular matrix, inflammation, and the angiogenic response. Cardiovascular research. 2010;86:226-35.

8. SUPPORTING INFORMATION

1. Characterization of RGD-QK by MALDI-TOF, NMR, DSC and FTIR.

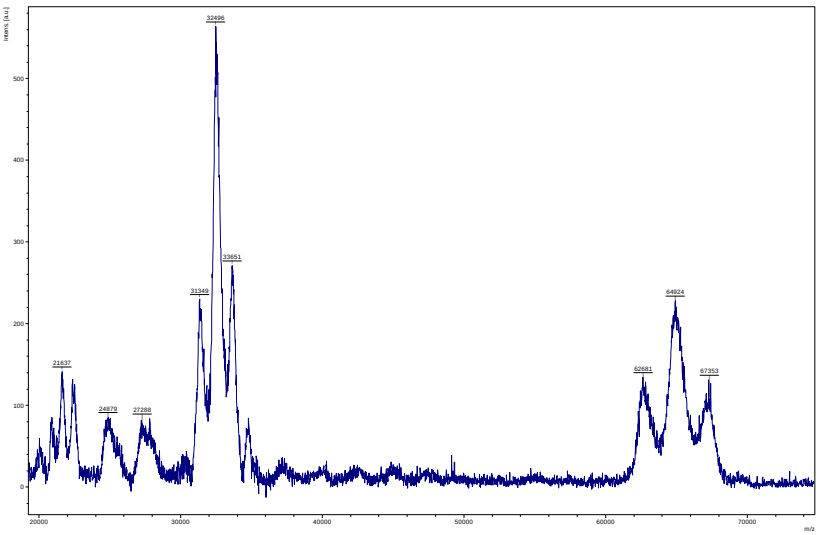

Figure S1. MALDI TOF spectrum of RGD-QK which represent a non-quantitative intensity against m/z (mass divided by net charge of the molecule).

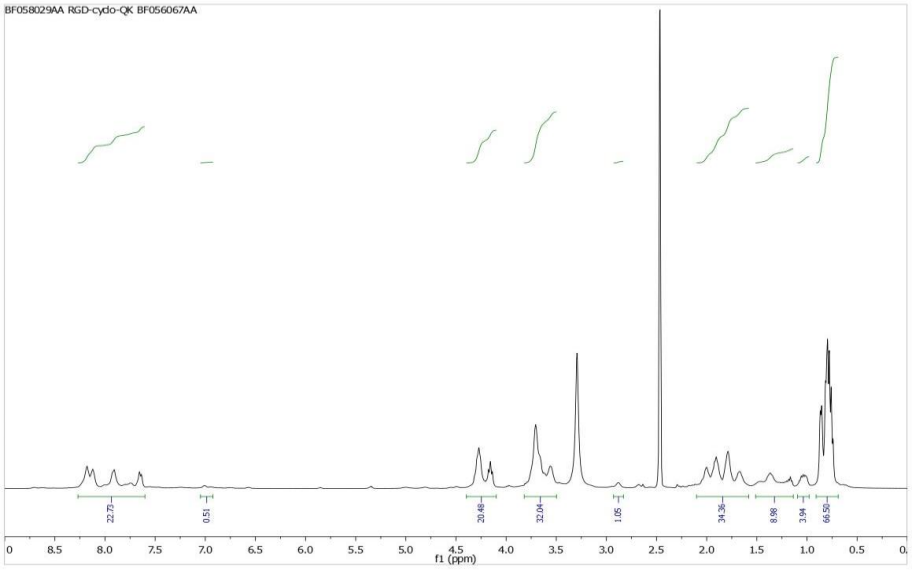

Figure S2. [1]H-NMR spectrum of RGD-QK ELR showing the integration of the poeaks corresponding to the different types of hydrogens.

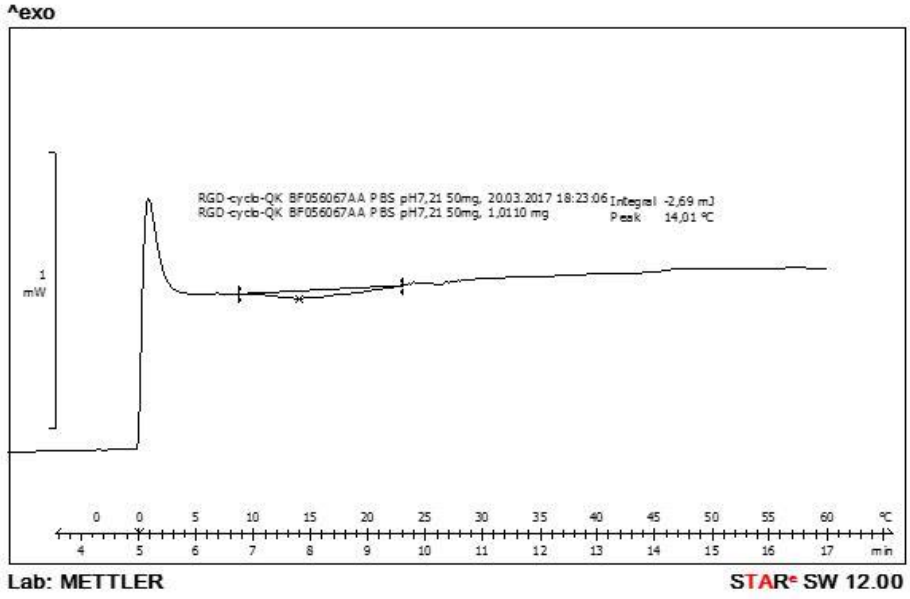

Figure S3. DSC thermogram of RGD-QK ELR showing the experimental Tt in PBS at a pH 7.21.

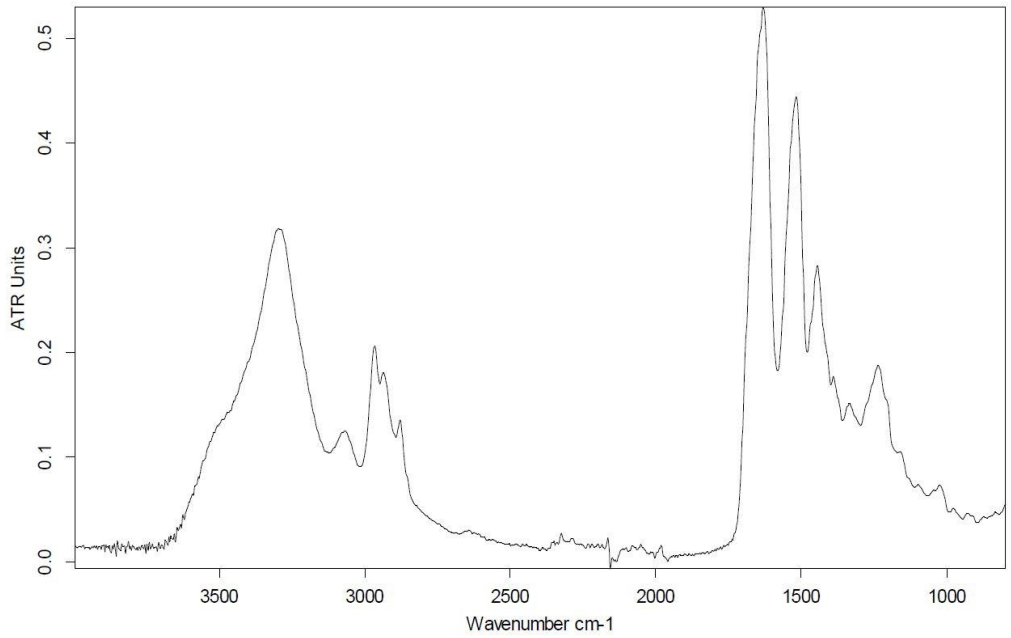

Figure S4. FTIR spectrum of RGD-QK ELR showing the presence of a peak at 2200 cm-1 confirming their chemical modification.

II. CHARACTERIZATION OF HRGD6 AND REDV RECOMBINAMERS

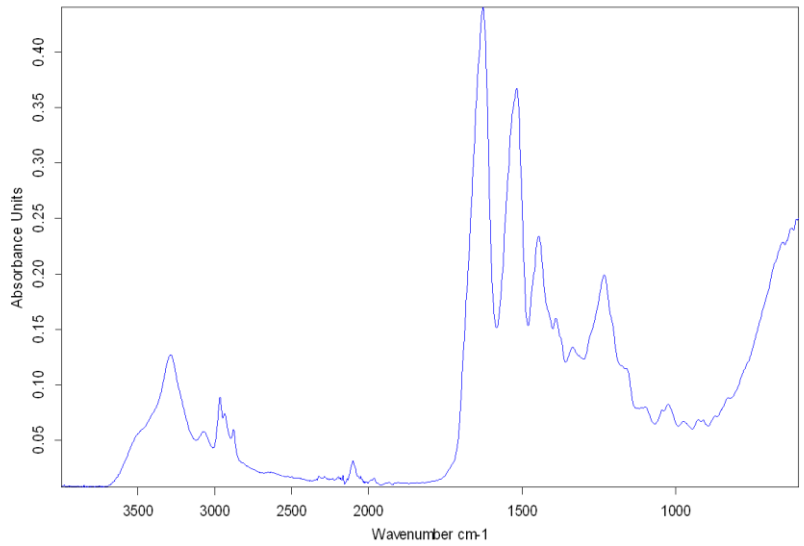

Figure S5. FTIR spectrum of HRGD6-N3

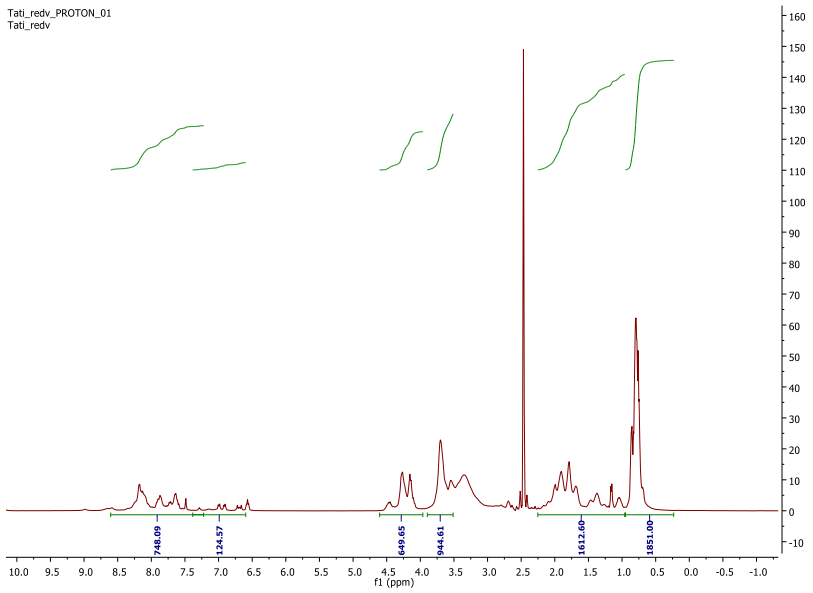

Figure S6. NMR spectrum of REDV-cyclootyne

CHAPTER 3

USE OF PROTEOLYTIC SEQUENCES WITH DIFFERENT CLEAVAGE KINETICS AS A WAY TO GENERATE HYDROGELS WITH PREPROGRAMMED CELL-INFILTRATION PATTERNS IMPARTED OVER THEIR GIVEN 3D SPATIAL STRUCTURE

Tatjana Flora, [1] Israel González de Torre, [2] Matilde Alonso, [1] José Carlos Rodríguez-Cabello,[1]

[1] BIOFORGE, CIBER-BBN, Universidad de Valladolid, Spain

[2] Technical Proteins NanoBioTechnology (TPNBT) S.L., Valladolid, Spain

Flora, Tatjana, et al. "Use of proteolytic sequences with different cleavage kinetics as a way to generate hydrogels with preprogrammed cell-infiltration patterns imparted over their given 3D spatial structure" *Biofabrication* (2019).In press

Abstract.

Control over biodegradation processes is crucial to generate advanced functional structures with a more interactive and efficient role for biomedical applications.

Herein, a simple, high-throughput approach is developed based on a 3D-structured system that allows a preprogramed spatial-temporal control over cell infiltration and biodegradation. The 3D-structured system is based on elastin-like recombinamers (ELRs) characterized by differences in the kinetics of their peptide cleavage and consists of a three-layer hydrogel disk comprising an internal layer containing a rapidly degrading component, with the external layers containing a slow-degrading ELR. This structure is intended to invert the conventional pattern of cell infiltration, which goes from the outside to the inside of the implant, to allow an anti-natural process in which infiltration takes place first in the internal layer and later progresses to the outer layers. Time-course *in vivo* studies proved this hypothesis, i.e. that it is possible to drive the infiltration of cells over time in a given 3D-structured implant in a controlled and predesigned way that is able to overcome the natural tendency of conventional cell infiltration. The results obtained herein open up the possibility of applying this concept to more complex systems with multiple biological functions.

1. Introduction

Over the past few years, the application of microfabrication and additive fabrication tools in the biomedical field has produced remarkable advances in the generation of complex structures with well-defined architectures that mimic those found in natural tissues and organs. [1] [2] Currently, the construction of well-defined three-dimensional (3D) structures is one of the most widespread strategies used in regenerative medicine. Indeed, this strategy has led to the construction of complex structures with controlled geometries and with precise control over the composition and spatial distribution. [3, 4] In most cases, these systems are conceived as transient, thus meaning that, once implanted, they either progressively degrade via a chemical process or are digested by the direct action of their cellular cargo or cells recruited from the surrounding tissues. In both cases, the implant is degraded and disappears from the implantation site, with natural tissue replacing the degraded implant. [5] [6]

Fabrication techniques for well-defined 3D structures still face technical challenges in terms of high-resolution cell deposition, controlled cell distributions and vascularization. [7] [8] Apart from these challenges, one evident drawback of current technology is the lack of spatial-temporal control during the degradation process. [8] In general, the well-defined 3D

structure of these implants is not related to their degradation process, at least in a controlled manner. Essentially, after implantation, the cells colonize and degrade the implant in an uncontrolled way, thus meaning that the spatial structure and biological function distribution of the implant are not connected with a predefined degradation program. [9] It would therefore be highly desirable for such sophisticated 3D structures to show a linked and programmable degradation sequence as a way of better controlling the evolution of the system once implanted. [10] [11] Currently, control of degradation rate over time is crucial for scaffolds used in tissue-engineering applications and is a key factor influencing the structure and properties of the scaffold. [12] [13] [14]

Elastin-like recombinamers (ELRs) are considered to be advanced biomaterials since they are multifunctional materials that can be tailored to exhibit a wide range of properties as well as functionalities such as cell adhesion, cell signaling, elasticity and biodegradability. [15] [16] [17] Moreover, they can be genetically engineered to exhibit complex biological functionalities as well as stimuli-responsiveness and, more specifically, they can change their physicochemical properties as a result of a change in a given stimulus. [18] [19] These smart biomaterials allow for the emulation of key properties of the natural ECM, specifically the ability to mimic its dynamic changes and complex functionalities. [20]

[21] These properties served as a basis and proved essential when choosing the materials to test the hypothesis of this work. Biomaterial-based implants that include protease recognition moieties in their amino acid composition are one of the most successful approaches towards the generation of functional devices. [22] [23] Proteolysis is one of the first and most sustained cell activities responsible for the structural remodelling and functional plasticity of tissues, which comprise basement membrane degradation, cell migration/ECM invasion, and capillary lumen formation. [24, 25] [26] During these processes, cells migrate and locally secrete a number of enzymes that promote the degradation and remodelling of matrix molecules in their pathway. Matrix metalloproteases (MMPs) and plasmin have been identified as particularly important proteases for cell migration. [27] [28] [29] In particular, the plasminogen activator-plasmin system plays an important role in tissue remodelling and is involved in several pathological processes. Two specific activators and their respective inhibitors, namely tissue plasminogen activator (tPA) and urokinase plasminogen activator (uPA), are mainly responsible for controlling this system. [30] [31] These activators are synthesized by different cell types, such as fibroblasts, epithelial cells, endothelial cells, smooth muscle cells, monocytes/macrophages and tumor cells. Moreover, uPA is actively

expressed under circumstances associated with cell migration (reparation, inflammation, angiogenesis, metastasis), where it provides efficient and spatially restricted extracellular proteolysis. [31, 32] [33]

Recent studies have shown the potential of the creation of 3D microenvironments that behave like actual ECM tissue. These 3D microenvironments can incorporate biological cues, such as protease epitopes, or growth factors to facilitate ECM degradation, cell proliferation, angiogenesis, or regeneration. They can also improve tissue specificity and facilitate maintenance of cell functions and phenotype. [34] [35]

Recently, Straley et al. demonstrated that the kinetics and sensitivity to proteolytic cleavage epitopes of uPA are not the same. Thus, whereas some epitopes, such as GTAR, exhibit a high sensitivity to proteolytic cleavage with a fast response, others, such as DRIR, exhibit a low cleavage efficiency, thus resulting in a delayed proteolytic sensitivity and slower degradation kinetics. [36]

We propose that the differences in peptide cleavage kinetics between those two epitopes can be used to program the degradation and cell-invasion sequence in a given 3D structure. To test this hypothesis, a model 3D structure (a sandwiched three layer disc) was constructed (Figure 1). This was accomplished using ELRs containing both adhesion (RGD sequence)

and specific proteolytic sites belonging to the plasminogen activator system (uPA enzyme) but with different degradation rates (fast and slow). The combination of these two types of bioactive signals allowed for the construction of a 3D system with a preprogrammed degradation sequence. This 3D model construct consisted of two external layers formed by a mixture of a proteolytic ELR with a slow degradation rate (DRIR-ELR) and an RGD-ELR, and a central layer composed of a proteolytic ELR with a fast degradation rate (GTAR-ELR) in addition to the RGD-ELR (Figure 1a). In essence, these three layers showed the same physical properties, cell adhesiveness and other biological functions. The concentration of cleavage sites was also the same but the central layer contained the fast degrading GTAR sequence while the two external layers contained the slow degrading DRIR sequence.

The resulting constructs were implanted subcutaneously in mice in order to analyse cell infiltration in a spatial-temporal distribution. (Figure 1b) It is hypothesized that the internal layer will be colonized first following an inside-to-outside pattern rather than the outside-to-inside pattern that is expected in conventional devices without such cell-infiltration programming (Figure 1c-1d).

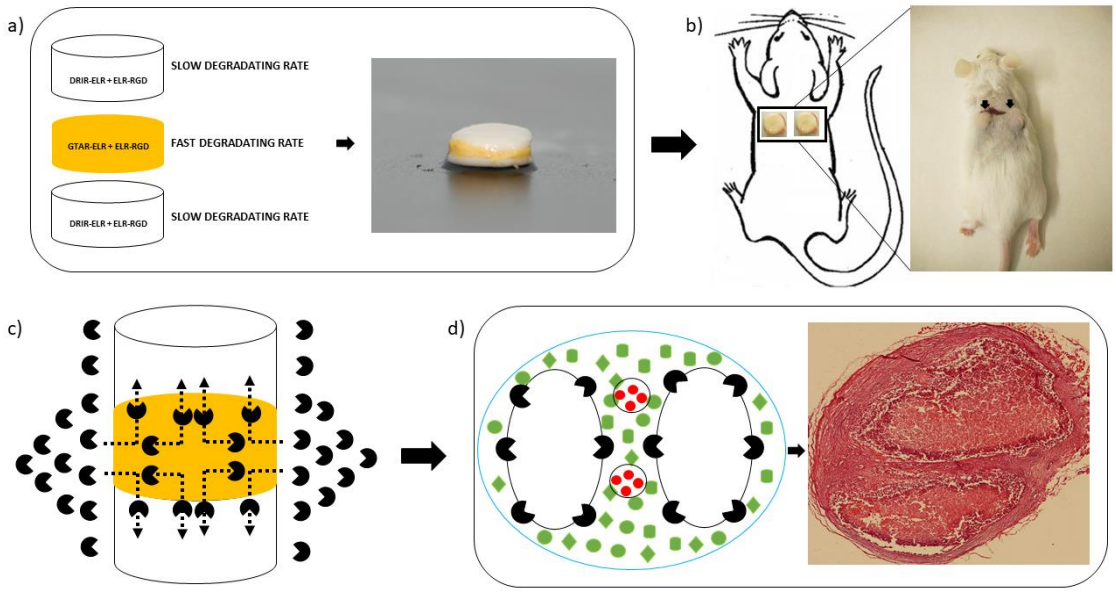

Figure 1. Representation of the 3D-structured system with preprogrammed cell invasion. **a)** A sandwiched three layer disc formed by two external layers (white color) characterized by a slow degradation rate and a central layer (yellow color) characterized by a fast degradation rate. **b)** This 3D structure was implanted subcutaneously into mice. **c)** Cells (the black structures) invaded the central layer of the system first following an outside-to-inside pattern. **d)** At six weeks post-implantation the central layer of the 3D system had been completely degraded, with the consequent formation of functional blood vessels (red circles). The other green structures with different shapes represent other kind of cells that invaded the 3D system. The last image is an H&E stained image showing that the two external layers of the 3D system with the slow degradation rate were not totally degraded, in contrast to the central layer, which was completely degraded.

2. Materials and methods

2.1 Synthesis of GTAR-ELR and DRIR-ELR

All gene-synthesis techniques, biosynthesis and purification protocols have been described in detail elsewhere. [15] [37] [38] The plasmid pUC57 containing the monomer peptides, GTAR and DRIR, was purchased from Nzytech (Lisbon, Portugal). Each monomer was flanked by an NheI recognition site. After extraction from pUC57 plasmid, they were inserted into a previously linearized and dephosphorylated pDrive vector (Qiagen) containing the $(((VPGIG)_2VPGKG(VPGIG)_2)_2$ block. The multi-block sequence was constructed using a directional oligomerization approach called the iterative-recursive method. [39]

A T4 ligase enzyme was used for ligation. This step was repeated four times in order to achieve four repetitions of each gene. Once the genes had been constructed, XL-1 blue component cells were transformed. They were then extracted from the pDrive vector and subcloned into a p7R expression vector which had previously been cut using SapI and dephosphorylated with SAP (Shrink alkaline Phosphatase). Incorporation into the expression vector was confirmed by analytical electrophoresis and subsequent DNA sequencing.

2.2 Expression and characterization of GTAR-ELR and DRIR-ELR

Expression vectors containing GTAR-ELR and DRIR-ELR genes were transformed into BL21 Star (DE3) *E.coli* strain. A screening of the colonies grown overnight (O/N) in auto-induction terrific broth (TB) medium was performed. The inoculum with a concentration of $1.6*10^9$ cells/mL was prepared in Luria-Bertani (LB) medium with ampicillin and glucose and incorporated into the fermenter once it had grown. Production in the fermenter allowed for the use of a higher culture volume and therefore a higher quantity of the desired ELR to be obtained. Bacteria had reached the stationary phase after 15 h, and production was stopped at 17 h. However, bacterial lysis ELRs remained in the soluble fraction afterwards. The ELRs were purified by inverse transition cycling (ITC), which comprises both hot and cold cycles and takes advantage of the smart behaviour of ELRs. The electrophoretic separation of proteins corresponding to the different purification steps, and the final product after purification, were studied in polyacrylamide gels stained with Coomassie Brilliant Blue.

In order to ensure the specific features of the final ELR products, physical and chemical characterizations were performed. To that end, SDS-PAGE, MALDI-TOF, nuclear magnetic resonance spectroscopy (NMR), amino acid analysis (HPLC) and differential scanning calorimetry (DSC) techniques were used. (Figure S1-S4, Supporting Information)

2.3 *In vitro* analysis of the degradation rate using a recombinant human uPA enzyme

The degradation rate of GTAR-ELR and DRIR-ELR was studied *in vitro* using a recombinant human uPA enzyme purchased from Hyphen BioMed (Neuville-sur-Oise, France). Each of the recombinamers (100 mM) was incubated with the enzyme at a concentration of 580 U/mL under sterile conditions. Samples were collected at specific time points (0, 15, 30, 60 minutes and 12, 24, 48, 72 hours) and subsequently analysed by SDS-PAGE electrophoresis. For analysis, 20 µL of each sample was mixed with 5 µL of loading buffer and heated at 100 °C for 10 minutes. The degradation rate was monitored on a 15% SDS-PAGE gel stained with Coomassie Brilliant Blue. Each sample was analysed in triplicate.

2.4 Hydrogel formation and physicochemical characterization

Hydrogels were obtained by substituting amine groups at the lateral chain of the lysine residues of each proteolytic ELR with a cyclooctyne group for subsequent crosslinking by a click reaction with RGD-ELR modified with an azide group. Two grams of each proteolytic ELR (DRIR-ELR and GTAR-ELR) was dissolved in 40 mL of dimethylformamide (DMF) at room temperature (RT) for 1 hour. Afterwards, 133.16 mg of Bicyclo [6.1.0] non-4-yn-9-ylmethyl N-succinimidyl carbonate (GalChimia, A Coruña, Spain) dissolved in 1 mL of DMF was added to the solution and

the resulting mixture was stirred for 48 h at RT. RGD-ELR was modified with an azide group as follows. 2-Azido ethyl (2,5-dioxopyrrolidin-1-yl) carbonate (51.69 mg) dissolved in 1 mL of DMF was added to the RGD-ELR solution previously dissolved in DMF as described above. The modified ELRs were purified by washing with 15 mL of diethyl ether and the supernatant was removed and washed with acetone (3 x 15 mL), dried under reduced pressure, re-dissolved in cold MQ water, dialyzed against MQ water and finally lyophilized. Their modification was studied by MALDI-TOF, NMR, FTIR and DSC (Figure S2.1-S2.2, Supporting Information).

2.5 Porosity studies of proteolytic ELR-based hydrogels

The porosity of the hydrogels was determined using the following equation:

$$\text{Porosity (\%)} = \frac{((W1-W2) \,/\, \text{d water}) * 100}{\text{V hydrogel}} \qquad \textbf{Equation 1}$$

Where W1 and W2 are the weight of the swollen and lyophilized gels, respectively, dwater is the density of pure water and Vhydrogel is the measured volume of the gel in the swollen state. Three replicas were measured for each condition.

2.6 Mechanical properties of proteolytic ELR-based hydrogels

To prepare the proteolytic ELR-based hydrogels, each proteolytic ELR (GTAR-ELR and DRIR-ELR) previously modified with a cyclootyne group was dissolved in PBS 1X at 4°C overnight (O/N). The same conditions were used for dissolution of the RGD-ELR previously modified with an azide group. The concentrations studied were 50, 100 and 150 mg/mL, with a molar ratio of 1:1. For each hydrogel, 50 µL of each proteolytic ELR-cyclootyne was mixed in an Eppendorf flask with 50 µL of RGD-ELR-azide. Subsequently, a specific mold was used to form the hydrogels, which were incubated at 4°C for 20 minutes. Three replicates were analysed for each concentration of each hydrogel. The mechanical properties were studied using a strain-controlled AR-2000ex rheometer (TA Instruments). A stainless steel with a diameter of 12 mm and a gap of about 1000 between the plates was adjusted, reaching a normal force of 0.2 N in order to prevent slippage. All measurements were conducted at 37°C with a frequency sweep of between 0.01 and 50 Hz at a fixed strain corresponding to the linear hydrogel region.

2.7 Morphological characterization by scanning electron microscopy (SEM)

Hydrogel structure and morphology were evaluated by SEM. After preparation as described above, they were dropped into liquid nitrogen, physically fractured, and immersed in liquid nitrogen again before finally

being freeze-dried. Images of lyophilized hydrogels were obtained by SEM (JEOL, JSM-820) with no prior footing procedures. Morphological details such as pore size were evaluated quantitatively using the ZEN (Blue Edition, 2012) software package (Carl Zeiss Microscopy).

2.8 *In vitro* degradation analysis of proteolytic ELR-based hydrogels

The degradation rate of proteolytic ELR-based hydrogels was studied by evaluating the variation of their elastic modulus after incubation with recombinant human uPA enzyme. Hydrogels with a concentration of 50 mg/mL previously prepared in a specific mold were incubated at 37°C with 1 mL of PBS 0.1 M and uPA enzyme at a concentration of 580 U/mL under sterile conditions. Their mechanical properties were analysed using the same approach described in section 2.6.

2.9 Cytocompatibility evaluation in a 2D cell culture

Human umbilical vein endothelial cells (HUVECs) were obtained from the ATCC (Madrid, Spain). Cells were cultured in MED200 medium (Gibco) supplemented with antibiotics gentamicin/amphotericin (1%, Gibco) and low serum growth supplement kit (LSGS, Gibco). They were maintained in a humidified atmosphere containing 5% CO_2 at 37ºC.

The alamarBlue (Invitrogen) bioassay was used to evaluate the cytotoxicity, determining the metabolic activity of HUVECs using a 2D

cell culture system consisting of seeding cells on top of the hydrogels. At each time point (4 hours, 3 days, and 7 days), the hydrogels were washed three times with PBS, then 10% alamarBlue in cell culture medium was added to the wells. After each time point, 70 µl of the solutions was transferred into a black, 96-well plate for fluorescence quantification using a microplate reader. A solution of 10% AB in cell culture medium and a 100% reduced solution of 10% AB in cell culture medium were used as negative and positive control, respectively.

2.10 *In vivo* studies of each proteolytic ELR-based hydrogel

In vivo experiments were performed in accordance with European Union Directive 2010/63/EU and Spanish Royal Decree RD 53/2013. The protocol was approved by the Animal Care and Use Committee of the University of Valladolid.

Mice were anesthetized by inhalation using 3% Isoflurane, then 30 µL of each hydrogel, with a concentration of 50 mg/mL, was injected intramuscularly using a syringe with a 20G needle in the hind limb area. Animals were euthanized by cervical dislocation at 3, 6 and 12 weeks.

2.11 Histology and immunohistochemistry analysis

The hydrogels were extracted from the animals at the established time point and were subsequently embedded in 4% paraformaldehyde at 4°C

for at least 24 hours. They were then dehydrated in ethanol solutions of increasing concentration (70%, 80%, 90% and 100%); the final step comprised two changes in xylene. All samples were fixed in paraffin for at least 5 hours at 50°C and stored O/N at -20°C. For a general histomorphological evaluation, microsections were cut with a rotatory microtome and stained with hematoxylin and eosin (H&E) according to standard protocols. [40] Three randomly chosen areas of histological staining were selected to perform quantitative analysis using ImageJ.

Immunofluorescence staining was performed on micro-sections previously deparaffinised and subsequently incubated for 1 hour in 10% donkey blocking serum (Santa Cruz Biotechnology, USA). Several washing steps in PBS 1X were then performed. All samples were subsequently incubated overnight (O/N) at 4°C with a goat polyclonal primary PECAM antibody (Santa Cruz Biotechnology, USA) at a concentration of 1 µg/mL in 1% blocking serum. After the primary antibody incubation, samples were washed three times with PBS 1X for five minutes each. Each sample was then incubated for 2 hours with donkey anti-goat (Santa Cruz Biotechnology, USA) fluorescein-conjugated secondary antibodies at a concentration of 1 µg/mL with 1.5% normal blocking serum. Incubation was carried out with minimal light exposure. After three washes in PBS 1X for five minutes, a vectashield

HardSet Antifade Mounting Medium with DAPI (Vector Laboratories, USA) was used to stain the nuclei of the cells. All images were acquired using a fluorescent microscope.

2.12 Preparation of the 3D-structured system

The 3D system consisted of three layers: two external layers formed by DRIR-ELR and RGD-ELR and the central layer formed by GTAR-ELR and RGD-ELR. For the preparation of each system, a specific mold with a diameter of 0.8 mm and a height of 0.4 mm was used. The first step involved depositing the first layer (DRIR-ELR + RGD-ELR) for 2 minutes at 4°C. The second layer (GTAR-ELR + RGD-ELR) was then deposited under the same conditions, and finally the third layer (DRIR-ELR + RGD-ELR) was deposited. The mold containing the entire structure was left for more than 20 minutes at 4°C under sterile conditions.

2.13 *In vivo* studies of the 3D-structured system

The 3D structures were implanted subcutaneously in mice anesthetized using ketamine and diazepam at a concentration of 100 and 5 mg/ml, respectively. A small incision was made on the dorsal area to form a skin pocket using surgical scissors. The entire cylinder (0.8 mm swollen previously in PBS 1X sterile and endotoxin free) was implanted and the wound was closed using absorbable sutures. Different time points were

analysed (1, 3, 6, 9 and 12 weeks), with the animals being euthanized by cervical dislocation at each time point. All samples were analysed by histology and immunohistochemistry as described above. Quantitative analysis were performed using Image J software as reported above.

2.14 Statistical analysis

All data are presented as mean ± SD (n = 3). Statistical analysis involved a one-way analysis of variance using the Holm–Sidak method. A p value of less than 0.05 was considered to be statistically significant. (**) $p < 0.001$, (*) $p < 0.05$, and $p > 0.05$. n.s.d indicates no significant differences.

3. Results

3.1 Construction, production and purification of proteolytic ELRs

The amino acid sequences of the resulting proteolytic ELRs (GTAR and DRIR) are shown in Table 1. Each proteolytic ELR comprises a main block $(((VPGIG)_2VPGKG\ (VPGIG)_2)_2$, which is repeated four times, with each cleavage peptide appearing in the middle. The entire DNA sequencing and restriction mapping analysis showed the accuracy of the gene-construction process. (Figure S1)

Purification were carried out using an ITC protocol and the production yields obtained were around 350 mg/L of bacterial culture. The purity, molecular mass and correctness of the biosynthetic process of the final product were confirmed by SDS-PAGE electrophoresis (Figure S2), FTIR (Figure S3), MALDI-TOF mass spectrometry (Figure S4), and amino acid analysis (Table S1).

Table 1. Amino acid sequence of the proteolytic ELRs

Proteolytic ELRs	Amino acid sequence
GTAR	MESLLPV $(((VPGIG)_2$ VPGKG $(VPGIG)_2)_2$YAVTG DRIR SASPASSA $((VPGIG)_2$ VPGKG $(VPGIG)_2)_2V)_4$
DRIR	MESLLPV$(((VPGIG)_2$ VPGKG $(VPGIG)_2)_2$YAVTG GTAR SASPASSA $((VPGIG)_2$ VPGKG $(VPGIG)_2)_2V)_4$

3.2. *In vitro* enzymatic degradation of proteolytic ELRs

The degradation rate of each proteolytic ELR (GTAR-ELR and DRIR-ELR) was studied *in vitro* by SDS-PAGE electrophoresis with Coomassie Brilliant Blue staining. A representative profile of the degradation rate of proteolytic ELRs within a range of time points is shown in Figure 2. At time zero, the molecular weight of the bands corresponding to the recombinamer was about 42 kDa. After 15 minutes, the full protein degraded into smaller fragments with molecular weights of approximately 35, 25, 15 and 5 kDa. The size of these bands corresponds to the theoretical length of the fragments generated upon cleavage at the proteolytic sites. The presence of other fragments that do not correspond to these molecular weights is due to the residual nonspecific cleavage of lysine sites. [41] After 60 minutes, a clear difference was noted between the recombinamer with a fast degradation rate and the recombinamer with a slow degradation rate. Thus, the upper bands of the recombinamer with a fast degradation rate (GTAR-ELR) were absent and the smallest band of 5 kDa increased in intensity. After 12 hours, GTAR-ELR was completely degraded and the only remaining band was that at 5 kDa. The recombinamer with a slow degradation rate did not reach complete degradation over the time period studied. One change that can be noticed for these time points is the loss of intensity in the upper bands, thus meaning that the band corresponding to

the full protein began to degrade. These results indicate that there is a clear difference between the ELRs with fast and slow degradation rates and that the degradation rate can be modified using these different cleavage sites.

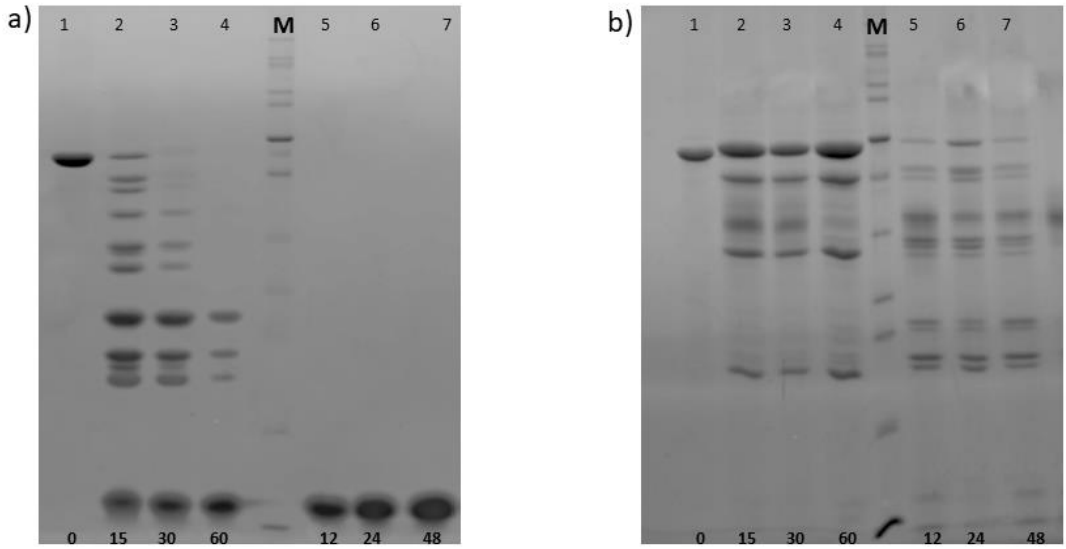

Figure 2. SDS-PAGE electrophoresis of the proteolytic ELRs: a) GTAR-ELR, b) DRIR-ELR. 15% SDS-PAGE stained with Coomassie. In both gels: Lines 1-4: proteolytic ELR degradation after 0, 15, 30 and 60 minutes. Line M: Page Ruler unstained Protein Ladder. Lines 5-7: protein degradation after 12, 24, and 48 hours.

3.3 Morphology studies of proteolytic ELR-based hydrogels

The morphology of the proteolytic ELR-based hydrogels at several concentrations in a frozen-lyophilized state was analysed by SEM microscopy. SEM micrographs of GTAR-ELR and DRIR-ELR hydrogels at several concentrations (50, 100 and 150 mg/mL) can be found in Figure

3a and 3b, respectively. It is evident that the dried porosity decreases with increasing concentration. In hydrogels with a concentration of 100-150 mg/mL, the shape of the pores is irregular and some zones are characterized by a non-pore size. It is also clear that their structure converts into a denser and tighter structure formed by smaller pores. The hydrogels with a concentration of 150 mg/mL present a collapsed network, thus leading to a shrunken state. There is an inverse correlation between concentration and pore size, which further affects the swelling ratio. Hydrogels with a concentration of 50 mg/mL display a higher number of pores with a regular and ordered porosity and also maintain high interconnectivity. A quantitative analysis of the pore size was performed using the ImageJ software, giving a range of about 13 μm. The microscopic structure of the proteolytic ELR-based hydrogels was studied in more detail in order to determine the porosity values, which are reported graphically in Figure 3c. The porosity of the hydrogels was evaluated as a function of concentration, demonstrating that porosity decreases with increasing concentration. These results are in agreement with the SEM analysis. Moreover, both ELR-based hydrogels (GTAR-ELR and DRIR-ELR) exhibit similar morphological features at a concentration of 50 mg/mL.

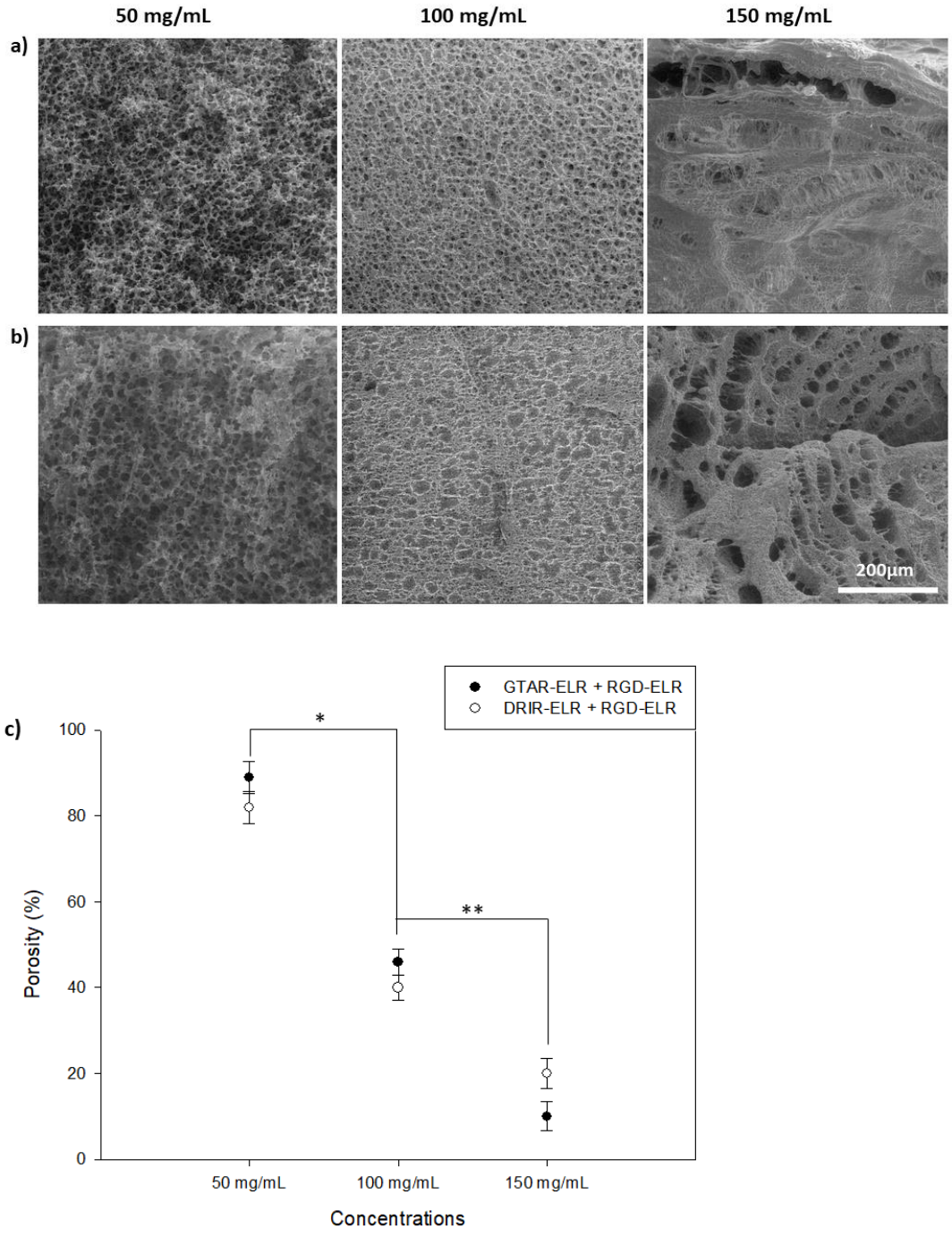

Figure 3. SEM micrographs of cryo-fractured proteolytic ELR-based hydrogels: a) GTAR-ELR + RGD-ELR based hydrogels at 50, 100 and 150 mg/mL from left

to right; b) DRIR-ELR + RGD-ELR based hydrogels at 50, 100 and 150 mg/mL. Scale bar for all images: 200µm. c) Graphical representation of porosity versus concentration. Data are reported as mean ± SD. Statistical analysis involved analysis of variance using the Holm–Sidak method. *p<0.05; **p<0.001.

3.4 Mechanical properties of proteolytic hydrogels

The mechanical properties of the hydrogels were determined by rheological measurement in oscillatory mode. Each hydrogel sample was used for only one test and each test was performed in triplicate. All rheological tests were performed at 1% strain as a previous measurement to demonstrate that the strain amplitude remained constant at 7-8%. The complex elastic modulus reported in Figure 4 represents the average of three tests performed at 37°C, together with the corresponding standard deviation.

As reported above, the complex elastic modulus of the hydrogels increased as a function of concentration to 1085±145, 2132±192 and 5253±248 Pa for 50, 100 and 150 mg/mL, respectively, at a frequency of 1 Hz. A statistically significant difference was found between the complex moduli of the hydrogels belonging to the different concentration groups, whereas relatively similar values, with no significant difference in complex modulus, were found for a given concentration for different proteolytic ELR-based hydrogels. The morphological analysis, mechanical properties

and swelling ratios demostrated that hydrogels with a concentration of 50 mg/mL exhibit similar properties to that for the scaffold used to regenerate soft tissues.[42] Moreover, the different cleavage site does not appear to affect their mechanical and morphological properties. [8, 43]

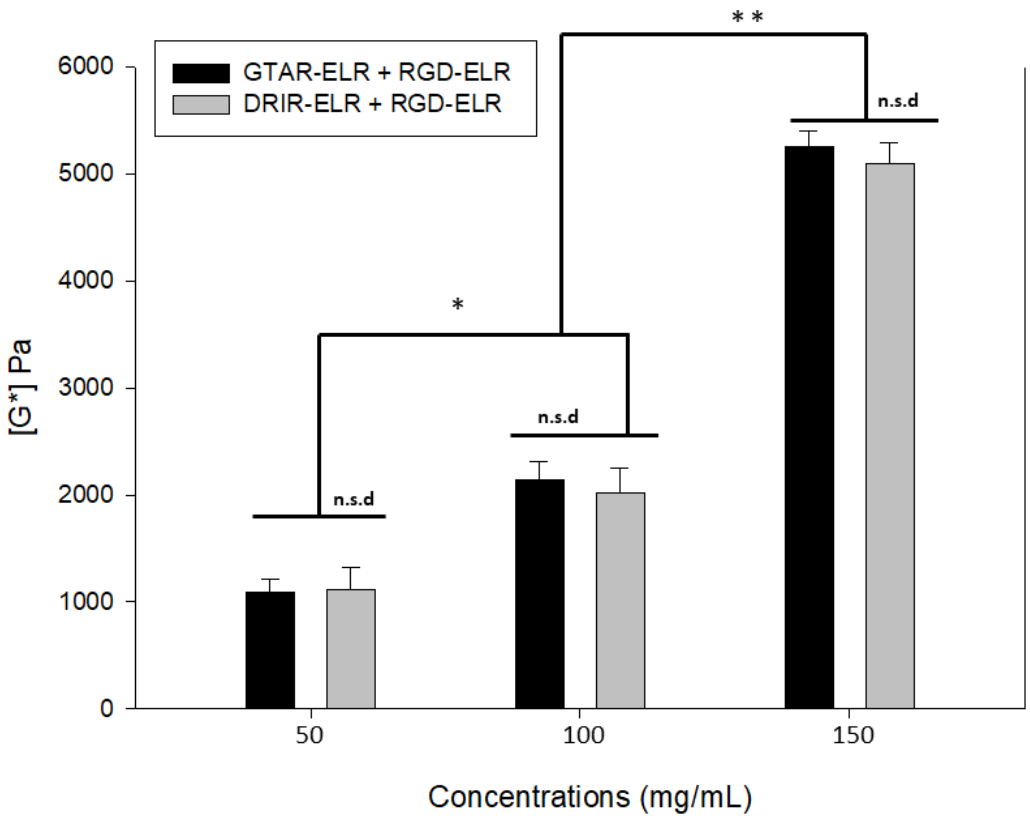

Figure 4. Representation of the complex modulus [G*] for GTAR-ELR + RGD-ELR and DRIR-ELR + RGD-ELR hydrogels at different concentrations. Data are reported as mean ± SD (n=3). Statistical analysis involved analysis of variance using the Holm–Sidak method. *p<0.05; **p<0.001; n.d.s. no significant differences.

3.5 Degradation rate of the proteolytic ELR-based hydrogels evaluated by analysing the mechanical properties

The degradation rate of the hydrogels was assessed by monitoring the variation of the elastic modulus for 24, 48, 72 and 168 hours. Rheological measurements were performed in oscillatory mode, as described above. The resulting complex modulus was compared to the measurements at time 0 in order to determine the variation in their magnitude after incubation with the corresponding concentration of uPA enzyme. As can be seen from Figure 5, the complex modulus [G*] at time 0 for the hydrogels with a concentration of 50 mg/mL was about 1100 Pa. After 24 hours, the complex modulus of the hydrogels with a fast degradation rate (GTAR-ELR + RGD-ELR) had decreased by nearly half, whereas the modulus of the hydrogels with a slow degradation rate (DRIR-ELR + RGD-ELR) remained unaffected. This behaviour was expected for the hydrogels with a fast degradation rate (GTAR-ELR + RGD-ELR) since the enzyme had cleaved the majority of the proteolytic sites. However, an interesting phenomenon was observed after 48 hours. Thus, the complex modulus of the hydrogels with a slow degradation rate (DRIR-ELR + RGD-ELR) decreased significantly whereas the modulus for the hydrogels with a fast degradation rate (GTAR-ELR + RGD-ELR) decreased only slightly. After 72 hours, the complex modulus of the hydrogels with a fast

degradation rate (GTAR-ELR+ RGD-ELR) was impossible to measure due to their loss of integrity. As such, the last two points for the measurements are not shown in the graph reported in Figure 5. As regards the hydrogels with a slow degradation rate (DRIR-ELR + RGD-ELR), the complex modulus started to slowly decrease, reaching a complex modulus of 676±62 Pa after 168 hours.

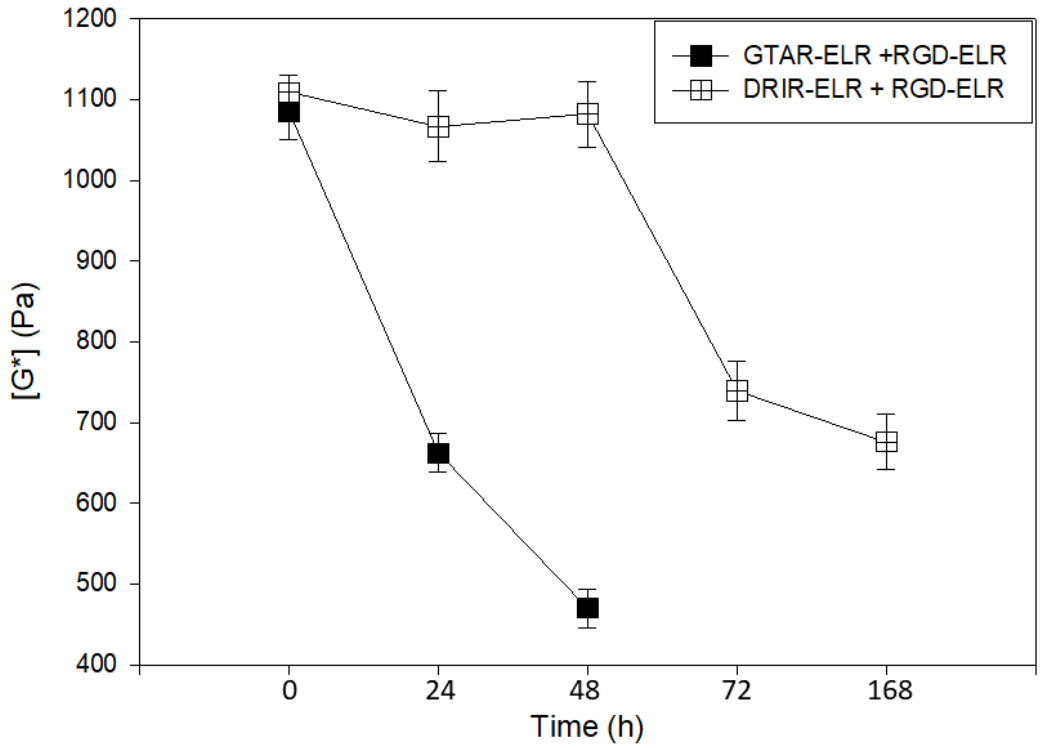

Figure 5. Graphical representation of the complex elastic modulus [G*] for the proteolytic ELR-based hydrogels after exposure to the uPA recombinant human enzyme at 0, 24, 48, 72 and 168 hours. It was not possible to measure the elastic

modulus of the last two time points for hydrogels with a fast degradation rate (GTAR-ELR + RGD-ELR). Data are reported as mean ± SD.

3.6 Cytocompatibility

The cytocompatibility of the hydrogels was evaluated using an alamarBlue bioassay considering three time points (4 hours, 3 days and 7 days). A representative graph is provided in Figure 6, where the cell number is reported for each hydrogel at each time-point. The metabolic activity assay revealed that hydrogels promote adherence and proliferation of HUVEC cells. After 4 hours, the endothelial cells adhered similarly in all the hydrogels, and at days 3 and 7 the cell metabolic activity increased, thus demonstrating that these hydrogels support cell growth and proliferation and confirming their cytocompatibility.

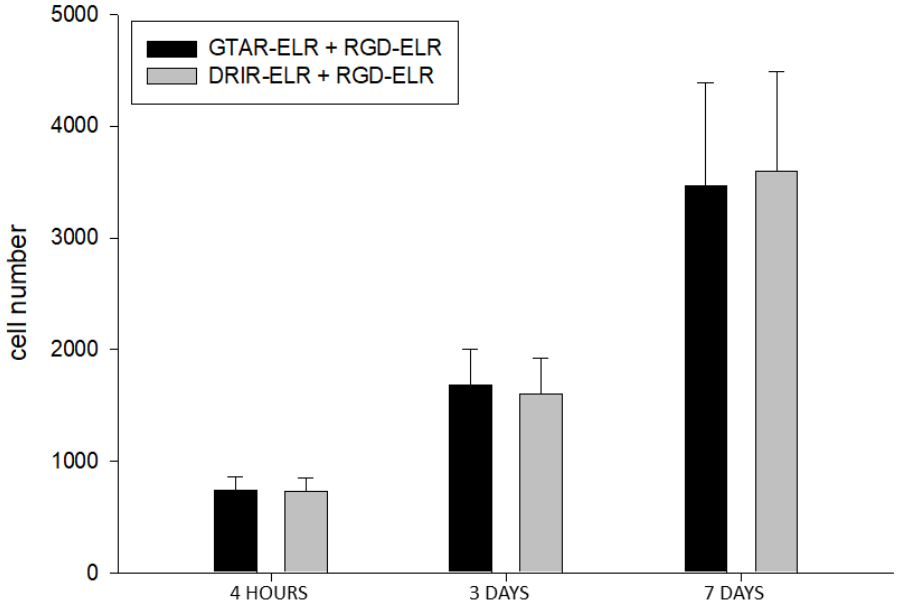

Figure 6. Cytocompatibility evaluation (adhesion and proliferation of endothelial cells) of proteolytic ELRs-based hydrogels using the alamarBlue assay. Error bars represent mean ± SD.

3.7 Individual *in vivo* behaviour of proteolytic ELR-based hydrogels

In this section, we investigate the *in vivo* behaviour of proteolytic ELR-based hydrogels in order to offering a general overview regarding their degradation rate based on the different cell invasion behaviours exhibited by them. Thus, the hydrogels were injected intramuscularly into mice using a syringe containing a solution of a specific proteolytic ELR and RGD-ELR previously mixed in an eppendorf.

The proteolytic ELR-based hydrogels integrated within the surrounding host tissue, although the tissue response after injection was distinct for the hydrogels with a fast degradation rate (GTAR-ELR + RGD-ELR) and those with a slow degradation rate (DRIR-ELR + RGD-ELR). A hydrogel comprising RGD-ELR and VKV-ELR was used as a control. VKV-ELR is a recombinamer that does not contain any proteolytic sites. As reported in Figure 7a (the first row), after three weeks post-injection, all hydrogels remained at the injection site and start to be invaded by cells. A graphic representation reported in Figure 7b show significant differences in cell number/mm^2 among the samples analysed, especially hydrogels with a fast degradation rate (GTAR-ELR+RGD-ELR) contained a higher number of cells compared to the other systems tested. On the other hand, the hydrogels with a slow degradation rate (DRIR-ELR+RGD-ELR) presented a higher number of cells rather than the control (VKV-ELR+RGD-ELR), which contained regions that were not invaded by any cells. In addition, cells migrated more deeply into the hydrogels with a fast degradation rate (GTAR-ELR+RGD-ELR) than into those with a slow degradation rate (DRIR-ELR+RGD-ELR), almost certainly as a consequence of their degradation rate. We hypothesize that the cells colonizing the hydrogels were a heterogeneous population of cells characteristic of the acute inflammatory response, which is a peripheral

reaction during inflammatory infiltration. These results offer an insight into how the different degradation rates influence cell migration into the hydrogels, thereby resulting in a marked variation in cell density. An interesting event occurred at six weeks post-injection (second row in Figure 7). As regards the hydrogels with a fast degradation rate (GTAR-ELR+RGD-ELR), these were found to be completely invaded by cells and the formation of small capillaries was observed. In hydrogels with a slow degradation rate (DRIR-ELR+RGD-ELR) cells migrated deeper, although some areas were not invaded completely. An initial inflammatory response starts which is characterized by the presence of macrophages that invaded the hydrogels and started to concentrate around the individual hydrogels. (Figure S3.2, Supporting Information) However, this inflammatory response was reduced or completely disappeared at the following time point. As the degradation process proceeded, a larger number of cells reached deeper within the proteolytic hydrogels, thus accelerating their degradation and leading to destruction of their structure. (Figure 7c) Moreover, the quantity of cells that invaded the control hydrogel was low due to the difficulty encountered by the cells when invading the hydrogel due to the lack of proteolytic sites.

At twelve weeks post-injection signs of degradation became more evident for both proteolytic hydrogels, especially their surface area which

decreased considerably. At three weeks the area of all the hydrogels was about 1.01 mm^2. After twelve weeks post-injection the remaining area was about 0.89 mm^2 for VKV-ELR+RGD-ELR, 0.30 mm^2 for GTAR-ELR+RGD-ELR and 0.63 mm^2 for DRIR-ELR+RGD-ELR. Degradation appeared to be more advanced in hydrogels with a fast degradation rate (GTAR-ELR+RGD-ELR), probably indicating resorption of the biomaterial. In summary, at six weeks post-injection, the hydrogels started to lose their internal structural integrity as the rate of hydrogel degradation was accelerated, thus resulting in a noticeably decrease in the volume of the injected hydrogel at twelve weeks post-injection.

Additionally, in hydrogels with a slow degradation rate (DRIR-ELR+RGD-ELR) very few macrophages were present around the remaining sample whilst in hydrogels with a fast degradation rate (GTAR-ELR+RGD-ELR), the inflammatory cells were no longer present. Moreover, in hydrogels with a slow degradation rate vascularization increased compared to the previous interval. (Figure S 3.1) Endothelial cells were found to be localized around the newly formed capillaries, thus contributing to their luminal structure. (third row of Figure 7a) The formation of neo-vascularization was confirmed by immunohistochemical staining using an antibody against the PECAM protein. The presence of cells positive for CD31 antigen was observed for hydrogels with a fast

degradation rate at six weeks post-injection (Figure 8a), and for hydrogels with a slow degradation rate at twelve weeks post-injection (Figure 8b).

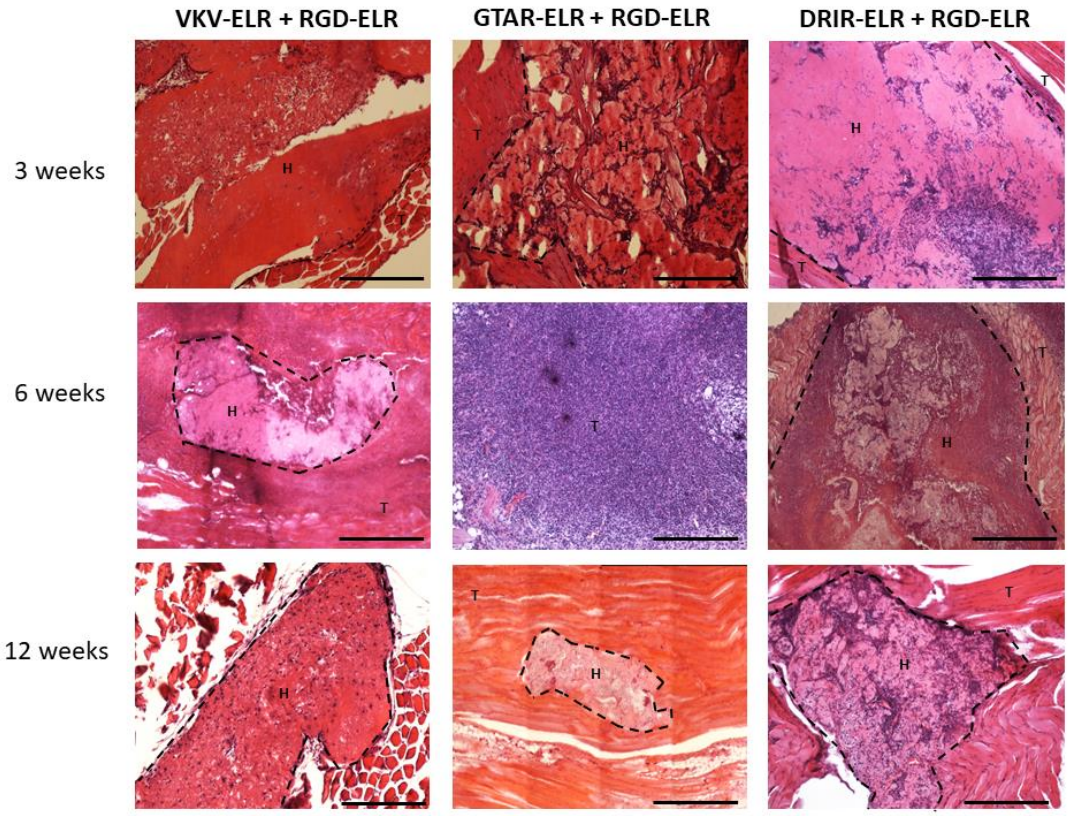

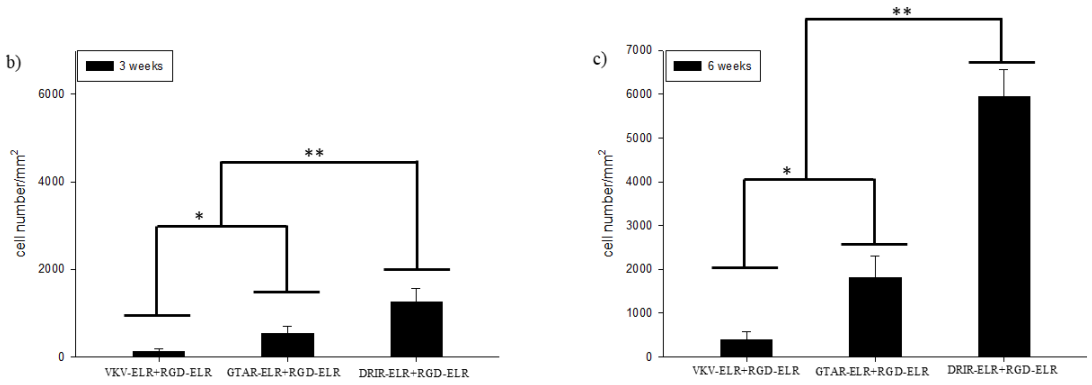

Figure 7. a) Histological hematoxylin and eosin (H&E) staining results for ELR-based hydrogels at 3, 6, and 12 weeks post-injection. The top row indicates the type of sample analysed and the left column indicates the different time points analysed. T: tissue. H: hydrogel. The dotted line represents the interface between tissue (muscle) and hydrogel. Scale bar: 200 µm. b) Graphic representation of number of cells/mm^2 for the hydrogels at three weeks post-injection and c) at six weeks post injection. Each data point represents the mean number of cells, and the bar represents the standard deviation. *p<0.05; **p<0.001.

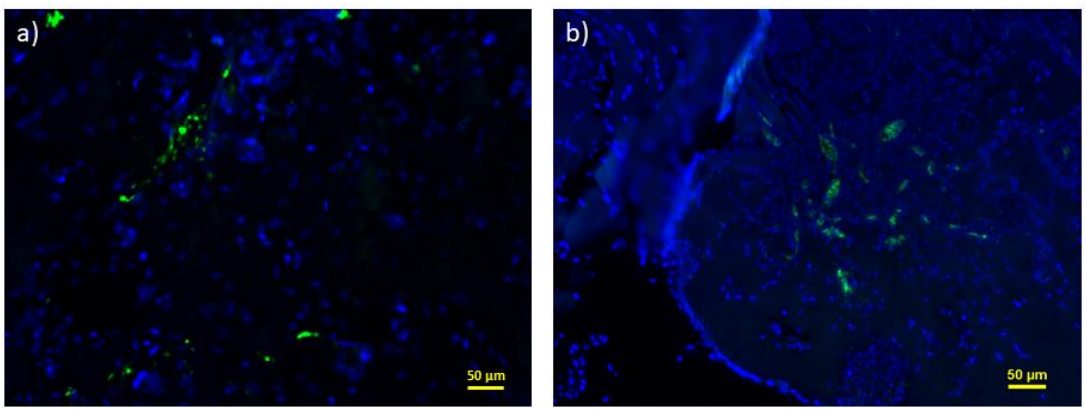

Figure 8. CD31 immunofluorescence staining images of: a) GTAR-ELR+RGD-ELR hydrogel at 6 weeks post-injection; b) DRIR-ELR+RGD-ELR hydrogel at 12 weeks post-injection. DAPI: nucleus staining (blue colour). CD31 protein (green colour). Scale bar: 50 μm.

3.8 *In vivo* studies of the sandwiched three-layer system

After the *in vivo* degradation studies of the individual proteolytic hydrogels, a three-dimensional system mainly comprising a three-layer disc was constructed. This three-layer disc comprised two external layers made of DRIR-ELR+RGD-ELR, characterized by a slow degradation rate, and a central layer made of GTAR-ELR+RGD-ELR, characterized by a fast degradation rate. These discs were implanted subcutaneously in mice and were explanted after 1, 3, 6, 9 and 12 weeks to evaluate the time-course of cell infiltration.

Histological examination upon staining with H&E at each time point is shown in Figure 9. As can clearly be seen (Figure 9a - 9a1), the three parts of the 3D structure can be easily recognized at one week post-implantation. Cell infiltration has not started yet.

At three weeks post-implantation, (Figure 9b - 9b1), a considerable part of the 3D structure was colonized by cells. As predicted, cell infiltration started in the central part of the 3D structure, specifically the layer characterized by a fast degradation rate (GTAR-ELR+RGD-ELR). Figure

9f shows the quantification of cell number/mm^2 that started to invade the central layer of the 3D structure and the cells that infiltrate the edges of the two external layers. There is a significant difference between the quantities of cells that invade the layers of the 3D system.

At six weeks, the central layer of the 3D system was completely invaded by cells and almost completely degraded (Figure 9c – 9c1), and a difference in the degradation rate was clearly observed at this time point. Thus, the external layer of the 3D structure was still not degraded, and the quantity of the cells that invaded these layers clearly increased even if there are significant differences between the quantity of cells that invade the central layer of the 3D system and the two external layers. (Figure 9g)

Moreover, at this time point neovascularization was underway as confirmed in Figure 10 a-b-c where is reported the whole central layer of the 3D system. The blotted circles indicates the presence of blood vessels or capillaries formed. In some of these structures is possible to detect the presence of endothelial cells surrounding the red blood cells, thereby suggesting the presence of a functional vasculature. (Figure a1, b1, c1) Immunofluorescent staining analysis for a well-known endothelial marker (CD31) was performed. A considerable amount of CD31-positive cells were detected in the central layer of the 3D system (Figure 10d) demonstrating a highly vascularized structure and confirming the presence

of blood vessel (Figure 10 d1) that favour the transport of nutrients between the 3D structure and the host tissue. It is evident that the two external parts of the 3D system have no vascularization yet.

At nine weeks post-implantation, the external layers of the 3D structure were almost completely degraded (Figure 9d – 9d1). Although some remnants of the hydrogels remained, they were completely invaded by cells.

The final time point was at 12 weeks. The animals were sacrificed at this point, and no hydrogels remained in the area where they were implanted. Given our previous findings, this allowed us to hypothesize that the entire system had been completely reabsorbed. A summary of the degradation process of the 3D structure when implanted subcutaneously, and how the size thereof changes with time up to the final time point, is provided in Figure 11. At the first three time points the three-layer disc is clearly visible under the skin, thus indicating that it had yet no degraded substantially, and there are no, or very few, macroscopic signs of inflammation or toxicity in the tissue surrounding the implant.

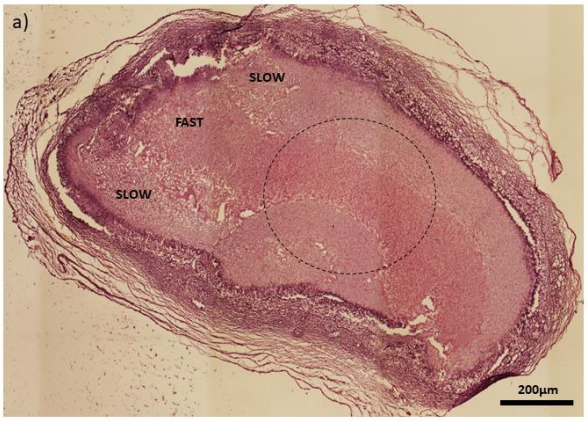
a)
SLOW
FAST
SLOW
200µm

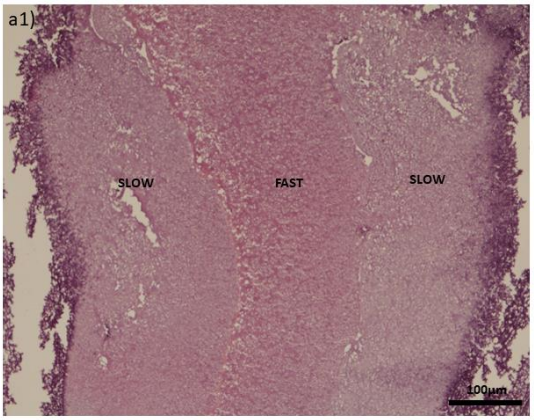
a1)
SLOW
FAST
SLOW
100µm

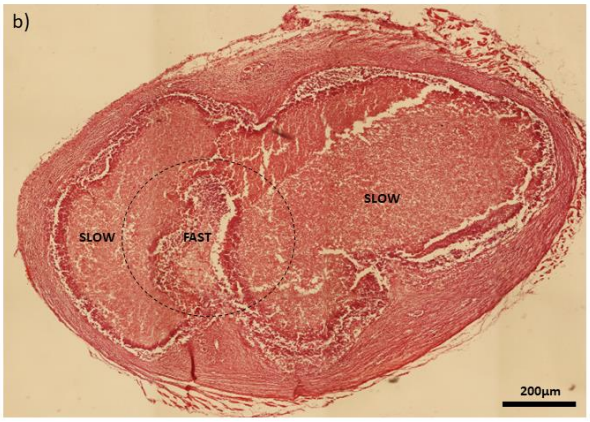
b)
SLOW
SLOW
FAST
200µm

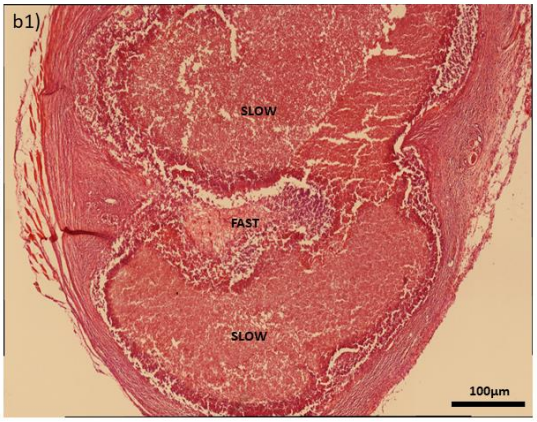
b1)
SLOW
FAST
SLOW
100µm

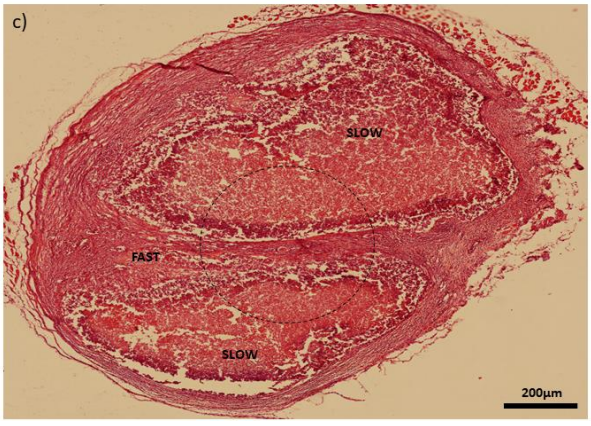
c)
SLOW
FAST
SLOW
200µm

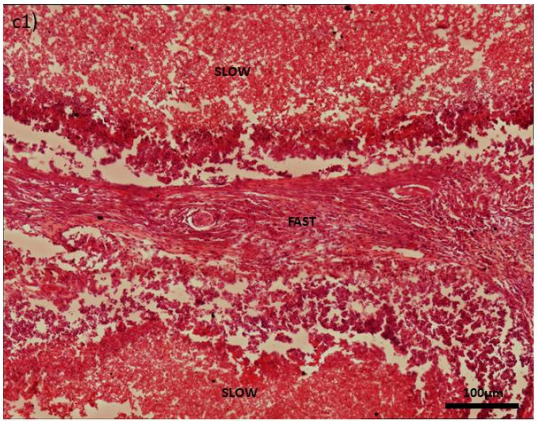
c1)
SLOW
FAST
SLOW
100µm

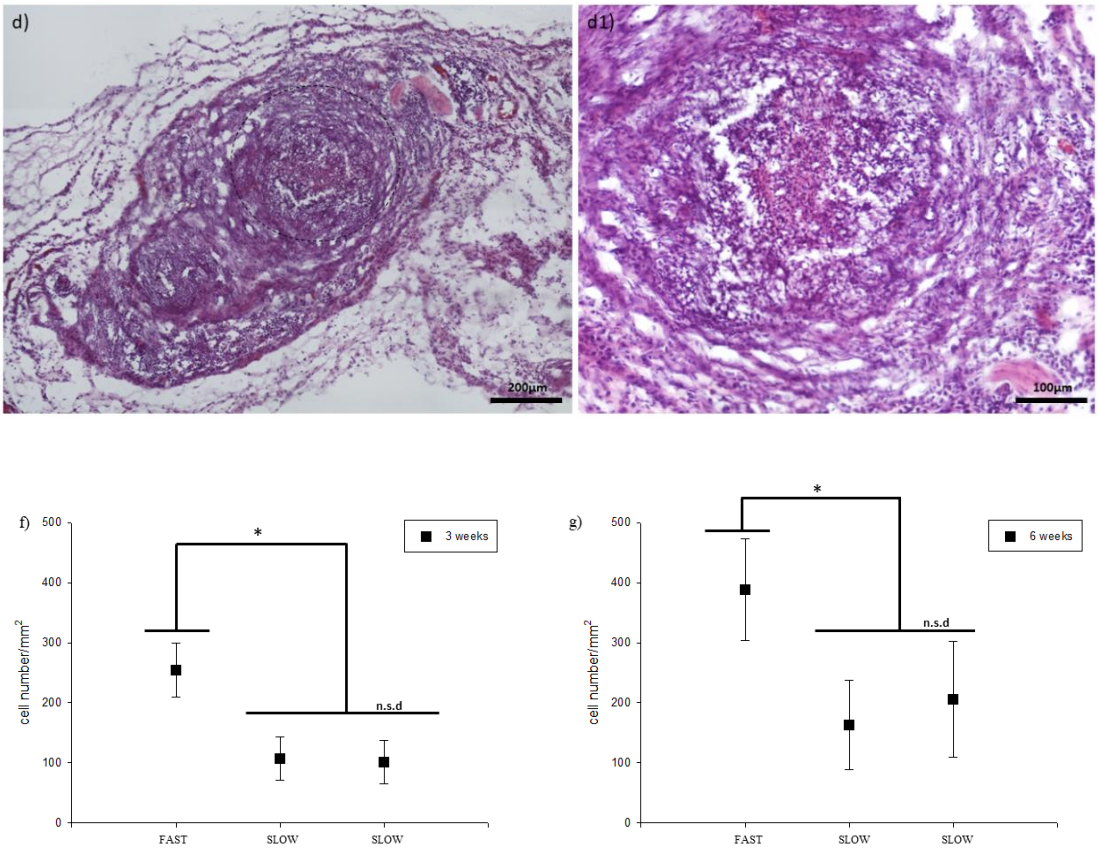

Figure 9. Histological analysis with H&E staining of the 3D structure at: a) 1 week post-implantation, a2) magnification of image where the three parts of the 3D system can be recognized a; b) 3 weeks post-implantation, b1) magnification of image b where it can be observed the initial phase of cell invasion; c) 6 weeks post-implantation, c1) magnification of image c where it can be noticed the complete degradation of the central part of the 3D system; d) 9 weeks post-implantation, d1) magnification of image d where it can be observed the complete cellular invasion and almost complete degradation of the two external parts of the 3D system. The dotted circle indicates the part of the image which was magnified f) graphic representation of number of cells/mm^2 that invaded the three parts of

the 3D system after three weeks post-implantation and g) after six weeks post-implantation. Data are reported as mean ± SD. *p<0.05; n.s.d no significant differences.

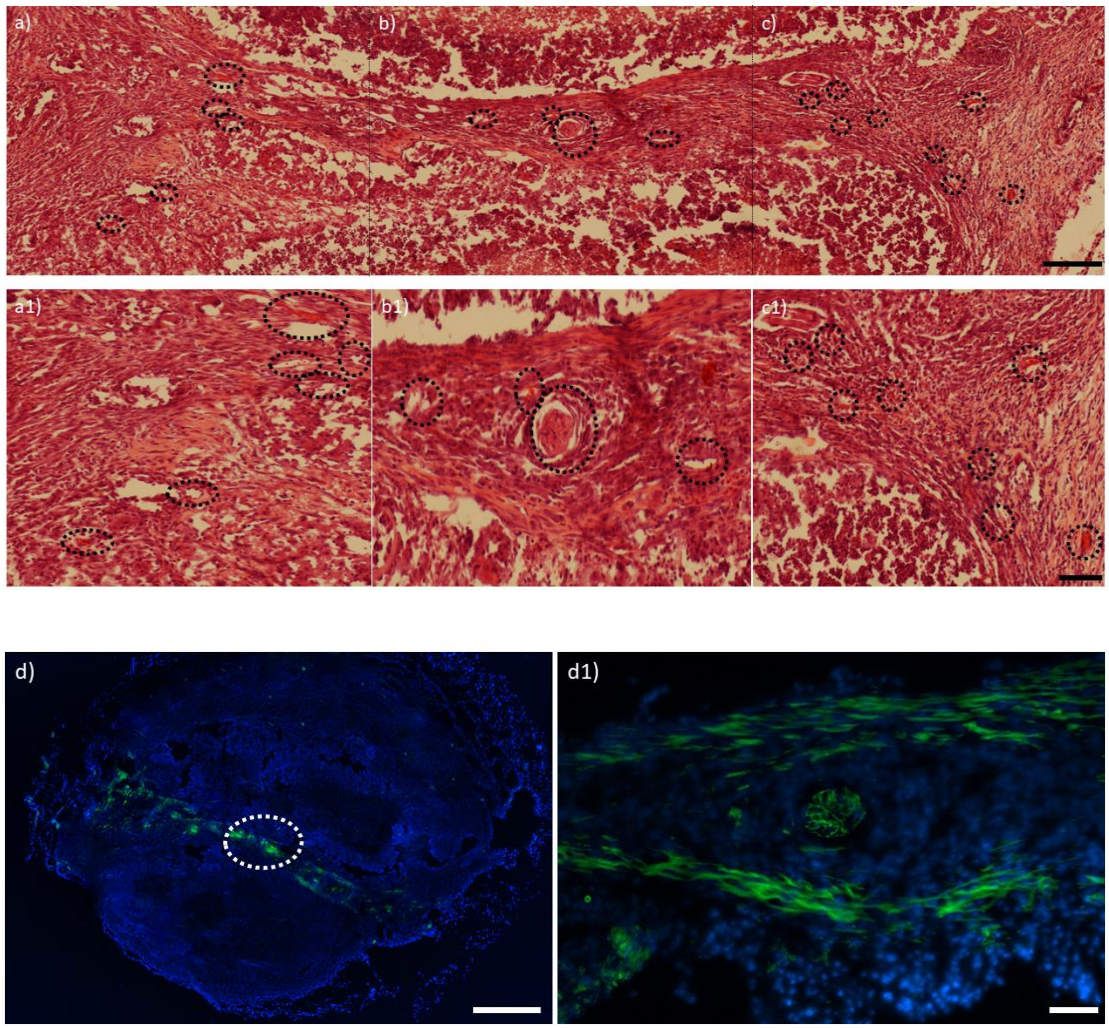

Figure 10. Histological analysis with: (a, b, c) H&E staining of the central part of the 3D-structured system at six weeks post-implantation. a1) magnification of zone a b1) magnification of zone b c1) magnification of zone c. Blotted circles indicates the presence of blood vessels or capillaries. d) CD31

immunofluorescent stain of the whole 3D system. Blotted circle indicates the area magnified in d1) magnification of the central area of the 3D system. Nuclei are stained blue with DAPI and overlaid with green-CD31. Scale bars: a, b, c, d) 100 μm; a1, b1, c1, d1) 50 μm.

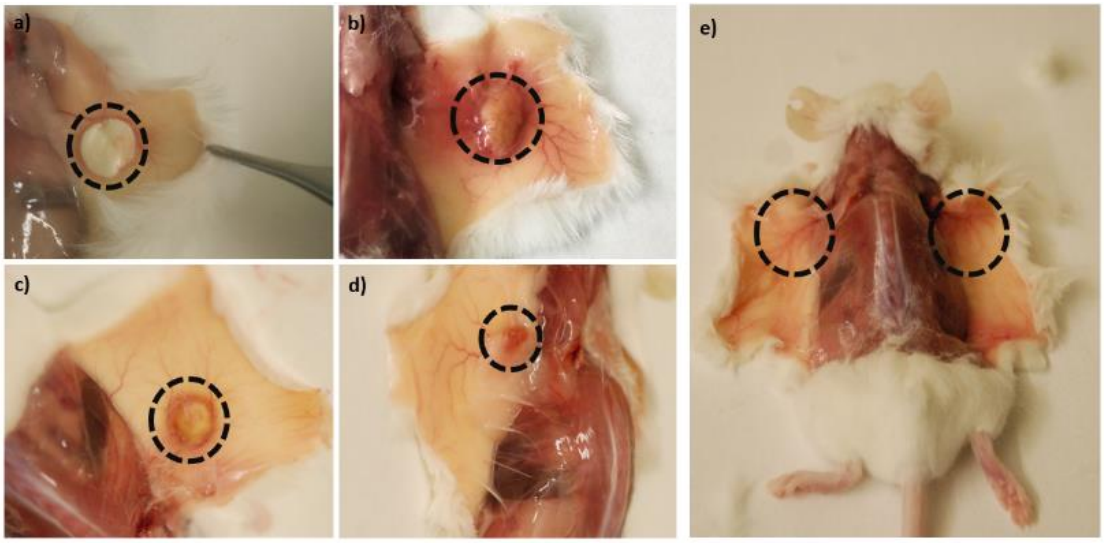

Figure 11. Summary of the 3D structure implantation in mice. The circles indicate the location of the 3D structure after: a) 1 week; b) 3 weeks; c) 6 weeks; d) 9 weeks post-implantation; and e) the complete absence of hydrogels after 12 weeks.

4. Discussion

Control of the biodegradation rate of biological substitutes remains a significant challenge in biomedical applications as a balance between neo-tissue formation and scaffold biodegradation must be achieved. [44, 45] Biomaterials with a controlled and predictable biodegradation are

therefore in high demand for the development of multi-functional scaffolds that can simultaneously provide mechanical support, reply to biological signals and resist physiological loads during the early stages of implementation. [46-48]

Protease-mediated degradation of biomaterials currently plays an important role in the development of 3D-structured systems employed in tissue engineering as it is able to provide a more precise and controlled environment for pre-programmed cell infiltration and biodegradation. [1] [49]

The 3D system presented herein consists of a bioactive 3D-structured ELR-based hydrogel that provides an appropriate microenvironment for cell growth and proliferation. In particular, this approach consists of controlling the orientation of cell infiltration over time while also controlling its structural transformation, thus meaning that it can be applied as a temporary soft tissue support for optimal regeneration processes.

This goal was achieved by synthesizing two different ELRs bearing proteolytic target sites with different degradation rates (fast and slow) belonging to the plasminogen activator system, specifically to the uPA enzyme, encoded into their backbone. Furthermore, for the construction of a 3D structure-system, an ELR containing a universal cell-adhesion

sequence (RGD) was employed, thereby resulting in the recruitment of a large number of cells inside the hydrogel that can trigger enzymes, thereby inducing proteolysis at the protease-sensitive sites. With regard to their physicochemical characterization (morphological features, mechanical properties and cytocompatibility), these ELR-based hydrogels proved to be effective as biological substitutes for future applications in tissue engineering. [50-52] [53] [54]

The degradation rate of these systems was initially studied *in vitro* using a human recombinant uPA enzyme, with a clear difference in terms of degradation being found. Initially, the ELR-based hydrogels containing each proteolytic ELR and RDG-ELR were investigated *in vivo* independently in order to determine how their degradation rates influence cell invasion and biodegradation. This study showed that there was a clear difference between the hydrogels containing the ELR with a fast degradation rate and the ELR-based hydrogels with a slow degradation rate in terms of cell-infiltration events, which is an important consideration for their subsequent application in tissue engineering. Tuning the design of these complex hydrogels by introducing proteolytic sites into the backbone of the protein has therefore been shown to improve adhesion and migration while adversely increasing hydrogel biodegradation.

These initial findings allowed us to develop a 3D-structured ELR-based hydrogel consisting of two external layers with an ELR characterized by a slow degradation rate and a central layer containing an ELR with a fast degradation rate to achieve predetermined cell invasion, thereby improving on conventional systems in which cells infiltrate in a more random manner. Several different approaches have been explored previously to control cell migration in hydrogels, including chemotaxis, which uses biochemical stimuli incorporated into the hydrogel, or durotaxis, which usies substrate rigidity and variations in the stiffness of hydrogels to enable cells to preferentially migrate from one region of a hydrogel to another. [55] [56]

Previous studies have demonstrated that synthetic scaffolds, such as PEG hydrogels containing MMP-sensitive peptides, display promising features that can support directed and guided cell behaviour and vascularization. Additionally, other synthetic scaffolds containing collagenase-sensitive peptide sequences have been used in a variety of tissue-engineering studies.[57] [57] [58] [59] However, these peptides exhibited slow cleavage rates and their incorporation into scaffolds resulted in slow rates of degradation, thus limiting *in vivo* cell invasion, vascularization and neo-tissue formation.

The 3D-structured ELR-based hydrogels designed herein were implanted subcutaneously in mice and cellular infiltration was found to start from the central layer of the structure, which comprises the recombinamer characterized by a fast degradation rate, subsequently migrating to the external layers, which are characterized by a slow degradation rate. At six weeks post-implantation, the entire central layer of the system was completely degraded and blood vessel formation had begun, thereby facilitating the transport of nutrients. Similarly, at nine weeks post-implantation, the two sections characterized by a slow degradation rate had been completely invaded by cells and, as a result, were almost completely degraded. Finally, at 12 weeks, no signs of the 3D-structured ELR-based hydrogel were found, in other words it had been completely reabsorbed. To the best of our knowledge, the ability to control cell infiltration *in vivo* using proteolytically mediated hydrogel degradation has not been reported previously.

In light of our results, cell invasion can easily be controlled by modulating the degradation rate of biomaterials used in the engineered constructs. Moreover, the presence of proteolytic target sites with a different degradation rate may potentially lead to more rapid and enhanced infiltration in a 3D system.

5. Conclusion

Hydrogel degradation rate is a crucial aspect that must be taken into consideration when such systems are used for biomedical purposes as their utility for a specific application depends on the length of time needed for tissue repair. In this study, we have examined a spatial-temporal control of cell infiltration into a 3D-structured ELR-based hydrogel made of two specific proteolytic ELRs with different degradation rates. A pre-programmed cell infiltration that progressed via an inside-to-outside pattern was observed.

This study offers an insight into the design of a simple 3D-structured system that can be used to promote directed and guided cell migration within engineered tissues and could easily be implemented for a specific type of tissue regeneration or even for the regeneration of more biologically complex structures such as organoids or organs.

6. Acknowledgements

The authors are grateful for funding from the European Commission (NMP-2014-646075, PITN-GA-2012-317306), the MINECO of the Spanish Government (PCIN-2015-010, MAT2015-68901-R, MAT2016-78903-R, MAT2016-79435-R), the Junta de Castilla y León (VA015U16) and the Centro en Red de Medicina Regenerativa y Terapia Celular de Castilla y León.

7. References

[1] Leijten J, Seo J, Yue K, Trujillo-de Santiago G, Tamayol A, Ruiz-Esparza GU, et al. Spatially and temporally controlled hydrogels for tissue engineering. Materials Science and Engineering: R: Reports. 2017;119:1-35.

[2] Drury JL, Mooney DJ. Hydrogels for tissue engineering: scaffold design variables and applications. Biomaterials. 2003;24:4337-51.

[3] Bishop ES, Mostafa S, Pakvasa M, Luu HH, Lee MJ, Wolf JM, et al. 3-D bioprinting technologies in tissue engineering and regenerative medicine: Current and future trends. Genes & diseases. 2017.

[4] Oliveira MB, Bastos HX, Mano JF. Sequentially Moldable and Bondable Four-Dimensional Hydrogels Compatible with Cell Encapsulation. Biomacromolecules. 2018.

[5] Li Y-C, Zhang YS, Akpek A, Shin SR, Khademhosseini A. 4D bioprinting: the next-generation technology for biofabrication enabled by stimuli-responsive materials. Biofabrication. 2016;9:012001.

[6] Ahearne M. Introduction to cell–hydrogel mechanosensing. Interface focus. 2014;4:20130038.

[7] Lu T, Li Y, Chen T. Techniques for fabrication and construction of three-dimensional scaffolds for tissue engineering. International journal of nanomedicine. 2013;8:337.

[8] O'brien FJ. Biomaterials & scaffolds for tissue engineering. Materials today. 2011;14:88-95.

[9] El-Sherbiny IM, Yacoub MH. Hydrogel scaffolds for tissue engineering: Progress and challenges. Global Cardiology Science and Practice. 2013:38.

[10] Hubbell JA. Biomaterials in tissue engineering. Nature Biotechnology. 1995;13:565.

[11] An J, Teoh JEM, Suntornnond R, Chua CK. Design and 3D printing of scaffolds and tissues. Engineering. 2015;1:261-8.

[12] Manavitehrani I, Fathi A, Wang Y, Maitz PK, Mirmohseni F, Cheng TL, et al. Fabrication of a Biodegradable Implant with Tunable Characteristics for Bone Implant Applications. Biomacromolecules. 2017;18:1736-46.

[13] Mahony O, Tsigkou O, Ionescu C, Minelli C, Ling L, Hanly R, et al. Silica-gelatin hybrids with tailorable degradation and mechanical properties for tissue regeneration. Advanced Functional Materials. 2010;20:3835-45.

[14] Zhang L, Liu X, Li G, Wang P, Yang Y. Tailoring degradation rates of silk fibroin scaffolds for tissue engineering. Journal of Biomedical Materials Research Part A. 2019;107:104-13.

[15] Girotti A, Reguera J, Rodríguez-Cabello JC, Arias FJ, Alonso M, Testera AM. Design and bioproduction of a recombinant multi (bio) functional elastin-like protein polymer containing cell adhesion sequences for tissue engineering purposes. Journal of Materials Science: Materials in Medicine. 2004;15:479-84.

[16] Staubli SM, Cerino G, De Torre IG, Alonso M, Oertli D, Eckstein F, et al. Control of angiogenesis and host response by modulating the cell adhesion properties of an Elastin-Like Recombinamer-based hydrogel. Biomaterials. 2017;135:30-41.

[17] Ibáñez-Fonseca A, Ramos TL, González de Torre I, Sánchez-Abarca LI, Muntión S, Arias FJ, et al. Biocompatibility of two model elastin-like recombinamer-based hydrogels formed through physical or chemical cross-linking for various applications in tissue engineering and regenerative medicine. Journal of tissue engineering and regenerative medicine. 2018;12:e1450-e60.

[18] Javier Arias F, Santos M, Fernández-Colino A, Pinedo G, Girotti A. Recent contributions of elastin-like recombinamers to biomedicine and nanotechnology. Current topics in medicinal chemistry. 2014;14:819-36.

[19] Urry DW, Parker TM, Reid MC, Gowda DC. Biocompatibility of the bioelastic materials, poly (GVGVP) and its γ-irradiation cross-linked matrix: summary of generic biological test results. Journal of Bioactive and Compatible Polymers. 1991;6:263-82.

[20] Nettles DL, Chilkoti A, Setton LA. Applications of elastin-like polypeptides in tissue engineering. Advanced drug delivery reviews. 2010;62:1479-85.

[21] MacEwan SR, Chilkoti A. Elastin-like polypeptides: Biomedical applications of tunable biopolymers. Peptide Science: Original Research on Biomolecules. 2010;94:60-77.

[22] Chan B, Leong K. Scaffolding in tissue engineering: general approaches and tissue-specific considerations. European spine journal. 2008;17:467-79.

[23] Rosso F, Giordano A, Barbarisi M, Barbarisi A. From cell–ECM interactions to tissue engineering. Journal of cellular physiology. 2004;199:174-80.

[24] Lyu S, Untereker D. Degradability of polymers for implantable biomedical devices. International journal of molecular sciences. 2009;10:4033-65.

[25] Akalp U, Bryant SJ, Vernerey FJ. Tuning tissue growth with scaffold degradation in enzyme-sensitive hydrogels: a mathematical model. Soft matter. 2016;12:7505-20.

[26] Werb Z. ECM and cell surface proteolysis: regulating cellular ecology. Cell. 1997;91:439-42.

[27] Lutolf M, Lauer-Fields J, Schmoekel H, Metters AT, Weber F, Fields G, et al. Synthetic matrix metalloproteinase-sensitive hydrogels for the conduction of tissue regeneration: engineering cell-invasion characteristics. Proceedings of the National Academy of Sciences. 2003;100:5413-8.

[28] Sokic S, Christenson M, Larson J, Appel A, Brey E, Papavasiliou G. Evaluation of MMP substrate concentration and specificity for neovascularization of hydrogel scaffolds. Biomaterials science. 2014;2:1343-54.

[29] Mecham RP, Broekelmann TJ, Fliszar CJ, Shapiro SD, Welgus HG, Senior RM. Elastin degradation by matrix metalloproteinases Cleavage site specificity and mechanisms of elastolysis. Journal of Biological Chemistry. 1997;272:18071-6.

[30] Lund LR, Green KA, Stoop AA, Ploug M, Almholt K, Lilla J, et al. Plasminogen activation independent of uPA and tPA maintains wound healing in gene-deficient mice. The EMBO journal. 2006;25:2686-97.

[31] Van Hinsbergh VW, Engelse MA, Quax PH. Pericellular proteases in angiogenesis and vasculogenesis. Arteriosclerosis, thrombosis, and vascular biology. 2006;26:716-28.

[32] Vassalli J-D, Sappino A, Belin D. The plasminogen activator/plasmin system. The Journal of clinical investigation. 1991;88:1067-72.

[33] Neurath H, Walsh KA. Role of proteolytic enzymes in biological regulation (a review). Proceedings of the National Academy of Sciences. 1976;73:3825-32.

[34] Yan Q, Dong H, Su J, Han J, Song B, Wei Q, et al. A Review of 3D Printing Technology for Medical Applications. Engineering. 2018.

[35] Banerjee A, Chatterjee K, Madras G. Enzymatic degradation of polymers: a brief review. Materials Science and Technology. 2014;30:567-73.

[36] Straley KS, Heilshorn SC. Dynamic, 3D-Pattern Formation Within Enzyme-Responsive Hydrogels. Advanced Materials. 2009;21:4148-52.

[37] Girotti A, Fernández-Colino A, López IM, Rodríguez-Cabello JC, Arias FJ. Elastin-like recombinamers: Biosynthetic strategies and biotechnological applications. Biotechnology journal. 2011;6:1174-86.

[38] Testera AM, Girotti A, de Torre IG, Quintanilla L, Santos M, Alonso M, et al. Biocompatible elastin-like click gels: design, synthesis and characterization. Journal of Materials Science: Materials in Medicine. 2015;26:105.

[39] Rodríguez-Cabello JC, Girotti A, Ribeiro A, Arias FJ. Synthesis of genetically engineered protein polymers (recombinamers) as an example of advanced self-assembled smart materials. Nanotechnology in Regenerative Medicine: Springer; 2012. p. 17-38.

[40] Fischer AH, Jacobson KA, Rose J, Zeller R. Hematoxylin and eosin staining of tissue and cell sections. Cold Spring Harbor Protocols. 2008;2008:pdb. prot4986.

[41] Ke S-H, Coombs GS, Tachias K, Corey DR, Madison EL. Optimal subsite occupancy and design of a selective inhibitor of urokinase. Journal of Biological Chemistry. 1997;272:20456-62.

[42] Vedadghavami A, Minooei F, Mohammadi MH, Khetani S, Kolahchi AR, Mashayekhan S, et al. Manufacturing of hydrogel biomaterials with controlled mechanical properties for tissue engineering applications. Acta biomaterialia. 2017;62:42-63.

[43] Hollister SJ. Porous scaffold design for tissue engineering. Nature materials. 2005;4:518.

[44] Nair LS, Laurencin CT. Biodegradable polymers as biomaterials. Progress in polymer science. 2007;32:762-98.

[45] Jammalamadaka U, Tappa K. Recent advances in biomaterials for 3D printing and tissue engineering. Journal of functional biomaterials. 2018;9:22.

[46] Khademhosseini A, Langer R. A decade of progress in tissue engineering. Nature protocols. 2016;11:1775.

[47] Miao S, Zhu W, Castro NJ, Leng J, Zhang LG. Four-dimensional printing hierarchy scaffolds with highly biocompatible smart polymers for tissue engineering applications. Tissue Engineering Part C: Methods. 2016;22:952-63.

[48] West JL, Hubbell JA. Polymeric biomaterials with degradation sites for proteases involved in cell migration. Macromolecules. 1999;32:241-4.

[49] Zhang YS, Khademhosseini A. Advances in engineering hydrogels. Science. 2017;356:eaaf3627.

[50] Coletta DJ, Ibáñez-Fonseca A, Missana LR, Jammal MV, Vitelli EJ, Aimone M, et al. Bone Regeneration Mediated by a Bioactive and Biodegradable Extracellular Matrix-Like Hydrogel Based on Elastin-Like Recombinamers. Tissue Engineering Part A. 2017;23:1361-71.

[51] Rodríguez-Cabello JC, de Torre IG, Ibañez-Fonseca A, Alonso M. Bioactive scaffolds based on elastin-like materials for wound healing. Advanced drug delivery reviews. 2018;129:118-33.

[52] de Torre IG, Ibáñez-Fonseca A, Quintanilla L, Alonso M, Rodríguez-Cabello J-C. Random and oriented electrospun fibers based on a multicomponent, in situ clickable elastin-like recombinamer system for dermal tissue engineering. Acta biomaterialia. 2018;72:137-49.

[53] Pescador D, Ibáñez-Fonseca A, Sánchez-Guijo F, Briñón JG, Arias FJ, Muntión S, et al. Regeneration of hyaline cartilage promoted by xenogeneic mesenchymal stromal cells embedded within elastin-like recombinamer-based bioactive hydrogels. Journal of Materials Science: Materials in Medicine. 2017;28:115.

[54] de Torre IG, Wolf F, Santos M, Rongen L, Alonso M, Jockenhoevel S, et al. Elastin-like recombinamer-covered stents: Towards a fully biocompatible and non-thrombogenic device for cardiovascular diseases. Acta biomaterialia. 2015;12:146-55.

[55] Sung H-J, Meredith C, Johnson C, Galis ZS. The effect of scaffold degradation rate on three-dimensional cell growth and angiogenesis. Biomaterials. 2004;25:5735-42.

[56] Azevedo HS, Reis RL. Understanding the enzymatic degradation of biodegradable polymers and strategies to control their degradation rate. Biodegradable systems in tissue engineering and regenerative medicine. 2005:177-201.

[57] Wade RJ, Bassin EJ, Rodell CB, Burdick JA. Protease-degradable electrospun fibrous hydrogels. Nature communications. 2015;6:6639.

[58] Galler KM, Aulisa L, Regan KR, D'Souza RN, Hartgerink JD. Self-assembling multidomain peptide hydrogels: designed susceptibility to enzymatic cleavage allows enhanced cell migration and spreading. Journal of the American Chemical Society. 2010;132:3217-23.

[59] Jun HW, Yuwono V, Paramonov SE, Hartgerink JD. Enzyme-mediated degradation of peptide-amphiphile nanofiber networks. Advanced Materials. 2005;17:2612-7.

8. Supporting Information

1. Characterization of proteolytic ELRs

1.1 DNA sequencing of GTAR-ELR and DRIR-ELR

a) GTAR-ELR

```
          S  R  N  N  F  V  *  L  *  E  G  D  I  H  M  E  S  L  L  P  V  P  G  I  G  V
1     CTCTAGAAATAATTTTGTTTAACTTTAAGAAGGAGATATACATATGGAATCACTACTACCCGTACCGGGCATTGGTGTTC   80
1     GAGATCTTTATTAAAACAAATTGAAATTCTTCCTCTATATGTATACCTTAGTGATGATGGGCATGGCCCGTAACCACAAG   80
          P  G  I  G  V  P  G  K  G  V  P  G  I  G  V  P  G  I  G  V  P  G  I  G  V  P  G
81    CGGGCATCGGTGTGCCGGGCAAAGGTGTTCCGGGCATTGGTGTGCCGGGCATCGGTGTGCCAGGCATTGGTGTGCCGGGC  160
81    GCCCGTAGCCACACGGCCCGTTTCCACAAGGCCCGTAACCACACGGCCCGTAGCCACACGGTCCGTAACCACACGGCCCG  160
           I  G  V  P  G  K  G  V  P  G  I  G  V  P  G  I  G  V  Y  A  V  T  G  G  T  A  R
161   ATCGGTGTTCCGGGCAAGGGTGTGCCGGGCATCGGTGTGCCAGGCATTGGTGTATACGCAGTTACCGGTGGCACCGCGCG  240
161   TAGCCACAAGGCCCGTTCCCACACGGCCCGTAGCCACACGGTCCGTAACCACATATGCGTCAATGGCCACCGTGGCGCGC  240
            S  A  S  P  A  S  S  A  V  P  G  I  G  V  P  G  I  G  V  P  G  K  G  V  P  G
241   TTCCGCTTCTCCGGCGTCCTCTGCAGTACCGGGCATTGGTGTTCCGGGCATCGGTGTGCCGGGCAAAGGTGTTCCGGGCA  320
241   AAGGCGAAGAGGCCGCAGGAGACGTCATGGCCCGTAACCACAAGGCCCGTAGCCACACGGCCCGTTTCCACAAGGCCCGT  320
          I  G  V  P  G  I  G  V  P  G  I  G  V  P  G  I  G  V  P  G  K  G  V  P  G  I  G
321   TTGGTGTGCCGGGCATCGGTGTGCCAGGCATTGGTGTGCCGGGCATCGGTGTTCCGGGCAAGGGTGTGCCGGGCATCGGT  400
321   AACCACACGGCCCGTAGCCACACGGTCCGTAACCACACGGCCCGTAGCCACAAGGCCCGTTCCCACACGGCCCGTAGCCA  400


          V  P  G  I  G  V  P  G  I  G  V  P  G  I  G  V  P  G  K  G  V  P  G  I  G  V  P
401   GTGCCAGGCATTGGTGTACCGGGCATTGGTGTTCCGGGCATCGGTGTGCCGGGCAAAGGTGTTCCGGGCATTGGTGTGCC  480
401   CACGGTCCGTAACCACATGGCCCGTAACCACAAGGCCCGTAGCCACACGGCCCGTTTCCACAAGGCCCGTAACCACACGG  480
            G  I  G  V  P  G  I  G  V  P  G  I  G  V  P  G  K  G  V  P  G  I  G  V  P  G
481   GGGCATCGGTGTGCCAGGCATTGGTGTGCCGGGCATCGGTGTTCCGGGCAAGGGTGTGCCGGGCATCGGTGTGCCAGGCA  560
481   CCCGTAGCCACACGGTCCGTAACCACACGGCCCGTAGCCACAAGGCCCGTTCCCACACGGCCCGTAGCCACACGGTCCGT  560
          I  G  V  Y  A  V  T  G  G  T  A  R  S  A  S  P  A  S  S  A  V  P  G  I  G  V  P
561   TTGGTGTATACGCAGTTACCGGTGGCACCGCGCGTTCCGCTTCTCCGGCGTCCTCTGCAGTACCGGGCATTGGTGTTCCG  640
561   AACCACATATGCGTCAATGGCCACCGTGGCGCGCAAGGCGAAGAGGCCGCAGGAGACGTCATGGCCCGTAACCACAAGGC  640
           G  I  G  V  P  G  K  G  V  P  G  I  G  V  P  G  I  G  V  P  G  I  G  V  P  G  I
641   GGCATCGGTGTGCCGGGCAAAGGTGTTCCGGGCATTGGTGTGCCGGGCATCGGTGTGCCAGGCATTGGTGTGCCGGGCAT  720
```

```
641     CCGTAGCCACACGGCCCGTTTCCACAAGGCCCGTAACCACACGGCCCGTAGCCACACGGTCCGTAACCACACGGCCCGTA   720
          G  V  P  G  K  G  V  P  G  I  G  V  P  G  I  G  V  P  G  I  G  V  P  G  I  G
721     CGGTGTTCCGGGCAAGGGTGTGCCGGGCATCGGTGTGCCAGGCATTGGTGTACCGGGCATTGGTGTTCCGGGCATCGGTG   800
721     GCCACAAGGCCCGTTCCCACACGGCCCGTAGCCACACGGTCCGTAACCACATGGCCCGTAACCACAAGGCCCGTAGCCAC   800
        V  P  G  K  G  V  P  G  I  G  V  P  G  I  G  V  P  G  I  G  V  P  G  I  G  V  P
801     TGCCGGGCAAAGGTGTTCCGGGCATTGGTGTGCCGGGCATCGGTGTGCCAGGCATTGGTGTGCCGGGCATCGGTGTTCCG   880
801     ACGGCCCGTTTCCACAAGGCCCGTAACCACACGGCCCGTAGCCACACGGTCCGTAACCACACGGCCCGTAGCCACAAGGC   880
          G  K  G  V  P  G  I  G  V  P  G  I  G  V  Y  A  V  T  G  G  T  A  R  S  A  S  P
881     GGCAAGGGTGTGCCGGGCATCGGTGTGCCAGGCATTGGTGTATACGCAGTTACCGGTGGCACCGCGCGTTCCGCTTCTCC   960
881     CCGTTCCCACACGGCCCGTAGCCACACGGTCCGTAACCACATATGCGTCAATGGCCACCGTGGCGCGCAAGGCGAAGAGG   960
          A  S  S  A  V  P  G  I  G  V  P  G  I  G  V  P  G  K  G  V  P  G  I  G  V  P
961     GGCGTCCTCTGCAGTACCGGGCATTGGTGTTCCGGGCATCGGTGTGCCGGGCAAAGGTGTTCCGGGCATTGGTGTGCCGG  1040
961     CCGCAGGAGACGTCATGGCCCGTAACCACAAGGCCCGTAGCCACACGGCCCGTTTCCACAAGGCCCGTAACCACACGGCC  1040
        G  I  G  V  P  G  I  G  V  P  G  I  G  V  P  G  K  G  V  P  G  I  G  V  P  G  I
1041    GCATCGGTGTGCCAGGCATTGGTGTGCCGGGCATCGGTGTTCCGGGCAAGGGTGTGCCGGGCATCGGTGTGCCAGGCATT  1120
1041    CGTAGCCACACGGTCCGTAACCACACGGCCCGTAGCCACAAGGCCCGTTCCCACACGGCCCGTAGCCACACGGTCCGTAA  1120
          G  V  P  G  I  G  V  P  G  H  P  C  A  R  A  K  V  F  P  G  I  G  V  P  G  H  P
1121    GGTGTACCGGGCATTGGTGTTCCCGGGCATCCGTGTGCCCGGGCAAAGGTGTTTCCGGGCATTGGTGTGCCCGGGCATCC  1200
1121    CCACATGGCCCGTAACCACAAGGGCCCGTAGGCACACGGGCCCGTTTCCACAAAGGCCCGTAACCACACGGGCCCGTAGG  1200
          C  A  Q  A  L  V  C  P  G  I  G  V  S  R  Q  G  C  A  R  A  S  V  C  P  G  I
1201    GTGTGCCCAGGCATTGGTGTGCCCGGGCATCGGTGTTTCCCGGCAAGGGTGTGCCCGGGCATCGGTGTGCCCAGGCATTT  1280
1201    CACACGGGTCCGTAACCACACGGGCCCGTAGCCACAAAGGGCCGTTCCCACACGGGCCCGTAGCCACACGGGTCCGTAAA  1280
```

b) DRIR-ELR

```
          G  N  N  F  V  *  L  *  E  G  D  I  H  M  E  S  L  L  P  V  P  G  I  G  V  P
1       AGGAAATAATTTTGTTTAACTTTAAGAAGGAGATATACATATGGAATCACTACTACCCGTACCGGGCATTGGTGTTCCGG   80
1       TCCTTTATTAAAACAAATTGAAATTCTTCCTCTATATGTATACCTTAGTGATGATGGGCATGGCCCGTAACCACAAGGCC
        G  I  G  V  P  G  K  G  V  P  G  I  G  V  P  G  I  G  V  P  G  I  G  V  P  G  I
81      GCATCGGTGTGCCGGGCAAAGGTGTTCCGGGCATTGGTGTGCCGGGCATCGGTGTGCCAGGCATTGGTGTGCCGGGCATC  160
81      CGTAGCCACACGGCCCGTTTCCACAAGGCCCGTAACCACACGGCCCGTAGCCACACGGTCCGTAACCACACGGCCCGTAG  160
          G  V  P  G  K  G  V  P  G  I  G  V  P  G  I  G  V  Y  A  V  T  G  D  R  I  R  S
161     GGTGTTCCGGGCAAGGGTGTGCCGGGCATCGGTGTGCCAGGCATTGGTGTATACGCAGTTACCGGTGACCGTATCCGTTC  240
161     CCACAAGGCCCGTTCCCACACGGCCCGTAGCCACACGGTCCGTAACCACATATGCGTCAATGGCCACTGGCATAGGCAAG  240
```

```
          A  S  P  A  S  S  A  V  P  G  I  G  V  P  G  I  G  V  P  G  K  G  V  P  G  I

241   CGCTTCTCCGGCGTCCTCTGCAGTACCGGGCATTGGTGTTCCGGGCATCGGTGTGCCGGGCAAAGGTGTTCCGGGCATTG   320

241   GCGAAGAGGCCGCAGGAGACGTCATGGCCCGTAACCACAAGGCCCGTAGCCACACGGCCCGTTTCCACAAGGCCCGTAAC   320

          G  V  P  G  I  G  V  P  G  I  G  V  P  G  I  G  V  P  G  K  G  V  P  G  I  G  V

321   GTGTGCCGGGCATCGGTGTGCCAGGCATTGGTGTGCCGGGCATCGGTGTTCCGGGCAAGGGTGTGCCGGGCATCGGTGTG   400

321   CACACGGCCCGTAGCCACACGGTCCGTAACCACACGGCCCGTAGCCACAAGGCCCGTTCCCACACGGCCCGTAGCCACAC   400

           P  G  I  G  V  P  G  I  G  V  P  G  I  G  V  P  G  K  G  V  P  G  I  G  V  P  G

401   CCAGGCATTGGTGTACCGGGCATTGGTGTTCCGGGCATCGGTGTGCCGGGCAAAGGTGTTCCGGGCATTGGTGTGCCGGG   480

401   GGTCCGTAACCACATGGCCCGTAACCACAAGGCCCGTAGCCACACGGCCCGTTTCCACAAGGCCCGTAACCACACGGCCC   480

          I  G  V  P  G  I  G  V  P  G  I  G  V  P  G  K  G  V  P  G  I  G  V  P  G  I

481   CATCGGTGTGCCAGGCATTGGTGTGCCGGGCATCGGTGTTCCGGGCAAGGGTGTGCCGGGCATCGGTGTGCCAGGCATTG   560

481   GTAGCCACACGGTCCGTAACCACACGGCCCGTAGCCACAAGGCCCGTTCCCACACGGCCCGTAGCCACACGGTCCGTAAC   560

          G  V  Y  A  V  T  G  D  R  I  R  S  A  S  P  A  S  S  A  V  P  G  I  G  V  P  G

561   GTGTATACGCAGTTACCGGTGACCGTATCCGTTCCGCTTCTCCGGCGTCCTCTGCAGTACCGGGCATTGGTGTTCCGGGC   640

561   CACATATGCGTCAATGGCCACTGGCATAGGCAAGGCGAAGAGGCCGCAGGAGACGTCATGGCCCGTAACCACAAGGCCCG   640

          I  G  V  P  G  K  G  V  P  G  I  G  V  P  G  I  G  V  P  G  I  G  V  P  G  I  G

641   ATCGGTGTGCCGGGCAAAGGTGTTCCGGGCATTGGTGTGCCGGGCATCGGTGTGCCAGGCATTGGTGTGCCGGGCATCGG   720

641   TAGCCACACGGCCCGTTTCCACAAGGCCCGTAACCACACGGCCCGTAGCCACACGGTCCGTAACCACACGGCCCGTAGCC   720

          V  P  G  K  G  V  P  G  I  G  V  P  G  I  G  V  P  G  I  G  V  P  G  I  G  V

721   TGTTCCGGGCAAGGGTGTGCCGGGCATCGGTGTGCCAGGCATTGGTGTACCGGGCATTGGTGTTCCGGGCATCGGTGTGC   800

721   ACAAGGCCCGTTCCCACACGGCCCGTAGCCACACGGTCCGTAACCACATGGCCCGTAACCACAAGGCCCGTAGCCACACG   800


          P  G  K  G  V  P  G  I  G  V  P  G  I  G  V  P  G  I  G  V  P  G  I  G  V  P  G

801   CGGGCAAAGGTGTTCCGGGCATTGGTGTGCCGGGCATCGGTGTGCCAGGCATTGGTGTGCCGGGCATCGGTGTTCCGGGC   880

801   GCCCGTTTCCACAAGGCCCGTAACCACACGGCCCGTAGCCACACGGTCCGTAACCACACGGCCCGTAGCCACAAGGCCCG   880

          K  G  V  P  G  I  G  V  P  G  I  G  V  Y  A  V  T  G  D  R  I  R  S  A  S  P  A

881   AAGGGTGTGCCGGGCATCGGTGTGCCAGGCATTGGTGTATACGCAGTTACCGGTGACCGTATCCGTTCCGCTTCTCCGGC   960

881   TTCCCACACGGCCCGTAGCCACACGGTCCGTAACCACATATGCGTCAATGGCCACTGGCATAGGCAAGGCGAAGAGGCCG   960

          S  S  A  V  P  G  I  G  V  P  G  I  G  V  P  G  K  G  V  P  G  I  G  V  P  G

961   GTCCTCTGCAGTACCGGGCATTGGTGTTCCGGGCATCGGTGTGCCGGGCAAAGGTGTTCCGGGCATTGGTGTGCCGGGCA  1040

961   CAGGAGACGTCATGGCCCGTAACCACAAGGCCCGTAGCCACACGGCCCGTTTCCACAAGGCCCGTAACCACACGGCCCGT  1040

          I  G  V  P  G  I  G  V  P  G  I  G  V  P  G  K  G  V  P  G  I  G  V  P  G  I  G

1041  TCGGTGTGCCAGGCATTGGTGTGCCGGGCATCGGTGTTCCGGGCAAGGGTGTGCCGGGCATCGGTGTGCCAGGCATTGGT  1120

1041  AGCCACACGGTCCGTAACCACACGGCCCGTAGCCACAAGGCCCGTTCCCACACGGCCCGTAGCCACACGGTCCGTAACCA  1120
```

```
          V  P  G  I  G  V  P  G  I  G  V  P  G  K  G  V  P  G  I  G  V  P  G  H  R  C  C
1121    GTACCGGGCATTGGTGTTCCGGGCATCGGTGTGCCGGGCAAAGGTGTTCCGGGCATTGGTGTGCCCGGGCATCGGTGTTG   1200
1121    CATGGCCCGTAACCACAAGGCCCGTAGCCACACGGCCCGTTTCCACAAGGCCCGTAACCACACGGGCCCGTAGCCACAAC   1200
            Q  A  L  V  C  P  G  I  R  V  S  G  Q  G  C  A  R  A  S  G  V  P  R  H  W  V
1201    CCAGGCATTGGTGTGCCCGGGCATCCGTGTTTCCGGGCAAGGGTGTGCCCGGGCATCCGGTGTGCCCAGGCATTGGGTGT   1280
1201    GGTCCGTAACCACACGGGCCCGTAGGCACAAAGGCCCGTTCCCACACGGGCCCGTAGGCCACACGGGTCCGTAACCCACA   1281
```

Figure S1. Amino acid sequence analysed by Bioedit program of a) GTAR-ELR and b) DRIR-ELR

1.2. SDS-PAGE electrphoresis

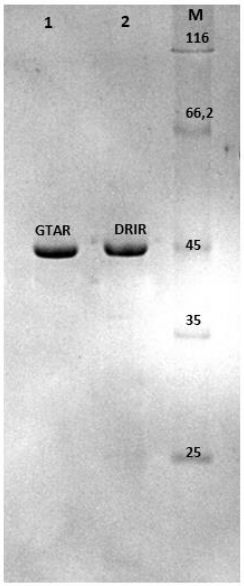

Figure S2. SDS-PAGE electrophoresis of GTAR-ELR (line 1) and DRIR-ELR (line 2). Line M: unstained protein molecular weight marker. The numbers on the top of the bands indicates the molecular weight of the standards.

1.3. Amino acid analysis

Table S1. Amino acid composition of GTAR-ELR AND DRIR-ELR.

GTAR			DRIR		
aa	**Calculated**	**Theoric**	**aa**	**Calculated**	**Theoric**
D	**0.00**		**D**	**3.89**	**4**
E	**1.55**	**1**	**E**	**1.55**	**1**
N	**0.00**		**N**	**0.00**	
S	**14.52**	**18**	**S**	**17.52**	**18**
Q	**0.00**		**Q**	**0.00**	
H	**0.00**		**H**	**0.00**	
G	**171.39**	**168**	**G**	**164.39**	**164**
T	**7.80**	**8**	**T**	**4.80**	**4**
R	**4.02**	**4**	**R**	**8.02**	**8**
A	**20.09**	**20**	**A**	**17.09**	**16**
Y	**3.42**	**4**	**Y**	**3.42**	**4**
C	**0.00**		**C**	**0.00**	
V	**83.51**	**85**	**V**	**84.51**	**85**
M	**1.07**	**1**	**M**	**1.07**	**1**
W	**0.00**		**W**	**0.00**	
F	**0.00**		**F**	**0.00**	
I	**64.71**	**64**	**I**	**68.71**	**68**
L	**2.63**	**2**	**L**	**2.63**	**2**
K	**17.76**	**16**	**K**	**17.76**	**16**
P	**83.94**	**85**	**P**	**83.94**	**85**

1.4. Fourier Transformation Infrared Spectroscopy (FTIR)

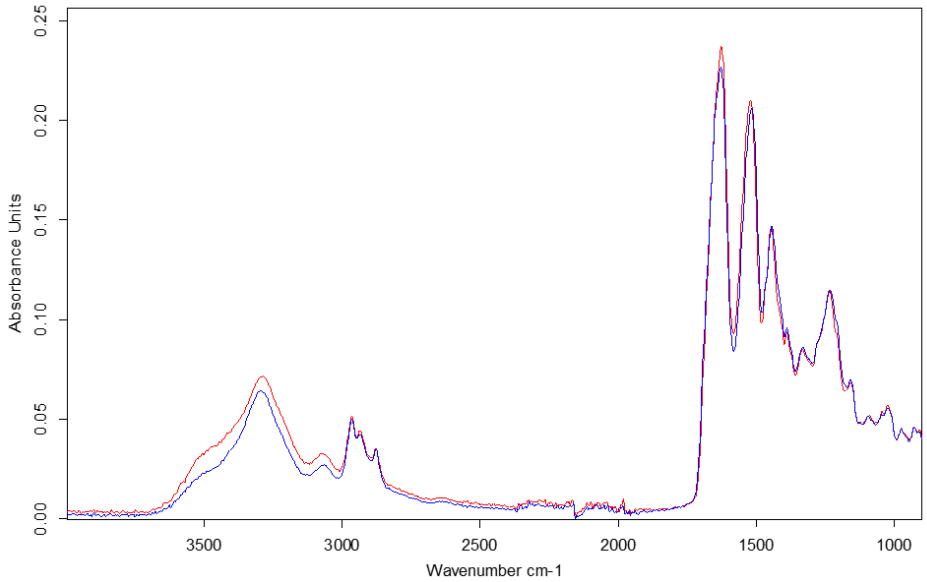

Figure S3. FTIR spectrum of GTAR-ELR and DRIR-ELR.

1.5. Matrix-Assisted Laser Desorption/Ionization Time Of Flight (MALDI-TOF)

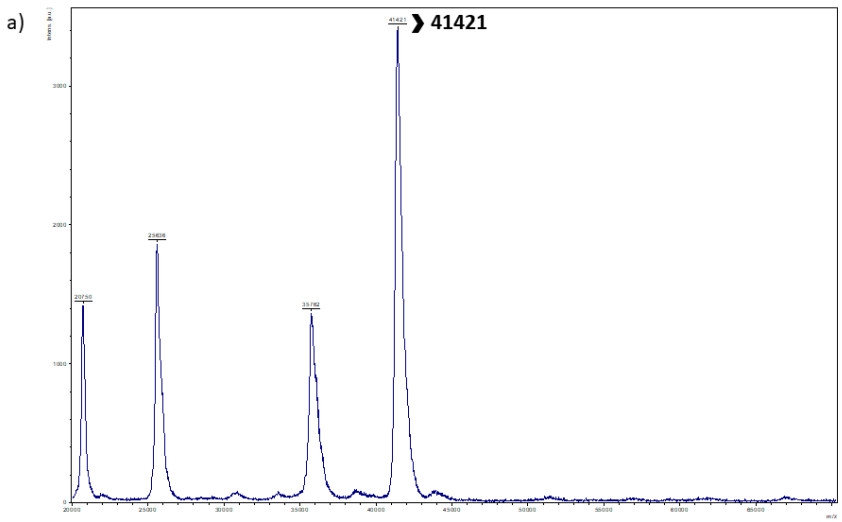

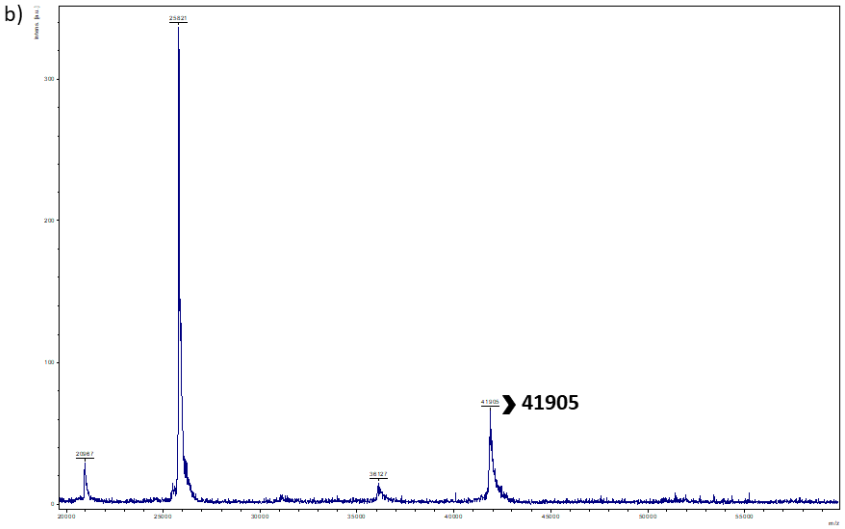

Figure S4. MALDI-TOF spectrum of a) GTAR-ELR and b) DRIR-ELR.

2. Characterization of proteolytic ELRs modified chemically via click reaction.

2.1 Differential scanning calorimetry (DSC)

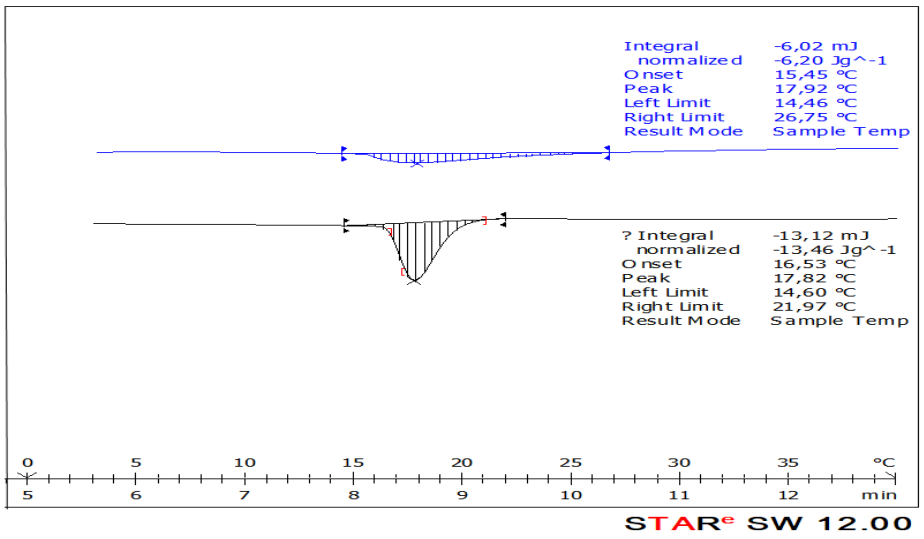

Figure S 2.1. DSC thermograms of GTAR-ELR and DRIR-ELR dissolved in PBS (pH=7.1)

2.2 Nuclear Magnetic Resonance (NMR)

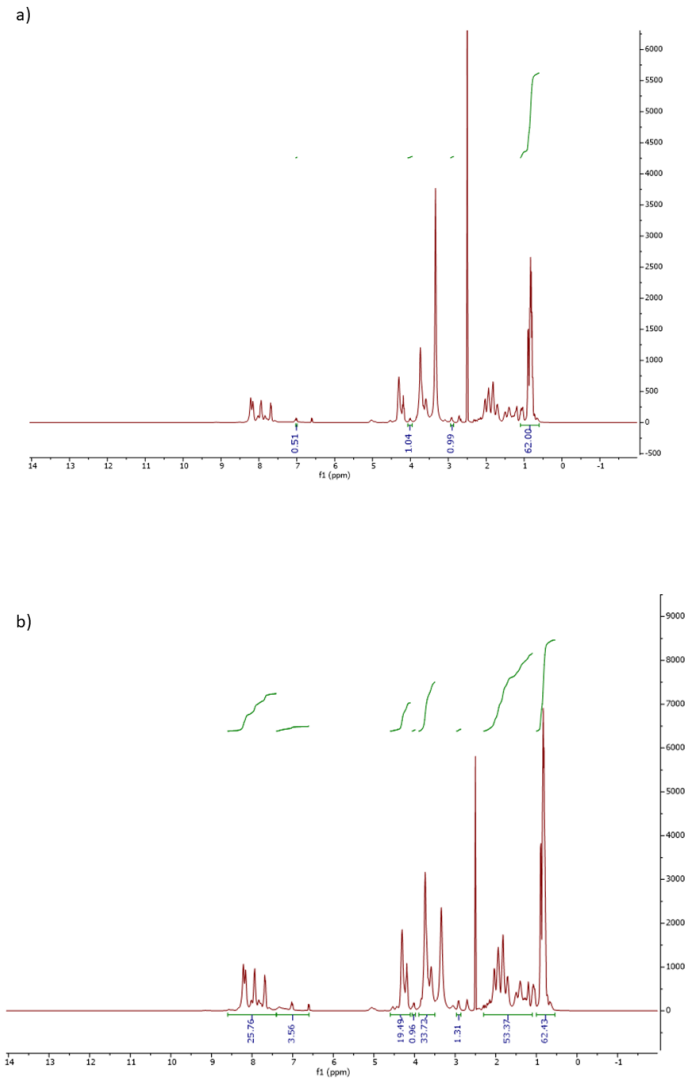

Figure S 2.2 NMR spectrum of a) GTAR-ELR and b) DRIR-ELR after their chemical modification.

3. *In vivo* studies of proteolytic ELR-based hydrogels.

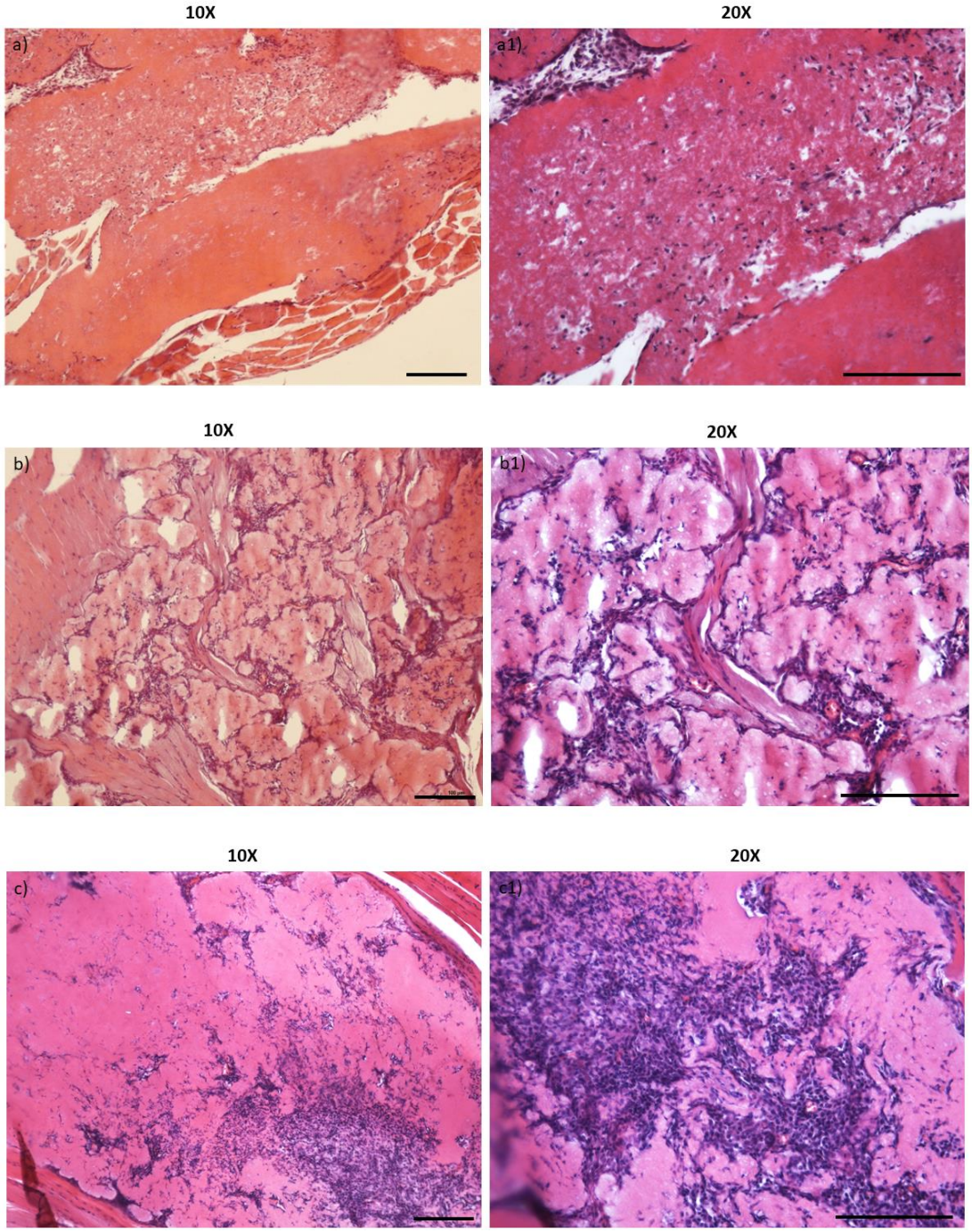

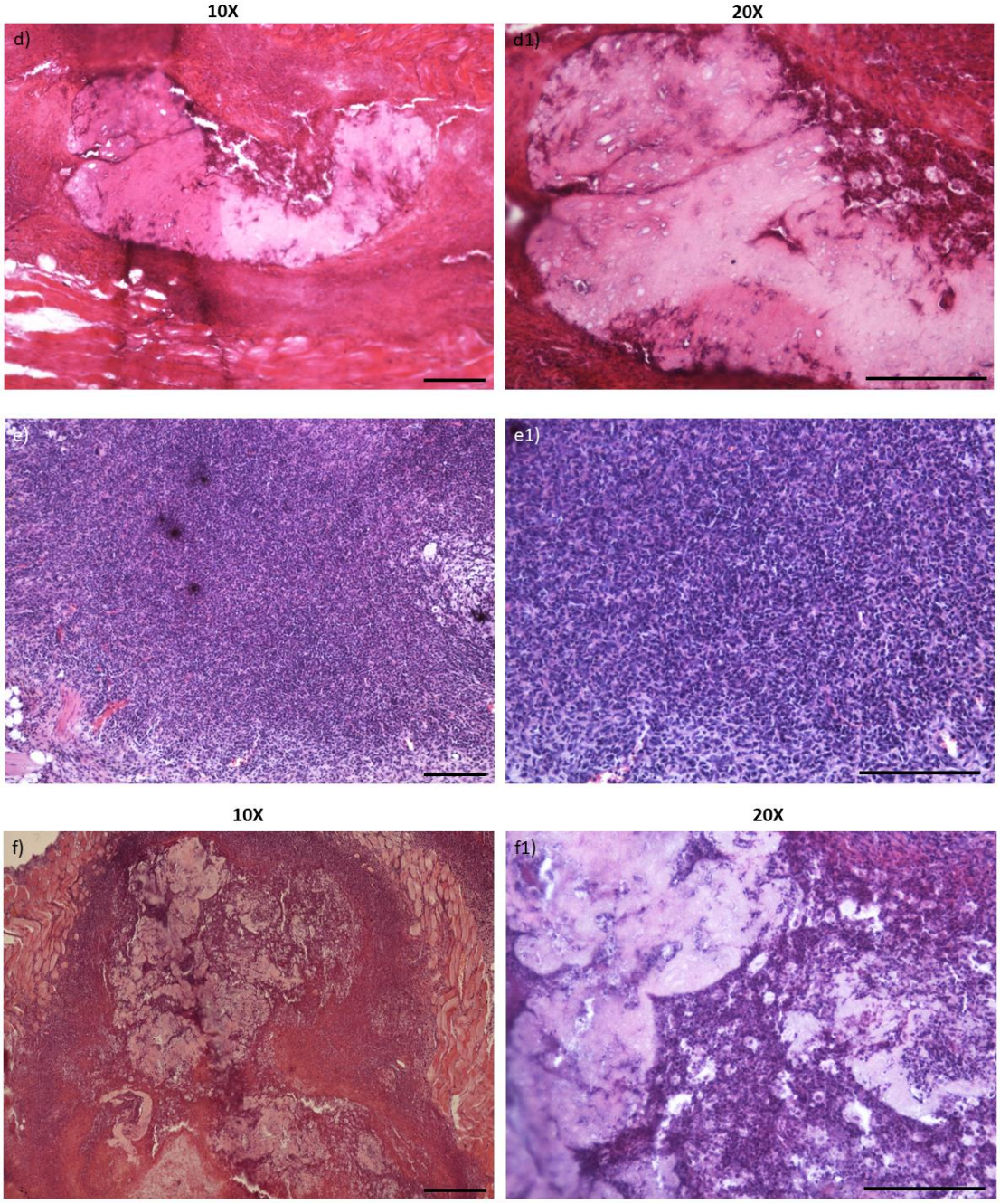
10X
20X
d)
d1)
e)
e1)
10X
20X
f)
f1)

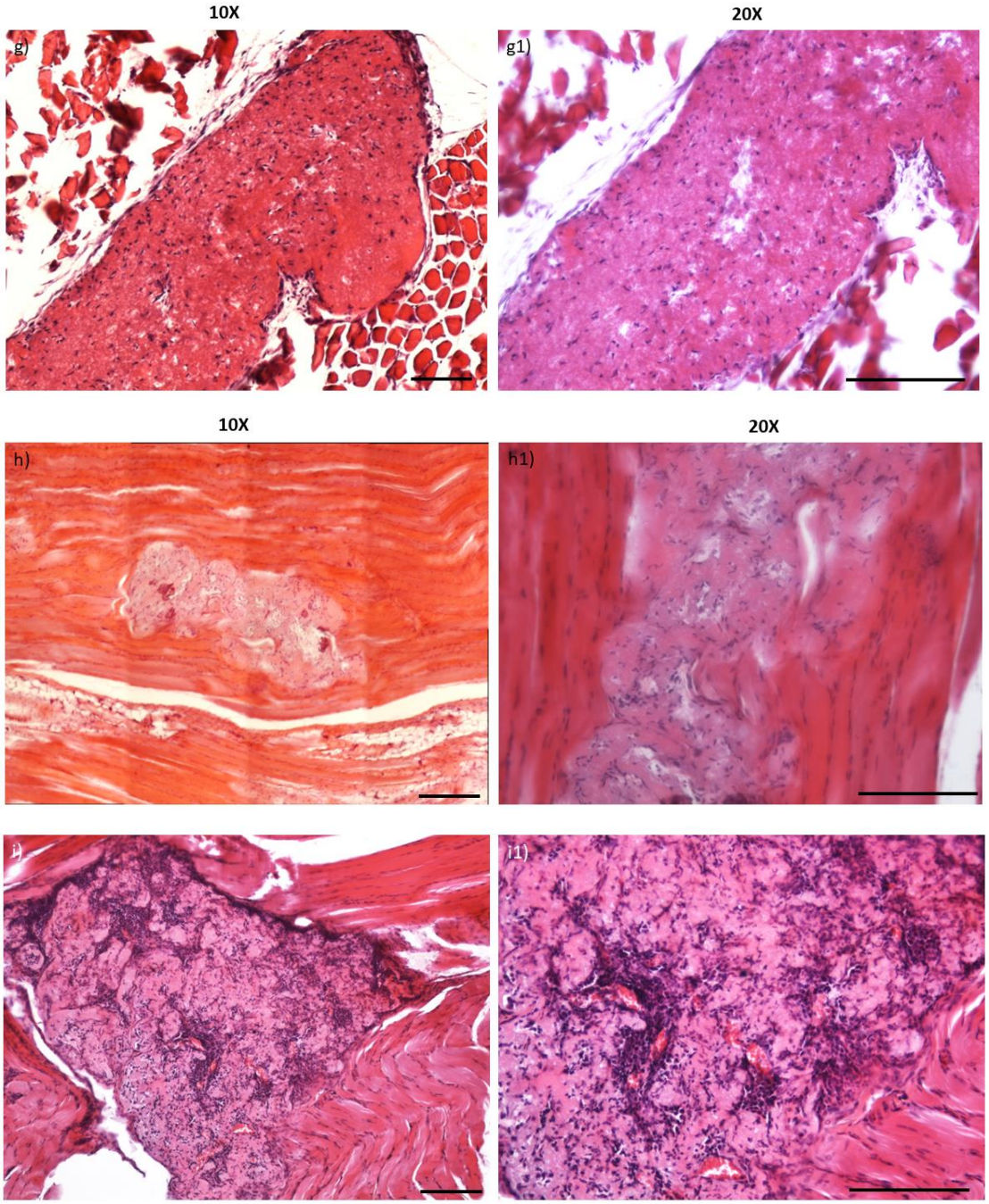

Figure S 3.1. Magnification of H&E staining of proteolytic ELR-based hydrogels at 3, 6, and 12 weeks post-injection. a) VKV-ELR+RGD-ELR at 3 weeks post injection a1) magnification of image a b) GTAR-ELR+RGD-ELR at 3 weeks post injection b1) magnification of image b c) DRIR-ELR+RGD-ELR at 3 weeks post injection c1)

magnification of image c d) VKV-ELR+RGD-ELR at 6 weeks post injection d1) magnification of image d e) GTAR-ELR+RGD-ELR at 6 weeks post injection e1) magnification of image e f) DRIR-ELR+RGD-ELR at 6 weeks post injection f1) magnification of image f g) VKV-ELR+RGD-ELR at 12 weeks post injection g1) magnification of image g h) GTAR-ELR+RGD-ELR at 12 weeks post injection h1) magnification of image h i) DRIR-ELR+RGD-ELR at 12 weeks post injection i1) magnification of image i. Scale bar images: 100µm.

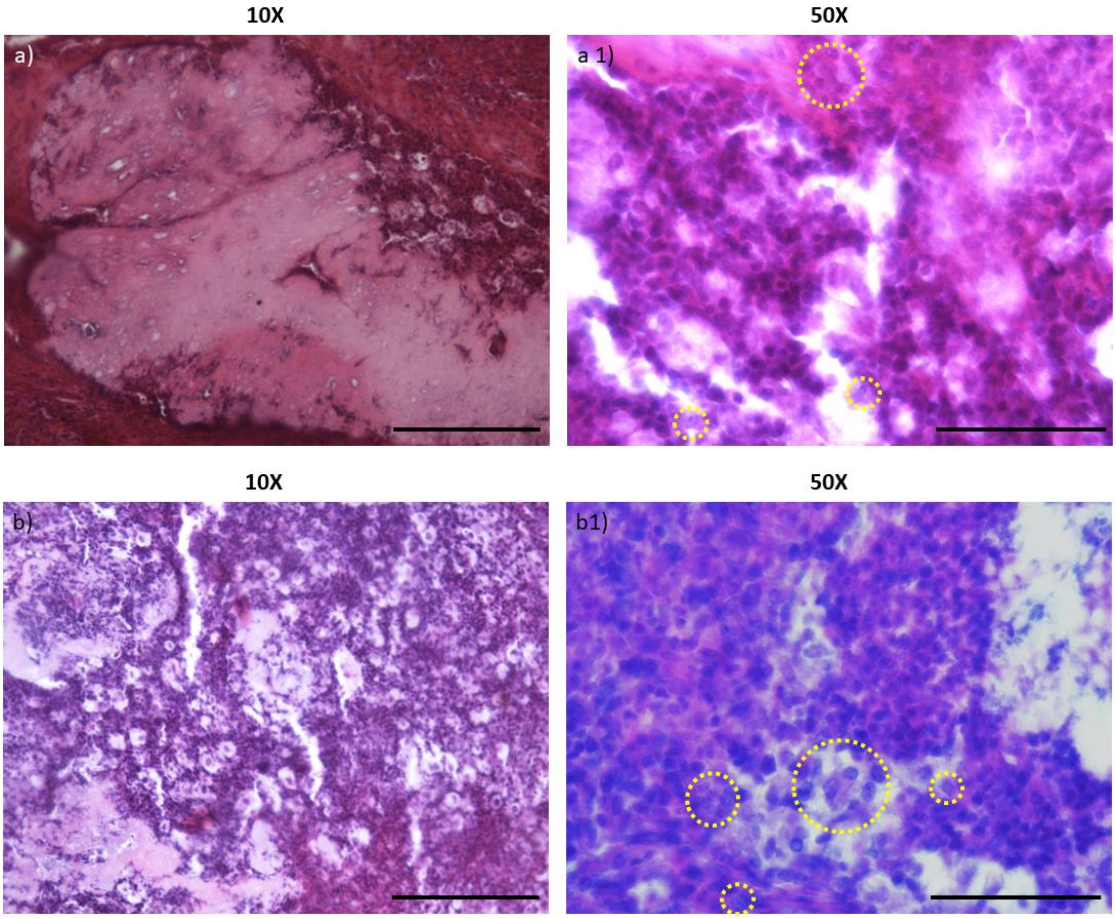

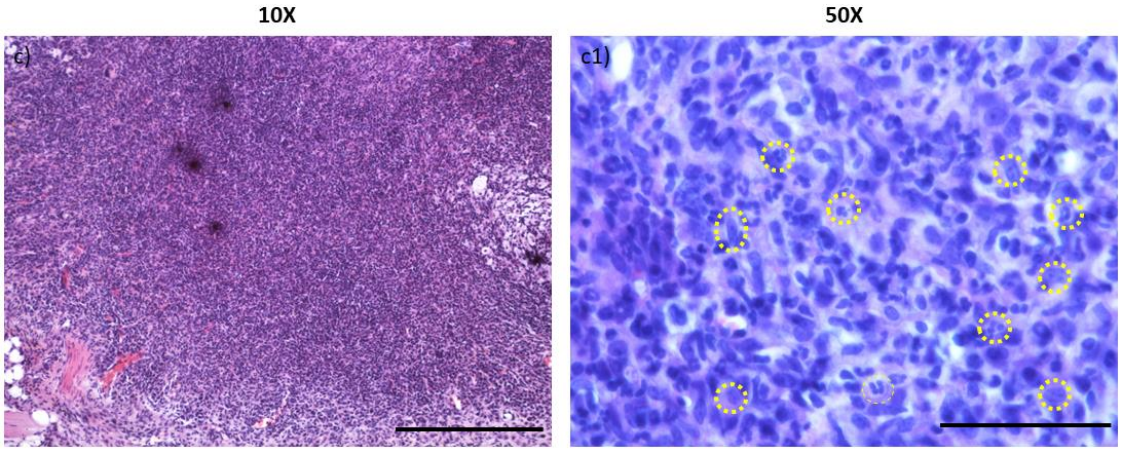

Figure S 3.2. H&E staining images of proteolytic ELR-based hydrogels at 6 weeks post-injection where macrophages are surrounded with a yellow circle. a) VKV-ELR+RGD-ELR a1) magnification of image a b) GTAR-ELR+RGD-ELR b1) magnification of image b c) DRIR-ELR+RGD-ELR c1) magnification of image c. Scale bar of images a, b, c: 100µm. Scale bar of images a1, b1, c1: 50 µm.

CONCLUSIONS

Conclusions

- The ELRs used here have demonstrated properties that were designed for obtaining multifunctional efficacious systems that opens up new possibilities for their application in tissue engineering and regenerative medicine.
- In the first study, spatial control and cell adhesion selectivity were obtained on model gold surfaces grafted with two different ELRs. Specifically, in the first part of this study was confirmed the functionalization of the surfaces with the ELRs by several techniques namely contact angle, XPS, AFM, SEM and QCM-D. Subsequently, an *in vitro* study determined that HUVEC cells adhere better on surfaces functionalized with a mixture made of 25% CC-RGD and 75% CCC-REDV ELRs. In the second part of this study, was obtained a spatial control of HUVEC cell adhesion. Particularly, was confirmed that the number of HUVEC cells adhered on the ablated areas was higher that in other areas of the surfaces functionalized with 100% CC-RGD. In summary, this work confirms that using complementary bioactivities is possible to obtain a spatial control over cell adhesion and this simple approach is useful for studies that require specific placement of

cells such as for generation of biosensors or tissue engineering application.

- In the second study, was demonstrated that when QK peptide is tethered chemically to the ELR-based hydrogels it influences the biological activity of cells *in vitro* namely adhesion and proliferation increase. When injected *in vivo*, after 21 days, it was observed that the ELR-based hydrogels tethering QK peptide present a considerable capillary network formation favoring perfusion and connection with the host tissue. This study confirmed that QK peptide have similar biological activity of VEGF in vitro and in vivo. These constructs could be used for specific tissue engineering application as they provide an alternative help to overcome critical barriers that limit vascularization in tissue engineered constructs.
- In the third study, we developed a 3D ELR-based system where cell infiltration and biodegradation is controlled spatial-temporarily. Primarily, ELRs with proteolytic sites with a different degradation rate (fast and slow) were designed, produced and characterized. The 3D structured system, which consists in a three-layer disk hydrogel, when implanted subcutaneously in mice was observed that the internal layer characterized by a fast degrading

rate was firstly invaded and degraded by cells achieving an inside-to-outside pattern of infiltration and biodegradation as hypothesized. This study confirmed that cell invasion and biodegradation could be preprogrammed using ELRs that present proteolytic sites with different degradation rate with the aim to optimize the regeneration of a specific tissue.

APPENDIX

Abbreviations

VEGF: vascular endothelial frowth factor

DSC: differential scanning calorimetry

ECM: extracellular matrix

ELP: elastin-like polymer

ELR: elastin-like recombinamers

HPLC: high-performance liquid cromatography

HUVECs: human umbilical vein endothelial cells

HFF1: human foreskin fibroblast

H-E: hematoxylin-eosin

ITC: inverse transition cycle

ITT: inverse temperature transition

LCST: lower critical solution temperature

MALDI-TOF: matrix-assisted laser desorption/ionization-time-of-flight

MMP: matrix metalloproteinase

uPA:urochinase plasminogen activator

tPA: tissue plasminogen activator

MQ: milliQ ultra-pure water

Mw: molecular weight

NMR: nuclear magnetic resonance

PBS: phosphate buffered saline

SDS-PAGE: sodium dodecyl sulfate-polyacrylamide gel electrophoresis

SELR: silk-elastin-like recombinamers

T_t: transition temperature

Table of standard amino acid abbreviations

Amino acid	3-letter code	1-letter code
Alanine	Ala	A
Arginine	Arg	R
Asparagine	Asn	N
Aspartic acid	Asp	D
Cysteine	Cys	C
Glutamic acid	Glu	E
Glutamine	Gln	Q
Glycine	Gly	G
Histidine	His	H
Isoleucine	Ile	I
Leucine	Leu	L
Lysine	Lys	K
Methionine	Met	M
Phenylalanine	Phe	F
Proline	Pro	P
Serine	Ser	S
Threonine	Thr	T

Tryptophan	Trp	W
Tyrosine	Tyr	Y
Valine	Val	V

Publications

- Rodríguez-Cabello, J. C, Ibañez-Fronseca, A., Flora, T., Acosta, S., &. (2019). Trends in the design and use of elastin-like recombinamers as biomaterials. *Matrix Biology*. SUBMITTED
- Reguera, J., Flora, T., Winckelmans, N., Rodríguez-Cabello, J. C., & Bals, S., (2019). Micellar self-assembly of Janus Au: Fe3O4 branched nanoparticles. *Angewandte chemie*. SUBMITTED
- Flora, T., de Torre, I. G., Alonso, M., & Rodríguez-Cabello, J. C. (2019). Use of proteolytic sequences with different cleavage kinetics as a way to generate hydrogels with preprogrammed cell-infiltration patterns imparted over their given 3D spatial structure. *Biofabrication*. In press
- Flora, T., de Torre, I. G., Alonso, M., & Rodríguez-Cabello, J. C. (2019). Tethering QK peptide to enhance angiogenesis in elastin-like recombinamer (ELR) hydrogels. *Journal of Materials Science: Materials in Medicine*, *30*(2), 30.

- Flora, T., de Torre, I. G., Quintanilla, L., Alonso, M., & Rodríguez-Cabello, J. C. (2018). Spatial control and cell adhesion selectivity on model gold surfaces grafted with elastin-like recombinamers. *European Polymer Journal*, *106*, 19-29.
- F.J. Arias, S. Acosta-Rodríguez, T. Flora, S. Serrano-Dúcar. *"Biomedical Applications of Recombinant Proteins and Derived Polypeptides"*. In "Biopolymers for Medical Applications" Ruso, J.M. and Messina, PV. (Eds) CRC Press (Taylor and Francis Group) Boca Raton (USA) (2017). ISBN: 978-1-4987-4496-6

- **Congresses and conferences**

2018

- 5th TERMIS WORLD CONGRESS, Kyoto (Japan). ORAL COMMUNICATION. Protease-sensitive recombinamers-based hydrogels able to stimulate angiogenesis.

2017

- XXXIX Congreso de la Sociedad Ibérica de Biomecánica y Biomateriales, Barcelona (Spain). ORAL COMMUNICATION. Tunable biodegradable Elastin-like recombinamer hydrogels able to stimulate angiogenesis.

- 28th Annual Conference of the European Society for Biomaterials (ESB), Athens (Greece). ORAL COMMUNICATION. Cell guided biodegradable Elastin-like recombinamer scaffold able to promote angiogénesis

- European Chapter Meeting of the Tissue Engineering and Regenerative Medicine International Society 2017, Davos (Switzerland). ORAL COMMUNICATION. Elastin-like recombinamers based hydrogels designed to support angiogénesis through a combination of cell adhesión, cell induced biodegradation and remodeling. **(BEST ORAL PRESENTATION, THIRD PLACE)**

2016

- European Chapter Meeting of the Tissue Engineering and Regenerative Medicine International Society 2017, Uppsala (Sweden). POSTER COMMUNICATION. Selective cell adhesiveness on model surfaces grafted with Elastin-Like Recombinamers.

- 10th World Biomaterials Congress, Montréal (Canada). POSTER COMMUNICATION. A 3D Elastin-Like Recombinamer approach toward angiogenesis.

2015

- 5th TERMIS WORLD CONGRESS, Boston (EE.UU). POSTER COMMUNICATION. Selective control of cell adhesiveness on Elastin-like Recombinamers biofunctionalized gold surfaces.

- Advanced Functional Polymers for Medicine, Galway (Ireland). POSTER COMMUNICATION. Biofunctionalization of gold surfaces with Elastin-like Recombinamers to selectively control cell adhesion.

Other contributions

- 15th IATI-BIOMED 2016 Conference and Exhibition, Tel Aviv, Israel
- Nature-inspired Nanomaterials; Synthesis, Characterisation and Applications for Ischemic Conditions. Research Summer School. (2014, May). Crete, Greece.
- Tissue Engineering and Regenerative Medicine I. Research Summer School. (2014, October). Valladolid, Spain.
- Tissue Engineering and Regenerative Medicine II. Research Summer School. (2015, March). Galway, Ireland.
- Entrepreneurship, IPR, Exploitation and Commercialization. Research Summer School. (2016, April). Tel Aviv, Israel.